Analysis of a Crawler Robot with Environmentally-adapted Mobility and its Modular Design

by

Qiquan Quan

M.S. (Harbin Institute of Technology) 2007

A dissertation submitted in partial satisfaction
of the requirements for the degree of

Doctor of Philosophy
in

Department of Robotics

in the

GRADUATE SCHOOL OF SCIENCE AND ENGINEERING

of the

RITSUMEIKAN UNIVERSITY, BIWAKO-KUSATSU CAMPUS

Committee in charge:

Professor Shugen Ma, Chair
Professor Sadao Kawamura
Professor Shinichi Hirai

Fall 2010

Analysis of a Crawler Robot with Environmentally-adapted Mobility and its Modular Design

by

Qiquan Quan

Abstract

Analysis of a Crawler Robot with Environmentally-adapted Mobility and its Modular Design

by

Qiquan Quan

Doctor of Philosophy in Department of Robotics

Ritsumeikan University, Biwako-Kusatsu Campus

Professor Shugen Ma, Chair

In recent years, many disasters are threatening the lives of human beings. For rescuing and exploring tasks in the ruined environment, scientists have developed various types of robot systems. Wheeled robots usually are deployed as the first choice to work on moderately smooth terrain since they can be programmed to traverse relatively flat areas easily; however, the diameter of wheels of the robot limits their locomotion over rugged terrain. Legged robots can step over obstacles, and walk up and down stairs like the legged animals, so as to operate well on uneven terrains, but they also encounter several challenges, including complexity of control, lack of stability and low speed owing to the intrinsic complexity of their mechanisms. Since tracked robots have many advantages, such as gap and obstacle-crossing ability, low pressure to the terrain, excellent stability, and high maneuverability, they are widely recognized to be an important locomotion system, especially for rescue robots and planetary exploration rovers. The performance of tracked mobile mechanisms, however, is still somewhat limited due to some mechanism parameters, such as the diameter of the front sprocket. The most common way to enhance the mobility and adaptability of tracked robot is to build a multi-track mechanism by linking several active or passive units in serial or parallel form. Unfortunately, the additional devices

including some extra actuators, mechanisms and control elements, increase weight of the robot and cost additional power consumption. Control of the robots also consequently becomes more challenging as the complexity of the system increases.

To address the encountering difficulties of the traditional wheeled, legged, and tracked robots, we have proposed a novel crawler mechanism, in which planetary gear reducer is employed as the main transmission device to provide two outputs in different forms using only one actuator. By determining the reduction ratio of two outputs in a suitable proportion, the crawler is capable of switching autonomously among locomotion modes according to the terrain. The proposed novel crawler is designed with excellent adaptability to the environment. There are three locomotion modes for the crawler: "moving mode", "rotating mode", and "recovering mode". The crawler can negotiate the encountering obstacle via the mechanism-realized three locomotion modes without any planning of control. Another premier feature of the crawler mechanism is the absorption of impact energy through specifically-designed redundant mechanism when collisions inevitably occur between the crawler and the environment. Compared with the crawler fully driven by two actuators, our crawler unit driven by one actuator can release impact energy possibly transmitted to the actuator and thus increase the security of the actuator when the robot collides with obstacles in irregular environments.

Using the proposed crawler mechanism, we can build several kinds of crawler-driven robots through proper connection. A dual-crawler-driven robot which is equipped with two crawler units can generate several configurations through cooperatively controlling the actuators located in both crawler units. This tracked robot, which uses two actuators to give four outputs, however could have less realizable postures than that where each output is provided by one actuator exactly. To figure out what postures can be generated by the introduced dual-crawler robot, quasi-static analysis of the robot is conducted while taking the rolling resistance into consideration and the realizable postures can be obtained numerically. The posture transition of the robot is also discussed subsequently. Experiments are conducted to verify the quasi-static analysis for each configuration.

To enlarge the application of the crawler mechanism in exploring and rescuing robot systems, we proposed a modular concept for the crawler mechanism, and achieved corresponding mechanical design of a modular crawler with waterproof and dust-proof qualities. Through placing four of the modularized crawler units to a robot body, a four-module-driven robot is realized via convenient assembly at the interface. Experiments are carried out to verify the proposed concept and mechanical design. A single-module crawler can well perform the proposed three locomotion modes for negotiating obstacles. The four-crawler-driven robot behaves good adaptability to the environment, capable of surmounting obstacles both passively and actively.

TABLE OF CONTENTS

Contents

List of Figures

List of Tables

Acknowledgements

At the time I am finishing the doctoral course in Ritsumeikan, I would like to acknowledge many people who have provided me with great help and much attention.

I am heartily thankful to my supervisor, Dr. Shugen Ma, a professor in Department of Robotics at Ritsumeikan University, whose encouragement, guidance and support from the initial to the final level enabled me to develop an understanding of the subject. He gives me a chance to work in his laboratory and creates many opportunities from which I have learned so much. He not only gives me great help on research, but also takes care of me on daily life. Although I will complete the doctoral course soon, a heart with thanksgiving will exist in my life forever.

I would like to thank my supervisor, Dr. Shinichi Hirai who is a professor in Department of Robotics at Ritsumeikan University. He especially gave me great help at the beginning of my doctoral course, providing a very good research environment and helping me considerably on life. In the seminar of graduate school, many constructive suggestions are proposed to direct my research.

I would like to express my appreciation to Dr. Sadao Kawamura who is a professor in Department of Robotics at Ritsumeikan University for his valuable suggestions in the seminar. Thanks for his comments on this thesis for a doctorate.

It is my pleasure to thank my colleagues in Ma laboratory. I feel very lucky to work with all of them. Thank my friends in Ritsumeikan University. Studying with them together in Ritsumeikan, I have shared a colorful campus life along with them.

I am grateful to the professors in my mother university, Harbin Institute of Technology. They consistently supplied me with tuition fee of my doctoral course for three years.

Thank the Kato Asao International Scholarship Foundation. During the last one and half years, they supported me on finance so that I can concentrate on my research without doing any part-time job.

Thank the staff in workshop of Ritsumeikan University. In the process of mechanical design, their constructive advice benefited the machining of prototype of the crawler robot.

Thanks to the dissertation template provided by U.C. Berkeley, through which the thesis was achieved smoothly.

Without the support and understanding of my family, it is impossible for me to complete this doctoral dissertation. Special thanks to my ex-girlfriend who supported me emotionally for many years both in Weihai and Harbin.

Curriculum Vitæ

Qiquan Quan

Education

1990-1995	Hanwei Primary School (Xisipo, Suzhou, Anhui, China) Pupil
1995-1998	Xisipo Junior High School (Xisipo, Suzhou, Anhui, China) Junior School Student
1998-2001	Sucheng No.1 Middle School (Suzhou, Anhui, China) High School Student
2001-2005	Harbin Institute of Technology (Weihai, Shandong, China) Bachelor, Automotive Engineering
2005-2007	Harbin Institute of Technology (Harbin, Heilongjiang, China) Master of Engineering, Mechanical Engineering
2007-2010	Ritsumeikan University, BKC (Kusatsu, Shiga, Japan) Doctor of Philosophy, Robotics

Personal

Born	October 3, 1983, Anhui, China.
Interests	Photography, Jogging, Badminton, Hiking, Table tennis.

Chapter 1

Research Background

Undoubtedly, robots are urgently required for search and rescue purposes. They should be able to enter dangerous places and environments that rescue personnel cannot reach. During the September 11 attacks in 2001, three hundred forty three fire fighters died at the World Trade Center in America. Rescuers often enter rooms that have unstable structures and yet there are no people to rescue actually. Sixty five of these rescuers died owing to searching the confined spaces after the disaster happened [1].

In order to prevent tragedy from happening again and again, robots can be the first responders and save lives of victims under the dangerous circumstances. Rescue workers have approximately 48 hours to retrieve victims due to survival constraints. Many hours are often lost as rescuers who cannot enter a building due to unsafe conditions. In South Africa, robots could find their useful application in the mining industry, where frequent mishaps occur that require search and rescue operations. Robots could also be deployed in destroyed buildings after earthquake for rescue purposes.

Research is being done on the design and development of robots that will assist in search and rescue scenarios. Different requirements that are needed on a robot are investigated involving video transmission, communication and robot control in these difficult environments. The types of robots being investigated are ground, aqueous and flying vehicles that will be able to adapt to their specific environments. Some of the limitations of these robots included ineffective traction systems, inability to withstand harsh conditions, limited wireless communication range in urban environments and unstable control systems.

As the most important key characteristic of a rescue robot, mobility of the mobile system has been paid great attention to. To a large extent, whether the robot has good motion ability or not determines that the task operation will succeed or not. Therefore, it is an urgent task to develop an efficient mobile mechanism for the robots operated in unstructured environments. Researchers have developed several kinds of mobile mechanisms for rescue robot systems. The typical mechanisms include wheeled, legged, and tracked types.

1.1 Wheeled Robots

Most mobile devices like vehicles and robots roll on wheels, which are simpler to control, pose fewer stability problems, use less energy per unit distance of motion, and can go faster [2], [3], [4], [5]. Stability is maintained by ensuring that the center of gravity of the vehicle is always within a triangle formed by three points contacting the ground. Wheeled vehicles are reasonably maneuverable, some are able to turn in their own length (conventional wheeled robots), and some can move sideways too (omni-directional wheeled robots). However, wheels are only usable on relatively smooth, solid terrain; on soft ground they may slip and get bogged down. In order to scale rough terrain, wheels have to be larger than the obstacles they encounter.

Figure 1.1. A wheeled robot of UGV (Unmanned Ground Vehicle)

The most familiar wheel layout for a vehicle uses four wheels placed at the corners of a rectangle. For four-wheeled vehicles a wheel suspension system is required to ensure that wheels are in contact with the ground at all times. Three-wheeled vehicles have the advantage that wheel-to-ground contact can be maintained on all wheels without a suspension system, such as a UGV wheeled robot shown in Figure 1.1 [6]. The center of a three-wheeled vehicle is the center of the circle defined by the ground contact points of the three wheels.

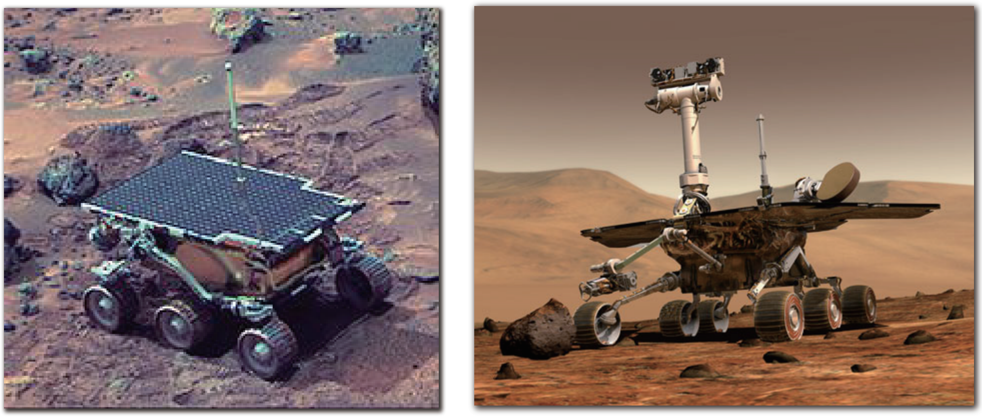

(a) "Sojourner" rover

(b) "Opportunity" rover

Figure 1.2. Mars pathfinders

The Mars pathfinders are a series of famous wheeled robots, such as "Sojourner" and "Opportunity" rovers, in which the rocker-bogie suspension is adopted to promote the locomotion in the irregular rocky environment [7]. Six wheels are mounted onto the suspension mechanism and the passive suspension ensures the consecutive contact between wheels and irregular terrain.

In one sentence, wheeled robots are usually selected to work in relatively smooth terrain; however, the diameter of wheels of the robot limits their locomotion over rugged terrain.

1.2 Legged Robots

There are many places on the surface of the earth where wheeled vehicles cannot go, but people and animals can. While it is more difficult to build and control legs than the wheeled vehicles, legged robots have a number of advantages: stepping over obstacles, walking up and down stairs, and giving a smooth ride over rough ground by varying the effective length of their legs to match the surface undulations [8], [9], [10], [11]. Legged robots are sorted into two classes: dynamically and statically stable systems [12], [13], [14]. For static stability, at least three feet must be firmly placed on the ground and the center of gravity of the vehicle must be within the triangle formed by the feet contact points. Dynamic stability is essential for vehicles with less than three feet, and useful for multi-legged vehicles. Dynamic stability is achieved by moving either the body or the feet to keep the center of gravity within the area formed by the contact points.

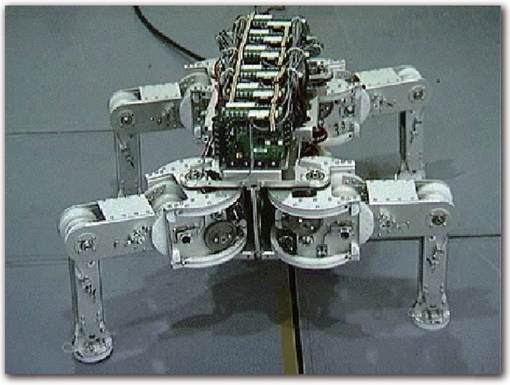

Figure 1.3. A legged robot of "Titan VIII"

Legged robots can step over obstacles and walk up and down stairs, so as to be operated well on uneven terrains, but they encounter several difficulties to resolve, including complexity of control, lack of stability and low speed due to the complexity of their mechanisms [15], [16].

1.3 Tracked Robots

Tracked vehicles, like bulldozers, handle rough terrain quite well. The development of tracked vehicles dates back to the 1770s when a crude continuous track was designed by Richard Lovell Edgeworth [17].

Tracked vehicles have better mobility than pneumatic tires over rough terrain. They smooth out the bumps, glide over small obstacles and are capable of crossing trenches or breaks in the terrain. Tracks are much less likely to get stuck in soft ground, mud, or snow since they distribute the weight of the vehicle over a larger contact area, decreasing its ground pressure.

In addition, the larger contact area, coupled with the cleats, or grousers, on the track shoes, allows vastly superior traction that results in much better ability to push or pull large loads where wheeled vehicles may dig in. Tracks can also give higher maneuverability, as some tracked vehicle can turn on the spot with no forward or backward movement by driving the tracks in opposite directions [18]. Modern tracked vehicles can travel cross-country at speed close to 100 kph, and operate reliably on different terrains [19]. They have become indispensable in many situations where roads are not available and goods and equipment need to be brought in. They help to explore new lands and to conserve the natural environment with their low ground pressure. Recently, track system has become an important locomotion system in robotics especially in rescue robots and outer space rovers.

Scientists have developed many kinds of tracked mobile mechanisms using different combination of tracks, wheels, manipulators and so on. Among the existing different solutions, the tracked robots can be divided into two main classes: 1) Search robots. Small and possibly fast vehicles with high mobility and able to move in destroyed areas where humans cannot go for information collection; 2) Task robots. Larger robots with good mobility and able to complete particularly heavy tasks to support physical strength of the rescuers [20]. It is extremely important to develop mobile platforms capable of traversing very rough terrain because of the unstructured environments in which they are expected to be utilized.

Since tracked robots have advantages, such as gap and obstacle crossing ability, low pressure to the terrain, excellent stability and high maneuverability, they are widely recognized as an important locomotion system especially for rescue robots and planetary exploration rovers. In the following contents, several different types of tracked robots will be introduced individually.

1.3.1 A Series of "Souryu" Robots

Professor Shigeo Hirose in Tokyo Institute of Technology has developed a series of tracked rescue robots named "Souryu" for exploring and rescuing tasks. Souryu-I, II, and III were developed with the purpose of entering collapsed buildings and finding survivors [21], [22], [23]. The crawler vehicles composed of three crawler bodies connected by active joints are capable of changing the body posture. The front and rear bodies are connected and can rotate symmetrically (with respect to the main central body) in vertical and lateral directions, by making use of two coupled-driven screw axes as joints. These front and rear screw axes are driven concurrently by two motors mounted in the central body.

(a) "Souryu I" (b) "Souryu II" (c) "Souryu III"

Figure 1.4. "Souryu" tracked robots I, II, III

The front and rear bodies of Souryu-I are fitted with wedge-shaped crawler units. The crawlers of all three bodies are driven concurrently by one motor via a power transmission axis, so the vehicle consists of only three motors. In Souryu-I, the joint mechanism can achieve yawing and pitching motion, and there is elasticity compliance in the direction of rolling. The next generation, Souryu-II similar to Souryu-I presents some new features, such as detachable bodies for more practical applications. Souryu-III is constituted by standard crawler bodies and both crawlers of each body are driven concurrently, so the vehicle consists of five motors totally. The joint can perform yawing and pitching motion, and it also has elasticity in the rolling direction.

With the their specifically-developed tracks, they had developed two improved models, namely Souryu-IV (composed of three independently actuated double-sided crawler bodies, a joint driving unit, a blade-spring joint mechanism, and cameras) and Souryu-V

(a) "Souryu IV" (b) "Souryu V"

Figure 1.5. "Souryu" tracked robots IV, V

(composed of mono-tread-crawler bodies, elastic-rod-joint mechanisms, and cameras). Concerning Souryu-IV, the independently actuated double-sided crawler allows for the rotation of the robot on the spot [24], [25], [26], [27]. With the joint driving unit and the blade-spring joint mechanism, it is possible to perform posture changes, which allow smooth changes in the configuration of the vehicle, so that it is not easily struck in rubble. Souryu-IV has three cameras: two are mounted in the front body mainly for search operations, and another one on the rear body utilized for teleoperating the robot. Regarding Souryu-V, the elastic rod-joint mechanism is a newly proposed mechanism devised to link the mono-tread-crawler bodies together. The mechanism consists of four elastic rods and rod-shortening/lengthening mechanisms, and bending actions result from the longitudinal difference and the elasticity of the elastic rods. Souryu-V has four cameras: two are mounted in the front body utilized mainly for search operations while another two are on the rear unit used for teleoperating the robot. Besides, each robot has dust-proof and waterproof mechanisms in order to protect them against the elements even in harsh environments.

1.3.2 Tracked Robots with Manipulator or Auxiliary Flipper Arm

(1) "Helios" Robots

Prof. Hirose has also developed another series of "Helios" robots, belonging to the type of task robot [28], [29], [30]. The concept consists of a crawler base equipped with a manipulator. The arm is mainly utilized to assist the motion of the vehicle itself. The use of a manipulator or active linkages is to improve the motion capabilities for the mobile platform.

Figure 1.6 shows the prototype and motor distribution of the robot “Helios VII”. The vehicle consists of two crawlers independently actuated by motors m1 and m2, respectively connected to the main body by actuators m3 and m4. The chassis acts as a base for an arm with 5 DOFs (Degree of Freedom) supplied by the motors m5, m6 and m7, and the pair of m8 and m9. Four passive wheels are installed on the joint shaft of the elbow and on the tip of the arm in order to support the motion of the vehicle and to protect the tip from damage when it touches the ground. Tracks are wrapped around three main wheels: the front and rear sprockets with equal diameter, but smaller than the middle one. By using this structure configuration and the manipulator, “Helios VII” presents several different motion capabilities including stair climbing, compact mode, upside-down recovery, manipulation at high positions, mobility on slopes, connection mode, and high-step climbing [20].

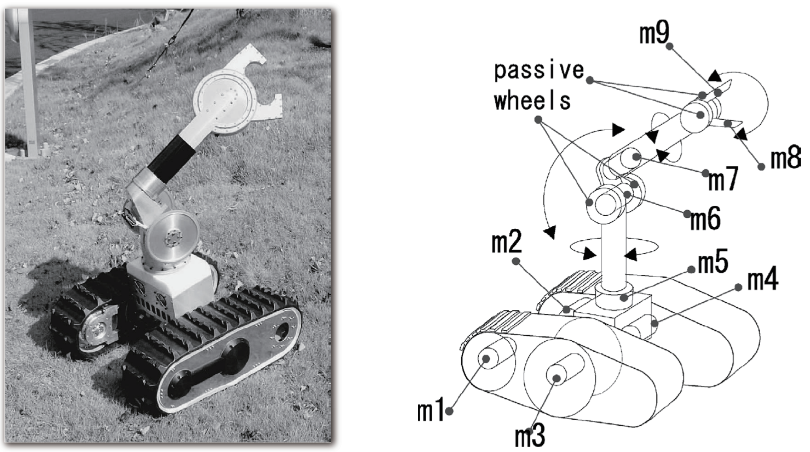

(a) “Helios VII” (b) Actuators distribution of this robot

Figure 1.6. “Helios” robots

(2) “PackBot” Developed by iRobot Corporation

The iRobot Corporation has developed several types of mature tracked robots with assistant flipper. PackBot can easily climb stairs, roll over rubble and navigate narrow, twisting passages [31]. Among the tracked robots, the iRobot “PackBot 510” is the ultimate protective tool for IED (Improvised Explosive Device) identification and disposal as shown in Figure 1.7(a). These flippers are capable of continuous 360-degree rotation and enable PackBot to traverse rocks, mud, snow, gravel and other tough terrain. PackBot's flexible polymer tracks eject debris and move the robot over all surfaces with sure-footed efficiency.

PackBot's shock-resistant chassis can survive shocks of up to 400Gs. This tough robot can withstand a six-foot (1.8 m) drop onto concrete, making it possibly being thrown through a windows, tumbling down stairs and being deployed from a low-altitude helicopter. The robot is fully sealed, with no exposed wires, making the robot operational in all weather conditions.

PackBot offers multi-mission flexibility and customization options on a proven chassis. State-of-the-art electronics enhance payload integration capabilities. Each of the eight payload ports is equipped with Ethernet, USB, power and two video channels. As a result, there is no limit to the types of payloads the robot can support.

The robot can be hand carried and deployed by one person in less than two minutes. PackBot is simple to learn and easy to use. The operator can view a 2-D or 3-D image of the robot on the control unit, allowing for precise positioning. The control unit is powered by onboard battery and can also be used with a supplementary power supply.

(a) The "PackBot 510" of iRobot

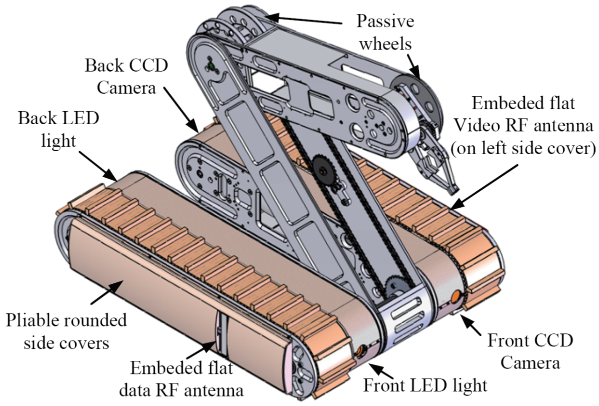

(b) Hybrid locomotion-manipulation tracked robot

Figure 1.7. Tracked robots with an assistant arm

(3) Hybrid Locomotion-manipulation Tracked Robot

As shown in Figure 1.7(b), another hybrid locomotion-manipulation tracked robot was made in University of Toronto [32], [33]. A novel architecture for a tracked hybrid mobile robot was proposed to hybrid the mobile platform and manipulator arm as one entity for improving robot locomotion as well as manipulation [34], [35]. The proposed idea is twofold and can be described as follows.

1) The mobile platform and the manipulator arm are integrated as one entity rather than two separate modules. Furthermore, the mobile platform can be considered as part of the manipulator arm and vice versa. Thus, some of the same joints that provide the manipulator's DOFs also offer the platform's DOFs.

2) The robot's adaptability is enhanced by "allowing" it to flip over and continue to operate instead of trying to prevent the robot from flipping over or attempting to return it back. Owing to a fully symmetrical design with the arm integrated, it is only required to command the robot to proceed towards its destination from the current position when a flip-over occurs. Furthermore, the undesirable effects of flipping over or free falling are compensated by a built-in dual suspension and tension mechanism.

(4) "Kenaf" and "Aladdin" Track-flipper Robots

The experimental robot "Kenaf" has been developed in the joint research project of Tohoku University in Japan. The robot's weight is about 20 kilograms, and it has a width of 450 millimeters, a length of 580 millimeters, and a height of 300 millimeters. This robot has four active flippers (each has a length of 280 millimeters) actuated independently to adapt to uneven terrains. The two tracks mounted at the bottom of the vehicle body are employed to prevent being stranded on rough terrains. In the tracked vehicle, two laser range sensors (URG-X04) are installed on both sides of the robot as shown in Figure 1.8(a). To detect the surface information of the terrain that flippers contact, each scanning plane is parallel to the workspace of the active flippers and perpendicular to the ground. In addition, three gyro sensors are embedded inside its body to measure its attitude [36], [37].

To determine a proper flipper angle to traverse uneven terrains, the robot fuses range data obtained from laser range sensors into the control algorithm. Controlling of flipper angles is utilized to ensure robust stability when the robot is working in irregular environment.

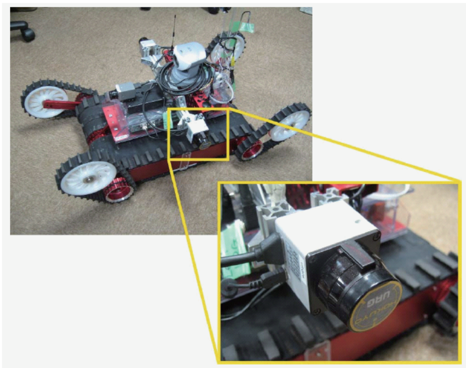

(a) Kenaf

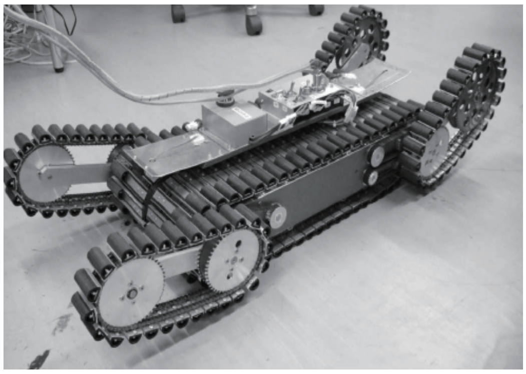

(b) Aladdin

Figure 1.8. Kenaf and Aladdin

“Aladdin” is another tracked robot with the shape similar to “Kenaf”, which was also developed in Tohoku University [38]. Like Kenaf, Aladdin can get over step by swinging these flippers. The robot has the following advantages: high mobility on rubble using four flippers and whole body’s crawler; enough capacity of embarkation inside the body [39], [40]. A strategy of semi-autonomous control for “Aladdin” was proposed to get over unknown steps. Control rule of flippers is founded on the judgment whether the robot body contacts ground or not.

(5) “Macbot” and “Double-track” Tracked Robots

“Macbot” and “Double-track” were developed in the universities of Korea as shown in Figure 1.9(a) and Figure 1.9(b), respectively. The “Macbot” composed of four track modules was designed for outdoor environment applications so that its design was focused on power, adaptability and reliability in operation. The front track module has a clutch mechanism based on a planetary gear train and the module provides two driving modes: one is the normal mode for regular terrain and the other is the obstacle mode for rough terrain. The switch between the two modes depends on the rotational direction of the motor installed at each track [41].

When the "Macbot" cannot go over a relatively higher step using the normal mode, the obstacle mode will be activated at once. First, the two front tracks reach the obstacle and start to climb it up through rotation of the front modules. After the two front tracks successfully stand on the obstacle, the two rear tracks approach the steps and consequently climb over the obstacle [42].

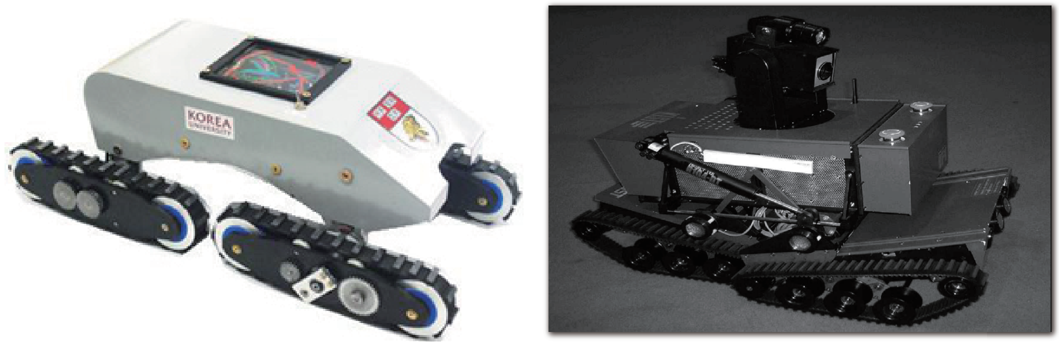

(a) Macbot (b) Double-track

Figure 1.9. "Macbot" and "Double-track" robots by universities in Korea

As shown in Figure 1.9(b), the "Double-track" robot consists of a driving mechanism and a robot body. The body is composed of a control block and camera while the driving mechanism is comprised of front and rear frames, thus the robot is called a double track [43]. The body is connected with the double track by four joints. It is designed for the body to be inclined according to the change of the relative angle between the front and rear frames. A hydraulic damper is attached on each side of the body in order to absorb impacts from rough landform. A pan-tilt stereo camera is employed to control the robot in remote areas, where the camera monitors the surrounding area. In the control block, controllers for the amplifiers and motors are inserted in the middle where the pan-tilt camera is positioned. A power control system is established on the front where an emergency switch is also attached. The switch can be turned on or off with a RF remote controller.

1.3.3 Wheel-track-integrated Robots

(1) “AZIMUT” Tracked Robot

AZIMUT addresses the challenge of making multiple mechanisms available for locomotion on the same robotic platform. AZIMUT possesses four independent articulations that can be wheels, legs or tracks, or a combination of these. By altering the direction of its articulations, AZIMUT is also capable of performing omnidirectional movement without changing its orientation. All these capabilities provide the robot with the ability to move in confined areas. AZIMUT is designed to be highly modular, placing for instance the actuators in the articulations so that the wheels can be easily replaced by leg-track articulations for all-terrain operations [44], [45].

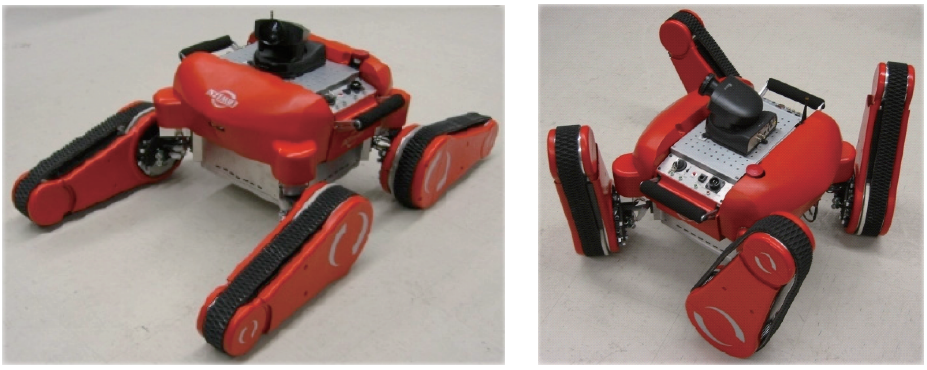

Figure 1.10. “AZIMUT’ robot developed in Canada

Stability and compliance of the platform are enhanced via adding a vertical suspension and using elastic actuators for the motorized direction of AZIMUT’s articulations. An elastic element is placed in the actuation mechanism and a sensor is used to measure its deformation, allowing to sense and control the torque at the actuators end. This technology makes the robot capable of “feeling” the surface so as to improve the locomotion over uneven terrains. AZIMUT’s design conception provides a rich framework to create a great variety of robots for indoor and outdoor applications [46], [47].

(2) "Andros F6A" Tracked Robot

As a leader in global security, Northrop Grumman Corporation has developed several kinds of mobile systems to support the challenge in public security. According to the advertisement of Northrop Grumman, the Remotec ANDROS F6A is the most versatile, heavy-duty robot on the market. Speed and agility unite to make it a first choice for a wide range of missions [48]. The robot is a highly stable, tough-as-nails partner for hazardous duty operations. The features of this tracked robot can be summarized as follows:

- Color surveillance camera with light, zoom, pan/tilt
- Surveillance camera with image stabilization - 216:1 total zoom (26x optical/12x digital)
- Stationary arm camera - 40:1 total zoom (10x optical/4x digital)
- 24-inch camera extender
- Multiple-mission tool/sensor mounts with plug-and-play capabilities
- Gripper with continuous rotation
- Manipulator arm's seven degrees of freedom ensure optimum dexterity
- Quick-release pneumatic wheels for rapid width-reduction, no tools required
- Patented articulating tracks allow for traversing ditches, obstacles and the roughest terrain

Figure 1.11. Andros robot for public security by company of Northrop Grumman

(3) "MOBIT" Tracked Robot

A new robotic platform, namely MOBIT (Mobile Robot of BIT), has been built at Beijing Institute of Technology in China [49], [50]. The robot is composed of four independent wheel-track-leg articulations and designed to be a light-weight, compact-size, low-consumption and highly robust for different kinds of maneuverability conditions as shown in Figure 1.12. This concept of wheel-track switch would allow the robot to move at high speed using wheels and be capable of traversing rough terrains using its various track locomotion modes [51], [52], [53].

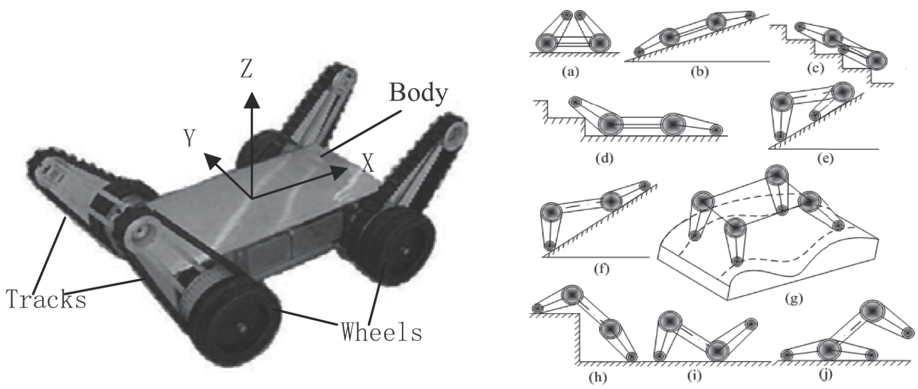

Figure 1.12. A wheel-track robot of "MOBIT" in China

1.3.4 Shape-transformable Tracked Robots

(1) "RLMA" Tracked Robot

The professor at Ryerson University in Toronto has proposed a kind of self-reconfigurable tracked mobile robot (SRTMR). The SRTMR under investigation is a Ryerson Linkage Mechanism Actuator (RLMA), which is a customized product made by ESI (Engineering Services Inc.). RLMA consists of a chassis, two tracks, two driving wheels, two supporting wheels, and two planetary wheels, as shown in Figure 1.13. The two driving wheels can be controlled independently to realize differential steering and the two planetary wheels are attached at the tip of the flippers. The two flippers which are installed at the flanks of the chassis through a hinge joint, are driven by one pitching motor to ensure synchronization of the left and right tracks [54]. A compressed-spring is installed in the linear joint to compensate the length when the track is changed so as to retain tension in each track. The tracks are equipped with a pattern of grousers, which are designed to improve the cohesion coefficient between the robot and the environment.

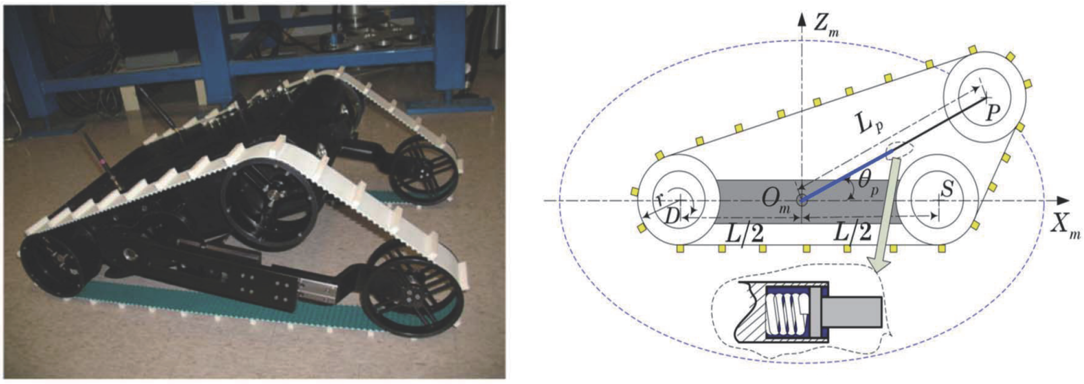

Figure 1.13. A self-reconfigurable tracked mobile robot

The motion of the flippers can be controlled to change the tracks configuration so as to surmount obstacles or climb stairs [55]. This mechanism of flippers can be controlled to adapt to environment actively by human.

(2) "Amoeba-I" Reconfigurable Tracked Robot

To improve the mobility and flexibility of the link-type structure, a link-type metamorphic robot was developed in SIA (Shenyang Institute of Automation) of China [56]. Restructuring is desired to change the configuration of the robot to adapt to different environments due to the complexity of unstructured environment. As shown in Figure 1.14, this kind of link-type structure can perform two types of locomotion: serial mode and parallel mode.

This link-type robot, with offset joints at both sides and with the link arm between adjacent modules, has enough flexibility to shift shape [57]. The number of module can be chosen by the designer and the connection and disconnection of the modules can be finished

(a) Serial mode (b) Parallel mode

Figure 1.14. Shape-shifting "Amoeba-I" tracked robot with two locomotion modes

manually [58]. As a manually reconfigurable structure, the primary prototype presents good mobility in various environments.

1.3.5 COG-transferring Mechanisms

A robot called "DIR-2" (Dexterous Inspection Robot) targeting an inspection robot market was developed in Advanced U-Corporation Inc. in Gunma, Japan. Figure 1.15 shows an assembly diagram of five robot components and eight driving parts in the robot. The robot is composed of two triangular-shaped crawler devices ("triangular crawler") placed in parallel, two-link mechanism ("Link A" and "Link B"), and a straight crawler device ("straight crawler"). As shown in Figure 1.15, each shaft ("center shaft") on the left and right side of Link A is inserted into the center hole of each triangular crawler. A servomotor embedded in the triangular crawler drives each crawler to rotate around each center shaft with 360 degrees. Both Link A and Link B, Link B and the straight crawler are connected by hinge joints and can be driven within the range of 240 degrees.

There are totally eight DOFs in this robot. Four motors are used for driving crawler belts of triangular crawlers and straight crawlers. Two motors are utilized to rotate triangular crawlers around each center shaft. Other two DOFs are used to drive joints between Link A and Link B, Link B and the straight crawler. In the ordinary locomotion style, the robot can move forwards, backwards, and turn to left and right.

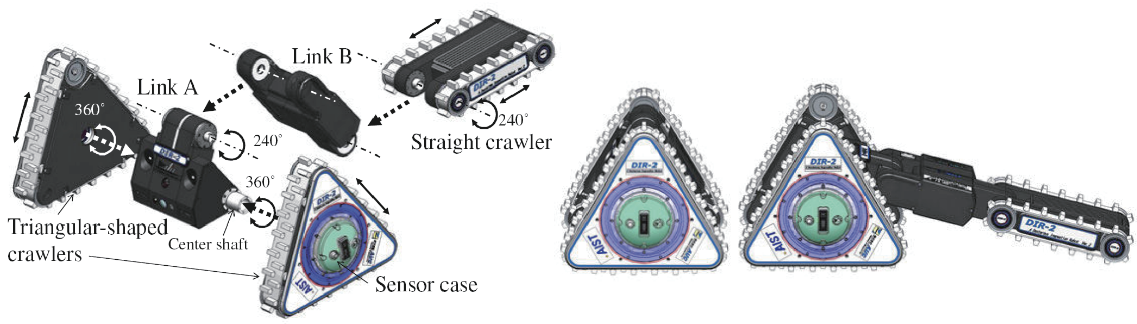

Figure 1.15. "DIR2" robot developed by the National Institute of Advanced Industrial Science and Technology (AIST) in Japan

Figure 1.15 shows a folding state and an extended state of the robot. The robot can fold Link B and the straight crawler completely inside the triangular crawler unit in the side view. The robot can also move and turn in a narrow space, ideally 35 cm in width and 25 cm in height, by that state. The folding state is so compact that it is easy for delivering and storing. In the extended state, Link B and the straight crawler part can be extended to about 40 cm backwards to overcome obstacles [59].

As described in this section, scientists have already proposed several kinds of tracked robot systems, including series of "Souryu"; tracked robots with manipulator or auxiliary flipper arm; wheel-track-integrated robots; shape-transformable tracked robots and COG-transferring mechanisms. The tracked mobile systems exhibit great virtues so as to adapt to the rough terrain in risky environment. Tracked mobile mechanisms, however, are still somewhat limited due to some mechanism parameters, such as the diameter of the front sprocket. As mentioned above, the most common way to improve the mobility and adaptability of the tracked robot is to build a multi-track robot by linking several active or passive units in serial or parallel form. Apparently, additional devices including some extra actuators, mechanisms and control elements, add weight and require additional energy. Control of the robots also consequently becomes more challenging as the complexity of the system increases [60]. To overcome the difficulties stated above, we have proposed a crawler mechanism with polymorphic locomotion.

1.4 A New Concept of Crawler-driven Mechanism

From the aforementioned tracked robot, the common way to improve locomotion of the tracked robot is to add an assistant tracked arm. Usually, two actuators are necessary for driving the pulley and the rotation of the arm. We want to find a way in which there is just one actuator to drive both the pulley and the arm rotation. Concretely, the power from the only one actuator should be divided into two parts to realize the idea that one actuator gives two outputs to drive the related mechanisms. A big problem is how to distribute the power to the related two parts separately.

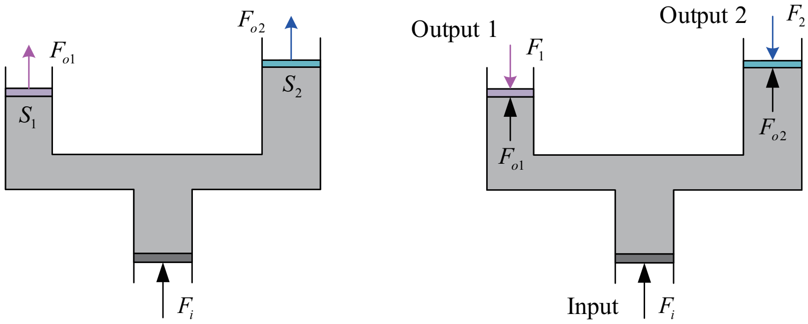

Figure 1.16. One input giving two outputs in a hydraulic system

Inspired from the knowledge of a hydraulic system as shown in Figure 1.16, the power splitting mechanism is composed of one input at the bottom and two outputs on the top [61]. The input is F_i at the bottom while the outputs are two pistons with the area of S_1, S_2, respectively. Assuming that all the objects are put in the horizontal plane without considering the influences of gravity, if only one input is exerted at the bottom, both the outputs will move freely and thus the movements of piston 1 and piston 2 cannot be determined definitely. If two external forces F_1, F_2 from the environment are acted on piston 1 and piston 2, the movements of piston 1 and piston 2 will be determined clearly because of the piston size. For instance, if $F_1 = F_{o1}$, $F_2 < F_{o2}$, the left piston 1 remains stationary while the right piston 2 moves upwards. In a word, the outputs of the device depend on the external constraints from the environment. Therefore, we want to apply this concept of one-input-two-output to design of the tracked crawler mechanism.

Based on the conception demonstrated above, we have proposed a novel crawler-driven mechanism, which makes use of only one actuator to provide two outputs [62], [63], [64], [65], [66]. The first output is used to drive the track pulley while the second output is employed to rotate the frame. By determining the reduction ratio of two outputs in a suitable proportion, the crawler is capable of switching autonomously among locomotion modes according to the terrain. The most important characteristic of the mechanism is that the polymorphic locomotion is provided by one actuator and switch among modes of locomotion occurs autonomously.

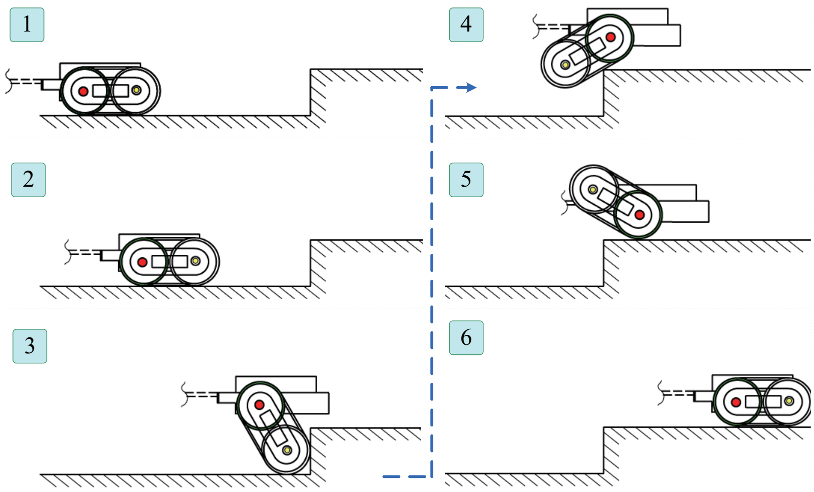

Figure 1.17. Concept of the proposed crawler mechanism

As depicted in Figure 1.17, there are three locomotion modes for the proposed crawler mechanism. On even ground or moderately rugged terrain, the power is transmitted to the crawler belt, and the crawler movement is like a typical tracked vehicle. When the crawler comes into contact with a high obstacle, the power is transmitted to the connecting frame. The crawler rotates and climbs over the obstacle. After the crawler climbs up the obstacle, the power is still transmitted to the connecting frame and drives the crawler to rotate continuously until it goes back to the initial position. This recovery can be achieved immediately after the rotation mode is performed or when the crawler comes into contact with the next obstacle.

1.5 Motivation of Our Research and Outline of this Thesis

The purpose of this research is to develop a crawler robot which may adapt to environment autonomously and find the advantages of the proposed crawler mechanism besides the intrinsic autonomy characteristic. Since the crawler mechanism is an under-actuated system, the controllability should be further studied for well performing rescuing tasks. The contents of this thesis are organized as follows.

Chapter 2 introduces the mechanical model and prototype of the proposed crawler-driven mechanism. The realization of making a crawler mechanism adapt to the environment through mechanical design is discussed in detail. Another important advantage of this crawler mechanism in impact absorption is analyzed when the crawler mechanism collides with obstacles in rough terrains.

Chapter 3 discusses two-dimensional posture analysis of a dual-crawler-driven robot which is comprised of two crawler mechanism units. All the possible configurations of the dual-crawler robot are analyzed in the quasi-static way and the controllable postures are obtained through numerical methods.

Chapter 4 presents control methods for posture control of the dual-crawler-driven robot. Three kinds of control methods are proposed for the robot to control the posture through the interaction between the front and rear crawler units.

Chapter 5 conducts a modular design of the crawler mechanism considering waterproof and dust-proof qualities. As the applications of the modular crawler, a one-module and a four-module crawler robots can be constituted via easily assembling the connecting interfaces.

Chapter 6 concludes this thesis and discusses the possible works in the future.

Chapter 2

A Crawler-driven Robot and its Features

Based on the conception of one-input-two-output, we proposed a new type of tracked crawler-driven mechanism with polymorphic locomotion. In this chapter, the concept and realization of the proposed crawler mechanism are presented first and then the features of this crawler mechanism are demonstrated.

2.1 Newly Proposed Crawler Mechanism

Based on the concept of one-input-two-output, we have proposed a novel crawler-driven mechanism, which makes use of only one actuator to provide two outputs. Since the planetary gear reducer has three movable parts (sun gear, carrier, and ring gear), one of them is selected to input the power, another two of them can be used as outputs. Thus, a planetary gear reducer is chosen as the main transmission in the crawler mechanism.

2.1.1 Mechanism of a Crawler Unit

The proposed crawler mechanism is capable of providing two different forms of outputs with just one actuator. The first output is transmitted to the crawler-belt and drives the

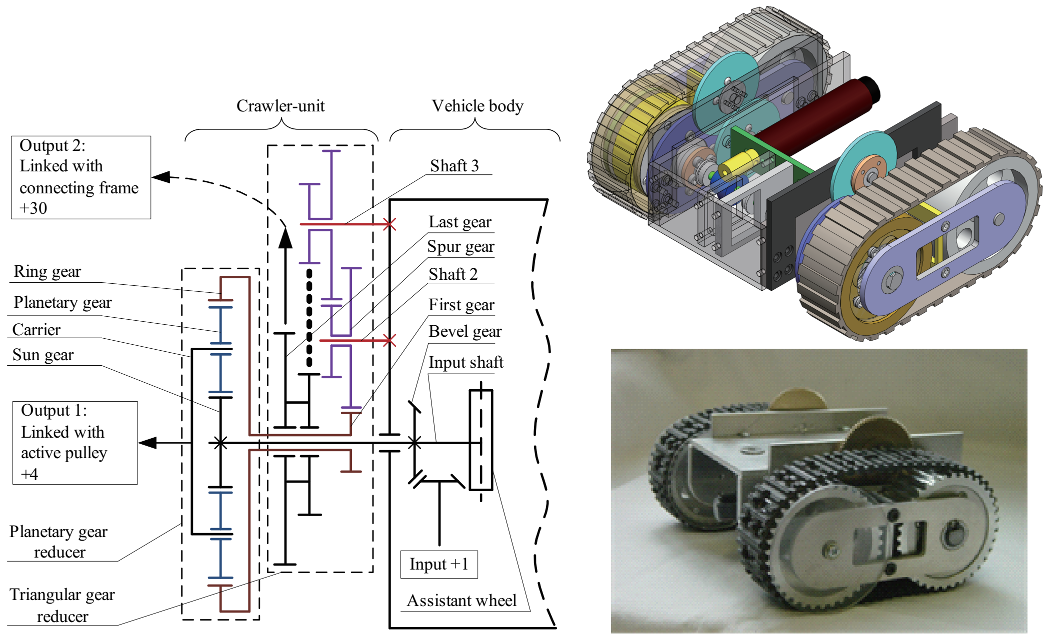

(a) Transmission system

(b) Mechanical model

Figure 2.1. Mechanism of one crawler unit

crawler to move forwards or backwards; the second one is employed to drive the connecting frame that links two sprockets of the crawler, as shown in Figure 2.1. The rotation of the connecting frame enhances the mobility when negotiating an obstacle.

The planetary gear reducer was adopted as the main power transmission for our crawler mechanism, as shown in Figure 2.1(a). The input torque of the actuator is transmitted to the sun gear of the planetary gear reducer through a pair of bevel gears. Since the carrier of the planetary gear reducer is linked with an active pulley, the torque is derived from the sun gear and transmitted to the active pulley, the crawler belt, and acts as the first output to drive the crawler mechanism to forward or backward on even ground or slopes. As the second output, the torque is derived from the sun gear and transmitted to the ring gear of the planetary gear reducer, and then to a triangular gear reducer, and lastly to the connecting frame. The triangular reducer consists of three pairs of spur gears. The rotation of the connecting frame drives the crawler unit to rotate wholly around the input axle.

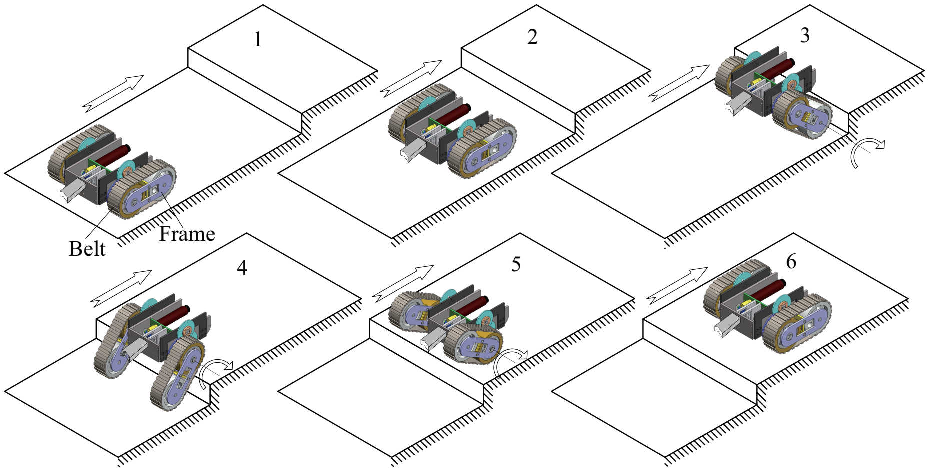

Figure 2.2. Locomotion modes for step climbing

2.1.2 Polymorphic Locomotion Modes

To describe the whole locomotion process while the crawler moves in irregular environment, we present three locomotion modes, referred to as “moving mode”, “rotating mode” and “recovering mode”.

1) Moving mode (1, 2, 6 in Figure 2.2): The crawler mechanism moves on an even terrain or slope like a normal tracked vehicle since the power of the actuator is transmitted to crawler-belt.

2) Rotating mode (3, 4 in Figure 2.2): When the crawler mechanism contacts an obstacle, since the rotation of the crawler belt is stopped by the resistance from the ground and the power has to be transmitted to the connecting frame, the rotation of connecting frame drives the crawler mechanism to climb over the obstacle.

3) Recovering mode (5 in Figure 2.2): Once the crawler mechanism has climbed up the obstacle, the power is transmitted to the connecting frame and drives the crawler mechanism to return continuously until it recovers to the initial position.

To achieve the proposed locomotion autonomously in irregular environments, the power transmission of the crawler should be designed to meet the following three conditions:

i) One motor input gives two outputs in the transmission.

ii) The two outputs must rotate in the same direction.

iii) The two reducer ratios are selected in a certain range.

The mechanism of our crawler model equipped with a planetary gear reducer meets conditions i) and ii). Concerning the most important condition iii), we can determine the proportion of reduction ratios of two outputs within a certain range. The reduction ratios on outputs 1 and 2 have been designed to be 4 and 30, and the two outputs have the same rotating direction [63], [66].

In motion mode, to drive the crawler mechanism to move on even ground or slope like a normal tracked vehicle, propulsion on the crawler belt has been designed larger than motion resistance. At the same time, rotation torque on the connecting frame is smaller than the rotation resistance generated by gravity of crawler mechanism and payload.

In the same way, when the crawler mechanism contacts an obstacle, to climb over the obstacle in the proposed locomotion mode instead of track-slipping, the propulsion on the crawler belt has been designed smaller than the friction resistance so that the crawler belt can be fixed. Concurrently, the rotation torque is larger than the rotation resistance to lift vehicle body to negotiate the obstacle.

After the crawler mechanism has climbed up the obstacle, it can recover to the initial position autonomously.

In this mechanism, the polymorphic locomotion is provided by one actuator and switch between modes of locomotion occurs autonomously.

2.1.3 Mechanism of a Dual-crawler-driven Robot

A tracked robot that is realized by connecting two units of the proposed crawler mechanism through a rigid body is shown in Figure 2.3. This robot can not only switch autonomously motion modes adapted to the terrain but also generate several postures through controlling cooperatively the two actuators [67].

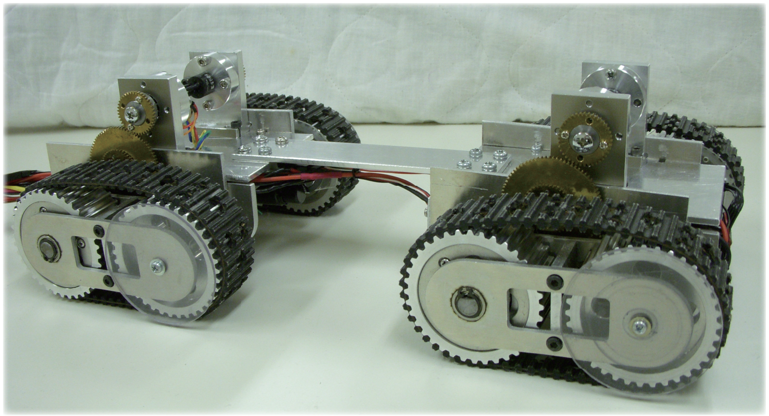

Figure 2.3. Prototype of a dual-crawler-driven robot

The dimension of the robot is shown in Figure 2.4 and its physical parameters that will be used later are listed in Table 2.1.

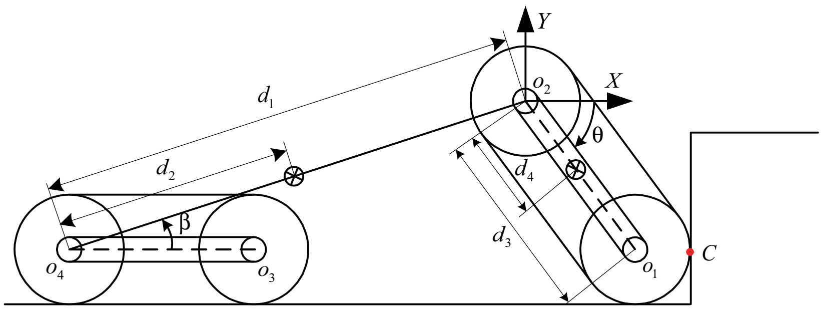

Figure 2.4. Dimensions of the robot with two crawler mechanisms

2.2 Features of the Proposed Crawler Mechanism

The crawler mechanism can switch the power of actuator correspondingly when its encountering terrain changes. This autonomy of the mechanism will be verified through experiments. This under-actuated mechanism may have another virtue of impact-absorption when collisions happen in rough terrain. We will try to model the impact of collision using the method of impact dynamics.

Table 2.1. Physical parameters of the dual-crawler-driven robot

G_1 (1.06 [kg])	Weight of the robot body
G_2 (0.14 [kg])	Weight of the frame
G_3 (0.14 [kg])	Weight of the active pulley
G_4 (0.14 [kg])	Weight of the passive pulley
m_a (0.42 [kg])	Mass of the robot arm
m_b (1.06 [kg])	Mass of the robot body
I_a (4.4e-4 [kg·m^2])	Inertia of the crawler arm
I_b (5.4e-2 [kg·m^2])	Inertia of the body
I_{pul1} (1.2e-6 [kg·m^2])	Inertia of the passive pulley
I_{pul2} (1.2e-6 [kg·m^2])	Inertia of the active pulley
I_{sun} (5.43e-2 [kg·m^2])	Inertia of the sun gear
I_{pla} (5.43e-6 [kg·m^2])	Inertia of the planetary gear
I_{ps} (4.86e-5 [kg·m^2])	Inertia of the planetary gear around the geometry center of the sun gear
I_{ring} (6.34e-4 [kg·m^2])	Inertia of the ring gear
I_{car} ([kg·m^2])	Inertia of the carrier mechanism
d_1 (0.19 [m])	Distance between the driven axles of two crawlers
d_2 (9.5e-2 [m])	Distance between axles of rear active pulley and Center of Mass of the body
d_3 (6.5e-2 [m])	Distance between the axles of the active and passive pulleys
d_4 (3.25e-2 [m])	Distance between the axle of the active pulley and CM of the frame
R (2.9e-2 [m])	Radius of the pulley
K (7.5)	Ratio of the reducer ratios (30 (output 2)/4 (output 1))
i_1 (4)	Ratio of reducer from the motor to the pulley
i_{21} (3)	Ratio of reducer from the motor to the triangle gear reducer
i_{22} (10)	Ratio of the triangle gear reducer
i_2 (30)	Ratio of reducer from the motor to the frame, $i_2 = i_{21} i_{22}$
r_1 (4e-3 [m])	Radius of the sun gear in the planetary gear reducer
r_2 (4e-3 [m])	Radius of the planetary gear in the planetary gear reducer
r_3 (1.2e-2 [m])	Radius of the ring gear in the planetary gear reducer

2.2.1 Autonomy of the Crawler Mechanism

The proposed crawler mechanism has good autonomy making the crawler robot overcome obstacles without any control. A one-crawler robot composed of the crawler mechanism and an assistant leg overcomes a step through the proposed three locomotion modes, as shown in Figure 2.5. Once the motion of the pulley is paused by the step (scene 1), the rotating mode will be activated to negotiate the step through the revolution of the frame (scenes 2, 3, 4 and 5) and consequently go back to the initial state (scene 6).

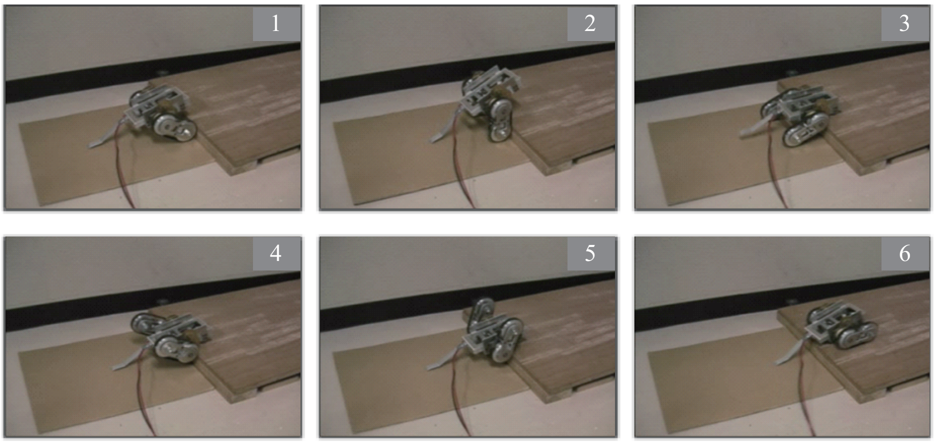

Figure 2.5. A crawler overcoming a step autonomously

A dual-crawler-driven robot constructed via connecting two crawler mechanisms rigidly negotiates a step autonomously, as shown in Figure 2.6. Both the front and rear mechanism units go through the three locomotion modes (moving, rotating, and recovering) and consequently overcome the step successively. Scenes 1, 2 and 3 show the passive climbing process of the front crawler unit while scenes 4, 5 and 6 depict the step-overcoming process of the rear crawler unit.

2.2.2 Impact-absorption Characteristic of the Crawler Mechanism

Due to the fact that collisions exist in the control of robot, researchers tried to find solutions to reduce this bad impact effect to actuators. Collision of a manipulator with its environment is detected by the difference between the actual input torques to the manip-

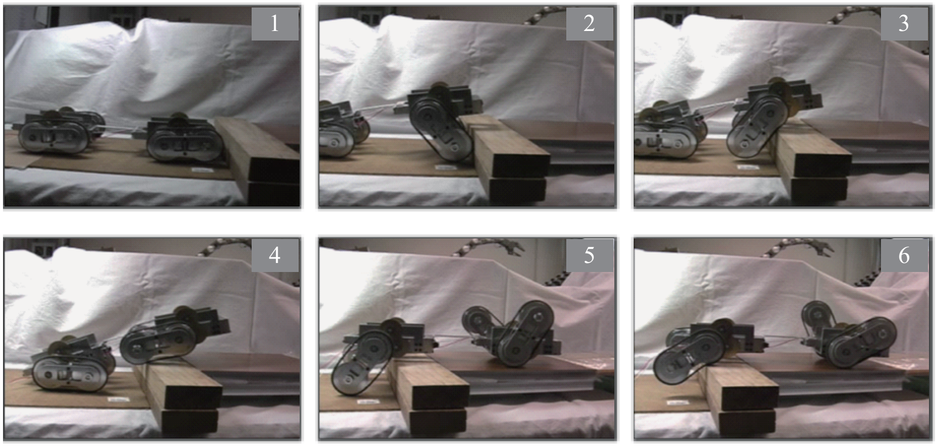

Figure 2.6. A dual-crawler-driven robot overcoming a step autonomously

ulator and the reference input torques calculated based on the manipulator dynamics on the base of nonlinear adaptive control and adaptive impedance control law [68], [69]. The proposed collision detection methods can get the collision event and stop the manipulator or change motion mode, but it inevitably gives an impact on the actuator already. Some researchers study on the specially-designed actuator for robots to absorb the impact energy through the elastic element inside. Compliance is introduced via elastic element between the actuator and the load in Series Elastic Actuator (SEA), which can be electrical, hydraulic, pneumatic, or other traditional servo systems. The elastic element, such as spring, is linked serially between the actuator and the load. Therefore, SEA has low impedance and friction, and thus can achieve high quality force control [70], [71], [72]. Once there is an impact acted on the SEA, the elastic element can absorb the impact energy. Compared with SEA, Differential Elastic Actuator (DEA) links the actuator and the elastic element in a differential form [73]. However, both SEA and DEA eventually decrease dynamic response or reduce the bandwidth of the system because of elastic elements exist between the actuator and the mechanism, and thus increase the order of the system. In our proposed crawler mechanism, two locomotion modes can switch autonomously according to the terrain. While there is a collision transmitted from one output, another output may release part of the impact energy. To find the advantage on this impact effect, impact analysis of the dual-crawler-driven robot is conducted and the simulation results show this advantage comparing with that where each output is individually given by one actuator [74], [75].

This analysis of impact absorption is organized as follows. Subsection (1) compares the difference of impact in two different driving methods: One-Actuator Drive (OAD) and Two-Actuator Drive (TAD). Subsection (2) presents the impact analysis of the external structure of the robot when the dual-crawler-driven robot collides with an obstacle. Subsection (3) gives the numerical results of impact analysis.

(1) Impact Analysis of the Inner Driving Mechanism

When the robot collides with an obstacle in the posture shown in Figure 2.4, impact will transmit from the collision point 'C' to the internal actuators. The actuator of the front unit will suffer from even worse impact compared with the actuator in the rear unit. Therefore the impact analysis of the front unit is our main topic here.

In the front unit of the robot, only one actuator which inputs power from the sun gear of the planetary gear reducer, gives the first output to the pulley via connecting it to the carrier and the second output to the frame via the ring gear, namely One-Actuator Drive (OAD), as shown in Figure 2.7(a).

To drive this kind of track-arm robot, two actuators usually are considered for each mechanism unit. The first actuator is used to drive the track while the second actuator is deployed to realize posture control for the arm, namely Two-Actuator Drive (TAD). For easier comparison, we adopt the same mechanism, as shown in Figure 2.7(b), where input of the first actuator is transmitted to the sun gear of the planetary gear reducer while input of the second actuator is transmitted to the carrier to drive the pulley directly. The output of the frame from the ring gear can be derived indirectly through controlling two actuators cooperatively. When a collision between the robot and an obstacle occurs, the impact acted on the front arm will be transmitted to the carrier and the ring gear, respectively. The impact to actuators in two driving methods could be different due to the fact that the number of the driving actuators is completely different. The impact analysis of each

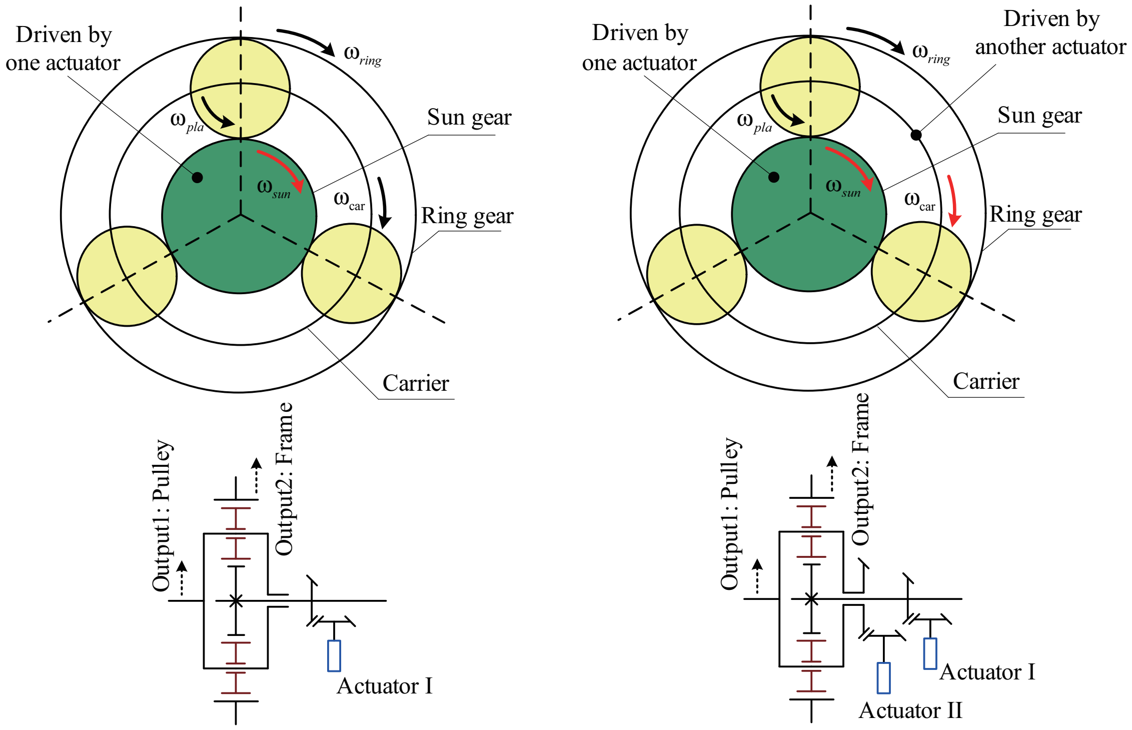

(a) OAD: One-Actuator Drive

(b) TAD: Two-Actuator Drive

Figure 2.7. Different driving methods for the track-arm mechanism

component in the planetary gear reducer will be conducted to figure out what the difference of two different actuating methods is.

Considering the impact to each component, the difference between OAD and TAD is just the different inertia of the carrier mechanism where in TAD, additional actuator is connected to the carrier, compared with that in OAD. The inertia of the carrier mechanism in TAD, which includes the inertia of the actuator and that of the transmission mechanism, should be much larger than that in OAD. In the following impact analysis, the inertia of carrier mechanism I_{car} will be treated as just one variable. However, I_{carI} and I_{carII} will be used to represent two different cases in the numerical calculation.

To get the velocity relation of each component before collision, we presume that the planetary gear reducer works in a general state shown in Figure 2.8. Using the simultaneous center method for the planetary gear, we have

$$2\omega_{pla}r_2 = \omega_{sun}r_1 - \omega_{ring}r_3 \tag{2.1}$$

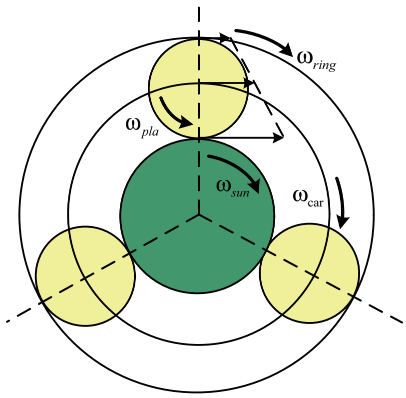

Figure 2.8. A generic working state of a planetary gear reducer

$$\omega_{sun} r_1 + \omega_{ring} r_3 = 2\omega_{car}(r_1 + r_2) \tag{2.2}$$

where ω_{pla}, ω_{sun}, ω_{ring}, ω_{car} are the angular velocities of the planetary gear, the sun gear, the ring gear and the carrier, respectively. Herein, the rotational direction of those components are defined according to the direction of robot movement, and shows in Figure 2.8.

Impact from the collision point 'C' of the robot transmits to the carrier by the moment impulse M_c and the ring gear by moment impulse M_{ring} via the outputs of the mechanism, the active pulley and the connecting frame. Here, we make an assumption that the velocities of the planetary gear, the sun gear, the ring gear and the carrier after collision are Ω_{pla}, Ω_{sun}, Ω_{ring} and Ω_{car}, respectively. From the conservation of angular momentum of the ring gear, the impact to the ring gear illustrated in Figure 2.9(a), causes the ring gear to change the angular velocity from velocity ω_{ring} to velocity Ω_{ring}, which is given by

$$M_{ring} - 3P_{rp1} r_3 = I_{ring}(\Omega_{ring} - \omega_{ring}) \tag{2.3}$$

where P_{rp1} is the reaction impulse from only one planetary gear, M_{ring} is the moment impulse transmitted to the ring gear.

The planetary gear rotates around its geometric center, and also revolves around the geometry center of the sun gear. Impact that comes from the ring gear, the sun gear and the carrier makes the planetary gear change the rotational velocities around the geometric axis of the sun gear and its own axis, as shown in Figure 2.9(b). Thus, the changes of the

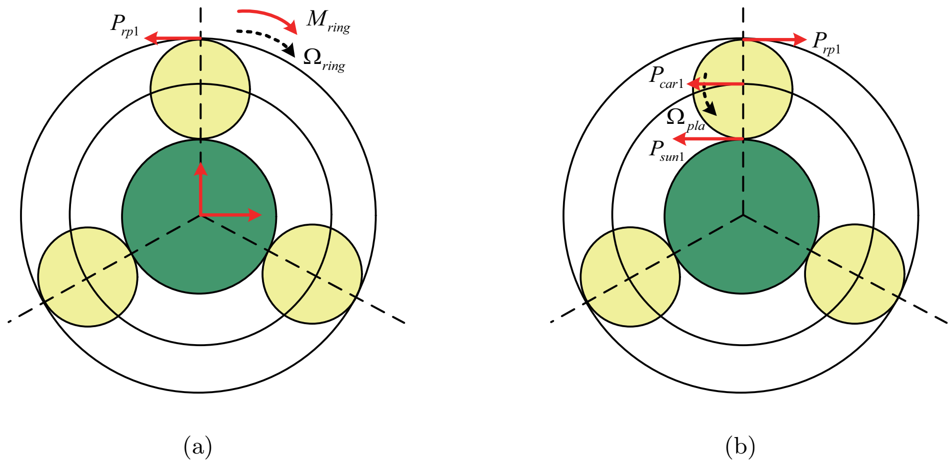

Figure 2.9. Impact of the ring gear and the planetary gear

rotational velocities can be described by

$$-P_{sun1}r_2 - P_{rp1}r_2 = I_{pla}(\Omega_{pla} - \omega_{pla}) \tag{2.4}$$

$$P_{rp1}r_3 - P_{sun1}r_1 - P_{car1}(r_1 + r_2) = I_{ps}(\Omega_{car} - \omega_{car}) \tag{2.5}$$

where P_{sun1} and P_{car1} are the reaction impulses from the sun gear and the carrier. I_{pla} is the inertia of the planetary gear around its center of mass; I_{ps} is the inertia of the planetary gear around the geometric center of the sun gear.

The impact of the carrier and the sun gear is shown in Figure 2.10. From the angular momentum conservation of the carrier, the velocity change of the carrier from ω_{car} to Ω_{car} is given by

$$M_c + 3P_{car1}(r_1 + r_2) = I_{car}(\Omega_{car} - \omega_{car}) \tag{2.6}$$

The impact of the sun gear which transfers from the planetary gear results in an effect that causes the sun gear to change the velocity from ω_{sun} to Ω_{sun}. According to the angular momentum conservation of the sun gear, this velocity change can be given by

$$3P_{sun1}r_1 = I_{sun}(\Omega_{sun} - \omega_{sun}) \tag{2.7}$$

Same as the the velocity relationship among the ring gear, the planetary gear and the sun gear before collision (Equations (2.1) and (2.2)), their velocity relationship after collision

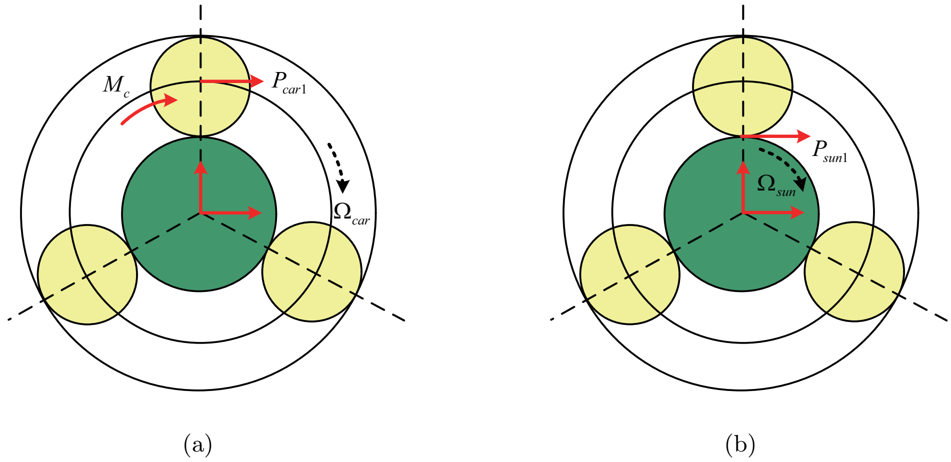

Figure 2.10. Impact of the carrier and the sun gear

is given by

$$2\Omega_{pla} r_2 = \Omega_{sun} r_1 - \Omega_{ring} r_3 \tag{2.8}$$

$$\Omega_{sun} r_1 + \Omega_{ring} r_3 = 2\Omega_{car}(r_1 + r_2) \tag{2.9}$$

Summarizing the equations above, we have an equation in matrix form, given by

$$\mathbf{Ax} = \mathbf{y} \tag{2.10}$$

where $\mathbf{x}(\begin{bmatrix} P_{rp1} & P_{sun1} & P_{car1} & \Omega_{sun} & \Omega_{ring} & \Omega_{pla} & \Omega_{car} \end{bmatrix}^T)$ describes the impulses and velocities after collision,

$$\mathbf{A} = \begin{bmatrix} 3r_3 & 0 & 0 & 0 & I_{ring} & 0 & 0 \\ r_2 & r_2 & 0 & 0 & 0 & I_{pla} & 0 \\ r_3 & -r_1 & -r_4 & 0 & 0 & 0 & -I_{ps} \\ 0 & 3r_1 & 0 & -I_{sun} & 0 & 0 & 0 \\ 0 & 0 & 3r_4 & 0 & 0 & 0 & -I_{car} \\ 0 & 0 & 0 & r_1 & -r_3 & -2r_2 & 0 \\ 0 & 0 & 0 & r_1 & r_3 & 0 & -2r_4 \end{bmatrix}$$

describes the structure parameters of the planetary gear reducer, also $r_4 = r_1 + r_2$. Herein,

$$\mathbf{y} = \begin{bmatrix} I_{ring}\omega_{ring} + M_{ring} \\ I_{pla}\omega_{pla} \\ -I_{ps}\omega_{car} \\ -I_{sun}\omega_{sun} \\ -M_c - I_{car}\omega_{car} \\ 0 \\ 0 \end{bmatrix}$$

Since three planetary gears are deployed in the planetary gear reducer, the total momentum impulses on the sun gear M_{sun}, the carrier M_{car} are derived by

$$M_{sun} = 3P_{sun1}r_1 \tag{2.11}$$

$$M_{car} = 3P_{car1}r_4 + M_c \tag{2.12}$$

The momentum impulses due to impact acted on actuators can thus be obtained while knowing the impact from the carrier (M_c) and the ring gear (M_{ring}).

(2) Impact Analysis of the Outer Robot Structure

In unstructured environments, it is inevitable for the robot to collide with obstacles. The collision will cause bad effect to the driving actuator, which may lead the actuator broken. The actuator of the front arm especially is subject to this impact. The dual-crawler-driven robot can be separated into three components: the front arm, the robot body and the rear arm. When collision occurs, the impact transfers from the collision point to the front arm, the robot body and then the rear arm. The impact analysis of the whole robot is conducted in the term that gravity of the robot and the effect from the horizontal surface are neglected due to the fact that values of friction and gravity are small enough, compared with the impulse of impact effect.

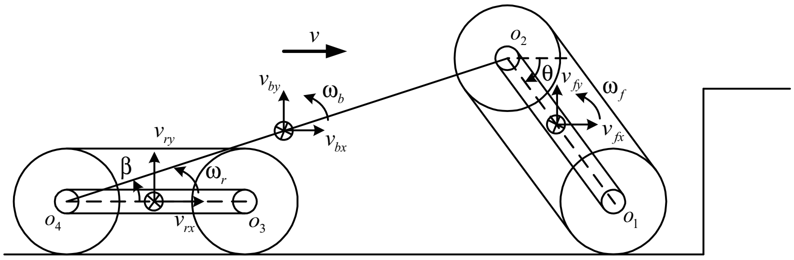

Figure 2.11. Initial state of the robot before collision

From Figure 2.11, we have the relationship between the incline angle of robot body β and that of front arm θ, given by

$$\beta = \arcsin(-d_3 \sin\theta / d_1) \tag{2.13}$$

When the robot moves forwards in velocity v while keeping a posture, the linear and the angular velocities of CM (Center of Mass) of each component are given by

$$v_{fx} = v, \quad v_{fy} = 0, \quad \omega_f = 0 \tag{2.14}$$

$$v_{bx} = v, \quad v_{by} = 0, \quad \omega_b = 0 \tag{2.15}$$

$$v_{rx} = v, \quad v_{ry} = 0, \quad \omega_r = 0 \tag{2.16}$$

where v_{fx}, v_{bx}, v_{rx} are the linear velocities of the front arm, the body, the rear arm in x direction before collision; v_{fy}, v_{by}, v_{ry} are their linear velocities in y direction before collision; ω_f, ω_b, ω_r are their angular velocities before collision, respectively.

From Equations (2.1) and (2.2), the velocities of each component of the planetary gear reducer before collision can be derived as

$$\omega_{sun} = \frac{2v(r_1 + r_2)}{Rr_1}, \quad \omega_{car} = v/R \tag{2.17}$$

$$\omega_{pla} = \frac{v(r_1 + r_2)}{Rr_2}, \quad \omega_{ring} = 0 \tag{2.18}$$

At the collision point 'C', collision causes the velocity of CM of the front arm in x direction to change from v_{fx} to V_{fx}, the velocity of CM of the front arm in y direction to change from v_{fy} to V_{fy}, and the angular velocity of the front arm to change from ω_f to Ω_f.

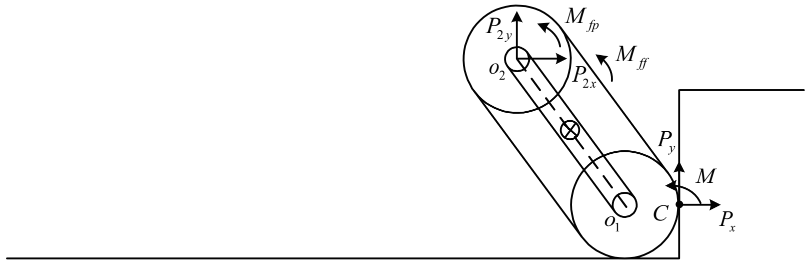

Figure 2.12. Impact of the front arm

Thus, the velocity of the front arm in x direction at the collision point 'C' changes from $v_{fx} - \omega_f l_1$ to $V_{fx} - \Omega_f l_1$ while velocity in y direction at this collision point changes from $v_{fy} + \omega_f l_2$ to $V_{fy} + \Omega_f l_2$. They are given by

$$V_{fx} - \Omega_f l_1 = -e_x(v_{fx} - \omega_f l_1) \tag{2.19}$$

$$V_{fy} + \Omega_f l_2 = -e_y(v_{fy} + \omega_f l_2) \tag{2.20}$$

$$e_m M = (1 + e_m) I_a \Omega_f \tag{2.21}$$

where e_x is the kinetic coefficient of restitution in normal collision direction (x) [76], $0 \leq e_x \leq 1$, which describes the relation of velocity changes between collision states before collision and after collision. $e_x = 0$, the largest possible amount of energy is lost because of the impact; for the perfect elastic case, $e_x = 1$, the rebound is a mirror image of the approach. Similar to e_x, e_y is the kinetic coefficient of restitution in tangential collision direction (y). e_m is the moment coefficient to describe the change of rotational velocities, and M is the moment impulse. Herein, $l_1 = (d_3 - d_4)\sin\theta$ and $l_2 = (d_3 - d_4)\cos\theta + R$. The most general way to account for the tangential effect is simply to define the impulse ratio μ as

$$P_y = \mu P_x \tag{2.22}$$

where P_x and P_y are the impulses from the obstacle at the collision point 'C' in x and y directions, respectively.

For the front arm shown in Figure 2.12, conservation of the linear momentum and the angular momentum is described by

$$P_x + P_{2x} = m_a(V_{fx} - v_{fx}) \tag{2.23}$$

$$P_y + P_{2y} = m_a(V_{fy} - v_{fy}) \tag{2.24}$$

$$P_y l_2 - P_x l_1 + P_{2x} l_3 - P_{2y} l_4 + M + M_{ff} + M_{fp} = I_a(\Omega_f - \omega_f) \tag{2.25}$$

where P_{2x} and P_{2y} are the reaction impulses from the robot body in x and y direction, M_{fp} and M_{ff} are the reaction moment impulses of the front arm from the pulley and the frame, respectively. Herein, $l_3 = d_3 \sin\theta$ and $l_4 = d_3 \cos\theta$.

The impact of the front passive and active pulleys is shown in Figure 2.13. The impact P_y causes the passive and active pulleys to change the rotational velocity around their own geometry center.

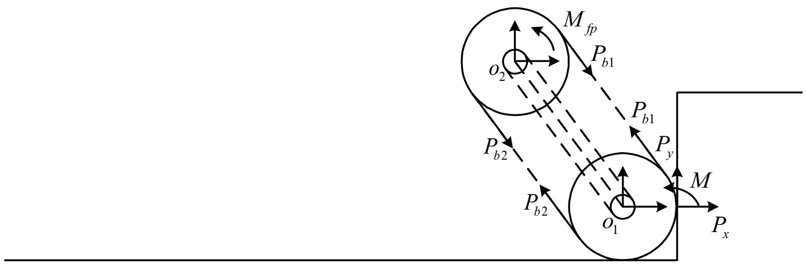

Figure 2.13. Impact of the front active and passive pulleys

Since the active pulley is connected to the output of the carrier, the passive and active pulleys keep the same rotational velocity around their geometry center as the angular velocity of the carrier. The impact effects on the passive and active pulleys can be derived by

$$-P_y R + (P_{b2} - P_{b1})R = I_{pul1}(\Omega_{car} - \omega_{car}) \tag{2.26}$$

$$-M_{fp} + (P_{b1} - P_{b2})R = I_{pul2}(\Omega_{car} - \omega_{car}) \tag{2.27}$$

where I_{pul1} and I_{pul2} are the inertia of the passive and active pulleys around their geometry center, P_{b1} and P_{b2} are the impulses of the driving belt on two sides, respectively.

From Equations (2.26) and (2.27), the moment impulse M_{fp} can be given by

$$M_{fp} = -P_y R - (I_{pul1} + I_{pul2})(\Omega_{car} - \omega_{car}) \tag{2.28}$$

The collision state of the robot body is shown in Figure 2.14. Conservation of the linear

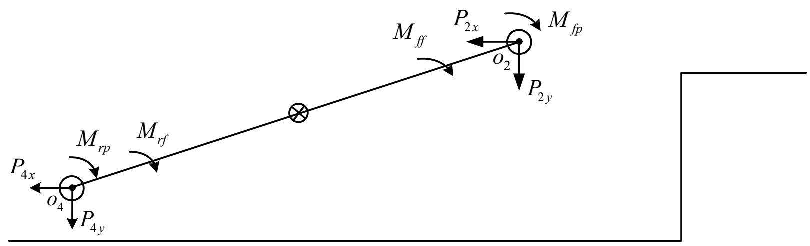

Figure 2.14. Impact of the robot body

momentum and the angular momentum is indicated by

$$-P_{4x} - P_{2x} = m_b(V_{bx} - v_{bx}) \tag{2.29}$$

$$-P_{4y} - P_{2y} = m_b(V_{by} - v_{by}) \tag{2.30}$$

$$-P_{2y}l_6 + P_{2x}l_5 + P_{4y}l_8 - P_{4x}l_7 - M_{rp} - M_{rf} - M_{fp} - M_{ff} = I_b(\Omega_b - \omega_b) \tag{2.31}$$

where P_{4x} and P_{4y} are the reaction impulses between the rear arm and the body in x and y directions, M_{rp} and M_{rf} are the reaction moment impulses of the rear arm from pulley and frame, respectively. V_{bx} and V_{by} are the velocities of CM of the robot body in x and y direction after collision, Ω_b is the angular velocity of CM of the robot body after collision. Herein, $l_5 = (d_1 - d_2)\sin\beta$, $l_6 = (d_1 - d_2)\cos\beta$, $l_7 = d_2 \sin\beta$, and $l_8 = d_2\cos\beta$.

Figure 2.15. Impact of the rear arm

For the rear arm shown in Figure 2.15, conservation of the linear momentum and the angular momentum is given by

$$P_{4x} = m_a(V_{rx} - v_{rx}) \tag{2.32}$$

$$P_{4y} = m_a(V_{ry} - v_{ry}) \tag{2.33}$$

$$M_{rp} + M_{rf} - P_{4y}d_4 = I_a(\Omega_r - \omega_r) \tag{2.34}$$

where V_{rx} and V_{ry} are the velocities of CM of the rear arm in x and y direction after collision, and Ω_r is its angular velocity of CM of the rear arm after collision, respectively.

At the joints o_2 and o_4, the velocity constraint in x and y directions at the pinned connection gives the following four equations,

$$V_{bx} - \Omega_b(d_1 - d_2)\sin\beta = V_{fx} + \Omega_f d_4 \sin\theta \tag{2.35}$$

$$V_{by} + \Omega_b(d_1 - d_2)\cos\beta = V_{fy} - \Omega_f d_4 \cos\theta \tag{2.36}$$

$$V_{bx} + \Omega_b d_2 \sin\beta = V_{rx} \tag{2.37}$$

$$V_{by} - \Omega_b d_2 \cos\beta = V_{ry} - \Omega_r d_4 \tag{2.38}$$

The impulse transmitted to the ring gear and the carrier of the front unit from the external impact can be derived by

$$M_{ring} = -M_{ff}/i_{22} \tag{2.39}$$

$$M_c = M_{fp} \tag{2.40}$$

where i_{22} is the reducer ratio from the ring gear to the frame.

From the above analysis, we know that the coefficients e_x, e_y and e_m are employed to describe the features of different collision conditions. From the analysis in impact of the planetary gear reducer, once the impulses to the ring gear (M_{ring}) and the carrier (M_c) are obtained, the impact to the driving actuators can be derived by Equation (2.10). To compare the impact effects to actuators in two driving methods, we execute numerical simulations in the next section.

(3) Numerical Calculation of the Impact Effect

The robot moves forwards initially in the velocity of 0.15 m/s. While the collision between the robot and an obstacle occurs, the velocity of the front arm, the body, the rear arm and each component of the planetary gear reducer before collision can be derived by Equations (2.14)–(2.18), that are listed in Table 2.2.

Table 2.2. Initial state of the robot and collision terms

v_{fx}	[m/s]	0.15	v_{by}	[m/s]	0	ω_r	[rad/s]	0	e_x		0.5
v_{fy}	[m/s]	0	ω_b	[rad/s]	0	ω_{sun}	[rad/s]	20.6897	e_y		0.1
ω_f	[rad/s]	0	v_{rx}	[m/s]	0.15	ω_{pla}	[rad/s]	10.3448	e_m		0.8
v_{bx}	[m/s]	0.15	v_{ry}	[m/s]	0	ω_{car}	[rad/s]	5.1724	μ		0.01

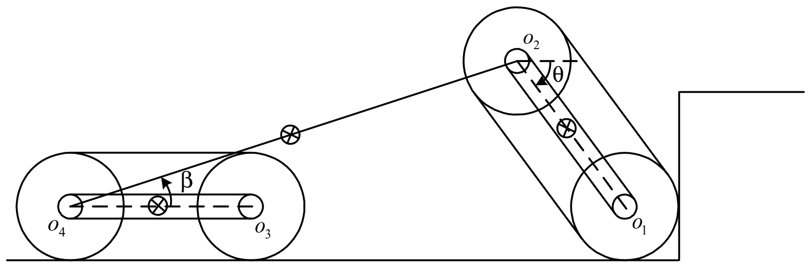

Figure 2.16. A robot posture ($-90° < \theta < 0°$)

When θ is in the range $(-90°, 0°)$, the incline angle of the robot body, β, is larger than $0°$, as shown in Figure 2.16; however, when θ is in the range $(0°, 90°)$, the incline angle of the robot body β is $0°$, as shown in Figure 2.17.

Consider the two different driving methods: OAD (One-Actuator Drive) is the case that just one actuator inputs to the sun gear and gives two outputs; TAD (Two-Actuator Drive) is the case that one actuator connects to the sun gear which is the same as that in OAD while another actuator inputs to the carrier. The actuator connected to the carrier drives the pulley and it cooperates with the actuator connected to the sun gear to drive the frame indirectly. For impact analysis, the difference of two cases is that the inertia of

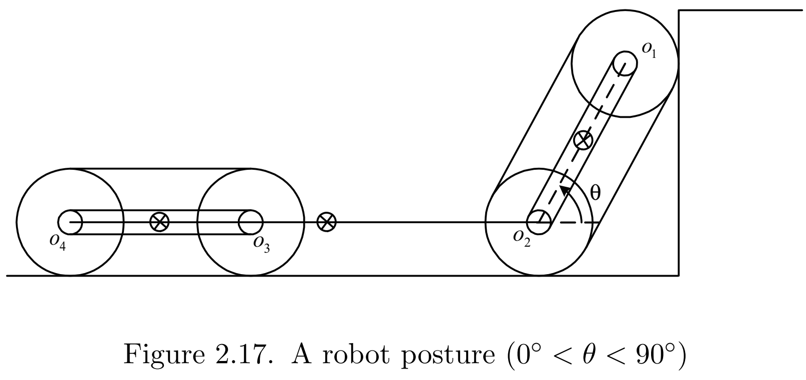

Figure 2.17. A robot posture ($0° < \theta < 90°$)

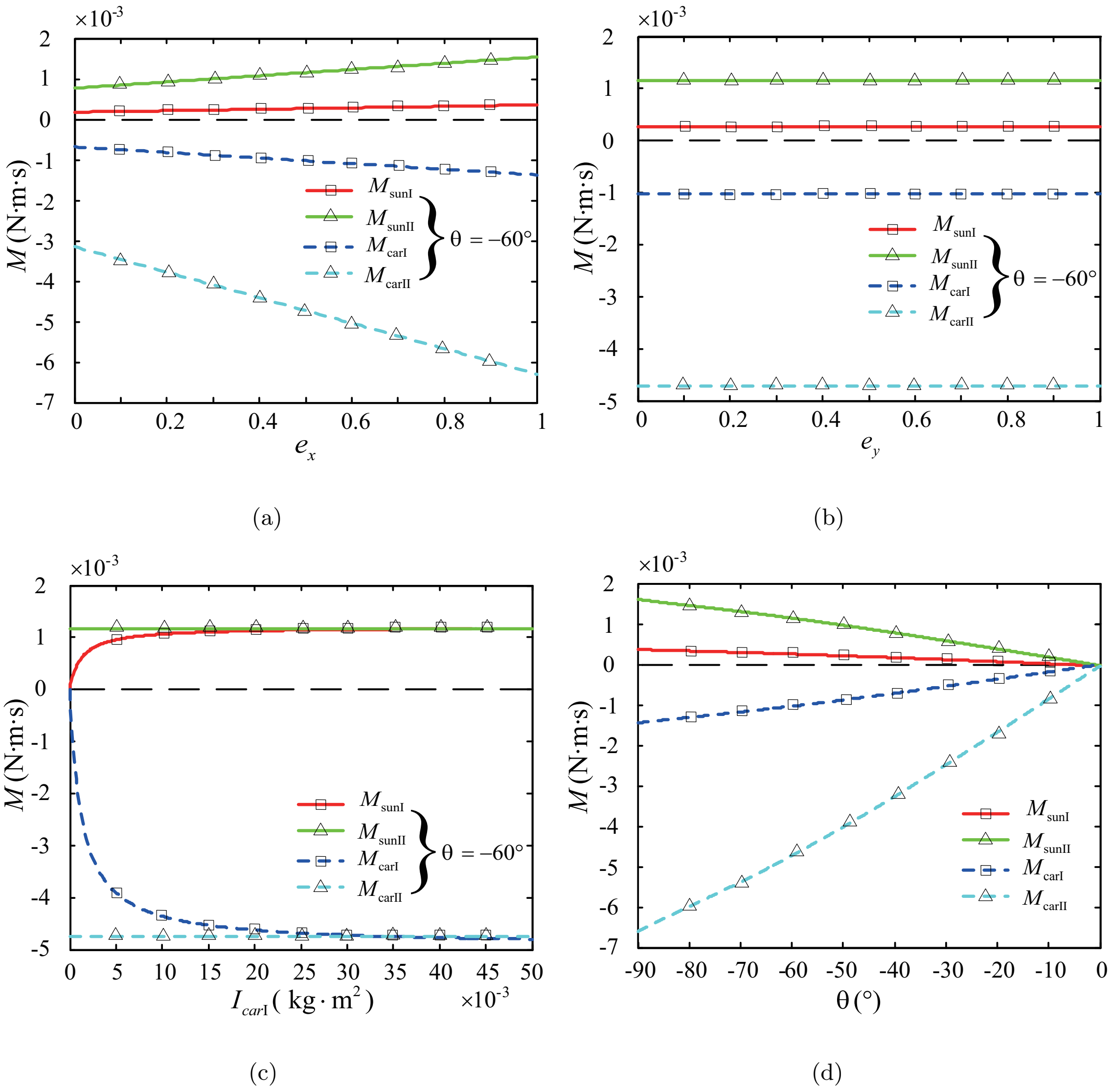

Figure 2.18. Numerical results for posture $(-90^\circ < \theta < 0^\circ)$

carrier mechanism (I_{car}) is different. I_{carII} in TAD is larger than that I_{carI} in OAD since the actuator connected to the carrier increases the inertia. Here, we use I_{carI}=3.5e-5 kg·m^2 for OAD and I_{carII}=3.5e-2 kg·m^2 for TAD.

When the robot moves in the posture $(-90^\circ < \theta < 0^\circ)$ as shown in Figure 2.16, the numerical results of impact to actuators are shown in Figure 2.18. When θ is -60°, the impulse to the sun gear M_{sunI} (acting on the driving actuator) and the carrier M_{carI} (no action on the actuator, just for reference) in OAD is much smaller than the impulse to the sun gear M_{sunII} (acting on the first actuator) and the carrier M_{carII} (acting on the second actuator) in TAD with the coefficient of restitution e_x in x direction varying from 0 to 1, as shown in Figure 2.18(a). Also, the impulses M_{sunI} and M_{carI} are smaller than M_{sunII} and M_{carII}, however, the values always keep constant while e_y varying from 0 to 1, as shown in Figure 2.18(b). When I_{carI} increases gradually, M_{sunI} and M_{carI} are approaching M_{sunII} and M_{carII}, as shown in Figure 2.18(c). When I_{carI} is equal to I_{carII}, the performances of impact absorption are completely the same.

As shown in Figure 2.18(d), when θ varies from $-90°$ to $0°$, M_{sunI} and M_{carI} are smaller than M_{sunII} and M_{carII} all the time. Also the impact near $\theta = -90°$ is larger than that at $\theta = 0°$.

When the robot moves in the posture ($0° < \theta < 90°$) shown in Figure 2.17, the numerical results are given in Figure 2.19. The results are very similar to that shown in Figure 2.18. The difference is that the collision causes the impact to actuators in opposite direction.

When the robot keeps the front arm lifted at the angle of 60°, the numerical results of impact effect for two driving methods are listed in Table 2.3. The angular velocities after collision and the impact of each component of the planetary gear reducer are also illustrated in the table.

Table 2.3. Comparison of the impact effect of two driving methods, OAD and TAD ($\theta = 60°$)

Impact Effect	OAD: One-Actuator (I)	TAD: Two-Actuator (II)
Ω_{sun} [rad/s]	20.6846	20.6677
Ω_{ring} [rad/s]	4.0638	0.1926
Ω_{pla} [rad/s]	4.2466	10.0450
Ω_{car} [rad/s]	8.2190	5.3114
$\Omega_{sun} - \omega_{sun}$ [rad/s]	-0.0051	-0.0219
$\Omega_{ring} - \omega_{ring}$ [rad/s]	4.0638	0.1926
$\Omega_{pla} - \omega_{pla}$ [rad/s]	-6.0982	-0.2999
$\Omega_{car} - \omega_{car}$ [rad/s]	3.0466	0.1390
M_{sun} [kg·m^2/s]	-2.8e-4	-1.2e-3
M_{car} [kg·m^2/s]	1.1e-3	4.9e-3

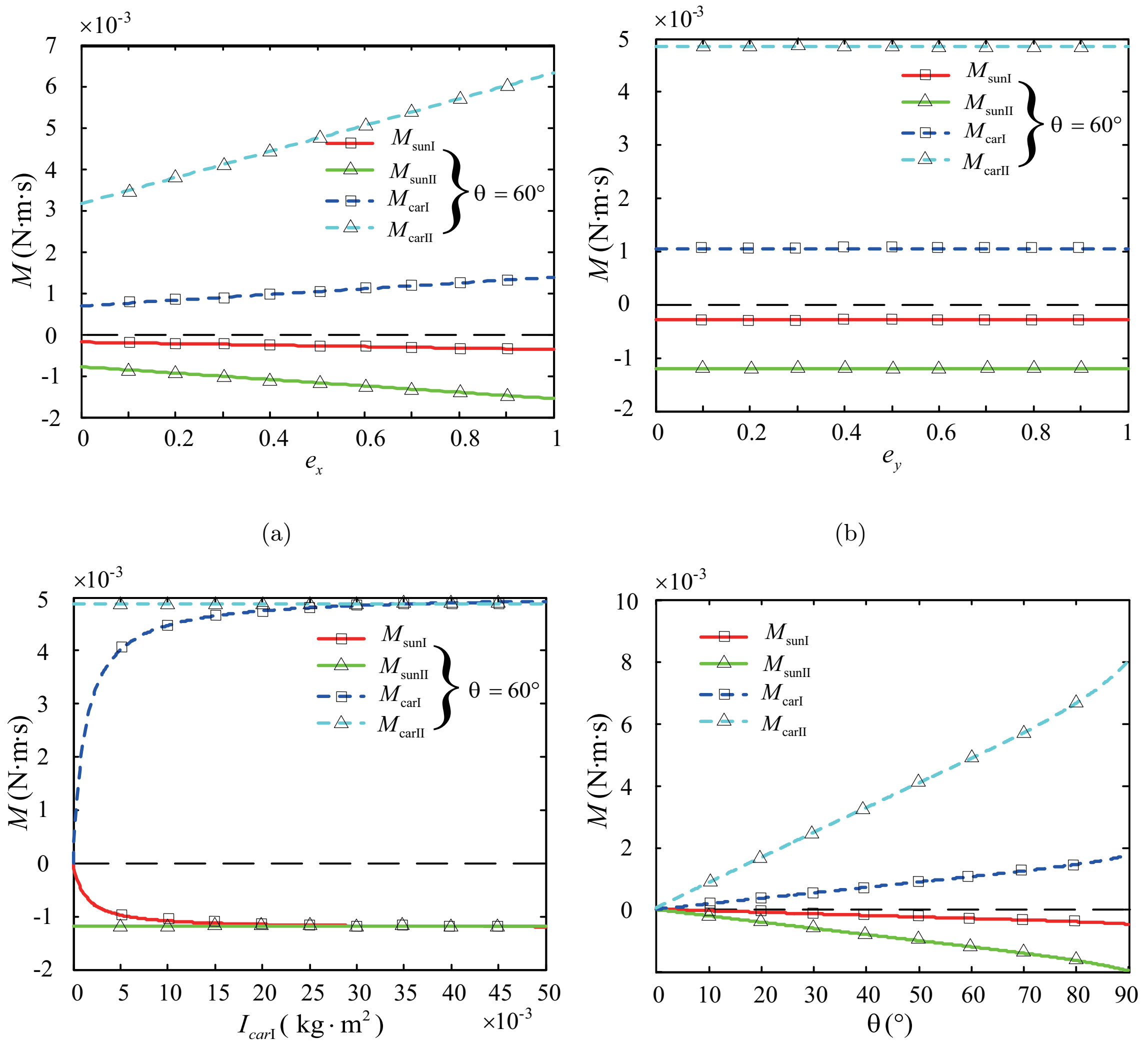

(a) (b) (c) (d)

Figure 2.19. Numerical results for posture ($0^\circ < \theta < 90^\circ$)

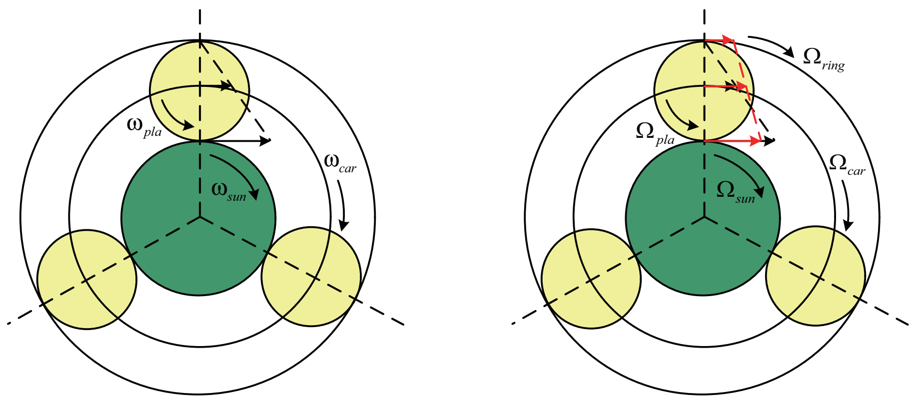

(a) Before collision (b) After collision

Figure 2.20. State change of the planetary gear reducer

From the above-mentioned results, we know that the resulted impact to actuators in OAD is smaller than that in TAD and our mechanism is advanced in impact absorption.

Lastly, we discuss the state changes of the internal planetary gear reducer since it is extremely important transmission components in this crawler-driven robot. As shown in Figure 2.20, before the collision occurs, the planetary gear reducer works in the state shown in Figure 2.20(a). The arm keeps the posture to move forwards, the output of the ring gear is zero. After collision, two impulses are transmitted to the planetary gear reducer since it gives two outputs for driving the pulley and the frame, as shown in Figure 2.20(b). For two different driving methods, since the inertia of the carrier mechanism in TAD is much larger than that in OAD, the angular velocity change of the carrier mechanism $\Omega_{carII} - \omega_{carII}$ is much smaller than $\Omega_{carI} - \omega_{carI}$. Due to this fact, the planetary gear in OAD gets a larger velocity change $\Omega_{plaI} - \omega_{plaI}$ than $\Omega_{plaII} - \omega_{plaII}$ in TAD, while a smaller velocity change of the sun gear is consequently resulted in OAD than that in TAD. As a result, we find that the resulted impact in OAD is smaller than that in TAD because the planetary gear absorbs more impact energy through larger change of its velocity.

To show the advantage of this mechanism for impact absorption, we have performed the impact analysis of the robot while the robot collides with an obstacle. Comparing the impact effect of two different driving systems (OAD and TAD), the impact to the actuator in OAD is much smaller than that in TAD. It is because that the second actuator in TAD increases the inertia of the carrier mechanism so as to limit the movement of the planetary gear. In other word, the planetary gear absorbs more impact energy in OAD than that in TAD. As a result, we know that the inertia of the carrier can be designed properly to reduce the impact effect to the actuator in OAD, and the advantage of our mechanism for impact absorption is thus clear.

2.3 Summary

In this chapter, we proposed a crawler mechanism in which a planetary gear reducer was adopted as the main transmission component to provide two outputs using only one actuator. The crawler mechanism has three locomotion modes and the switching between locomotion modes can be employed to adapt to irregular terrain autonomously. Another big advantage is that the redundant-driven mechanism can absorb the impact energy caused by the inevitable collision between the crawler and the working environment.

Chapter 3

Two-dimensional Posture Analysis of the Dual-crawler-driven Robot

There is only one actuator in our crawler mechanism. However, this actuator provides two different kinds of outputs to drive the track pulley and rotation frame, respectively. Apparently, this crawler mechanism belongs to the under-actuated system. This under-actuated factor probably influences on the realizable postures of the crawler robot. In order to figure out what kind of configurations of the robot can be achieved, the posture analysis of the robot in two-dimensional environment will be conducted through quasi-static method.

The dual-crawler-driven robot is considered as the research object. Generally speaking, this kind of tracked robot is usually driven by four actuators: two for the front and rear tracks; another two for the front and rear frames, as shown in Figure 3.1(a). If the ground can provide enough friction conditions, the controllable range of the fully-driven tracked robot should be the whole rectangular area where both θ_f and θ_r vary from 0° to 360°. However, due to the under-actuated factor in our proposed crawler tracked robot, two actuators are employed to drive the front and rear units. In each mechanism unit, only one actuator is used to drive the track and rotation frame concurrently. Compared with the traditional fully-driven tracked robot, our proposed dual-crawler-driven robot may perform

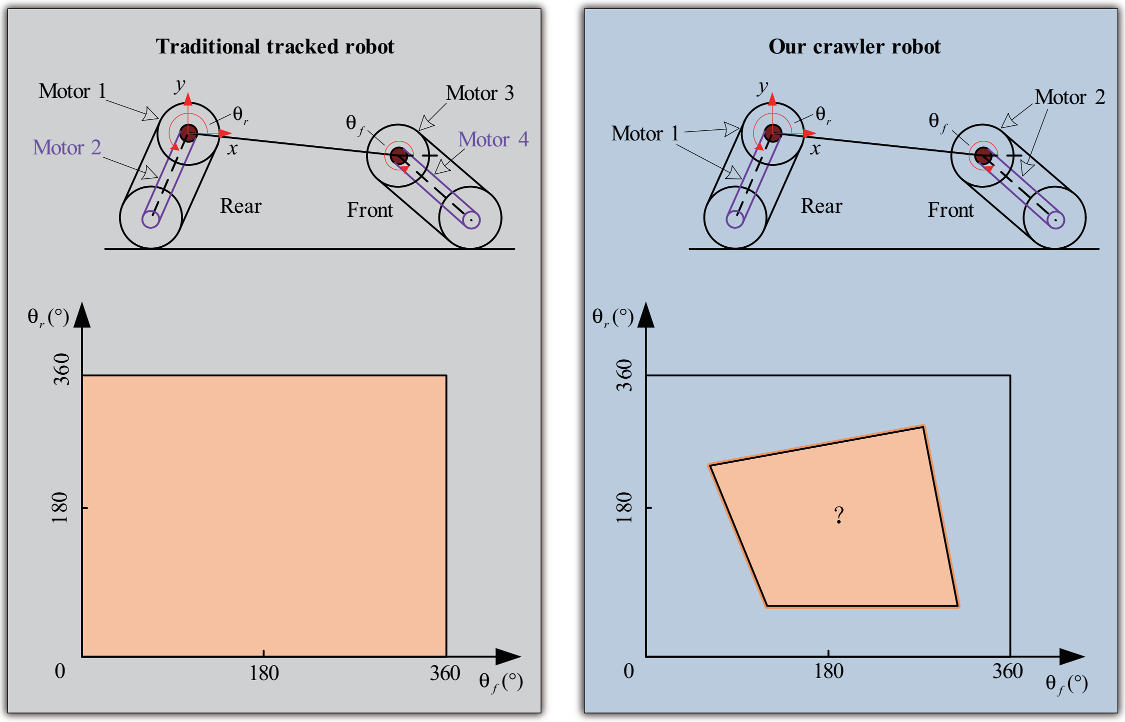

(a) Traditional fully-driven tracked robot (b) Our proposed under-actuated tracked robot

Figure 3.1. Comparison between the traditional tracked robot and our crawler robot

less realizable postures, for example, the whole rectangular area decreases to a relatively small area, as shown in Figure 3.1(b).

To answer the aforementioned question, we try to figure out the controllable postures for all the configuration of the dual-crawler-driven robot.

3.1 All Possible Configurations of the Crawler Robot

A tracked robot that is realized by connecting two units of the crawler mechanism through a vehicle body is shown in Chapter 2. This robot can not only switch autonomously between different locomotion modes adapting to the terrain, but also generate several postures through controlling the two actuators cooperatively. Figure 3.2 shows the corresponding dimensions of the robot, which can be used to describe different configurations.

The dual-crawler-driven robot consists of the rear crawler unit, the robot body, and the

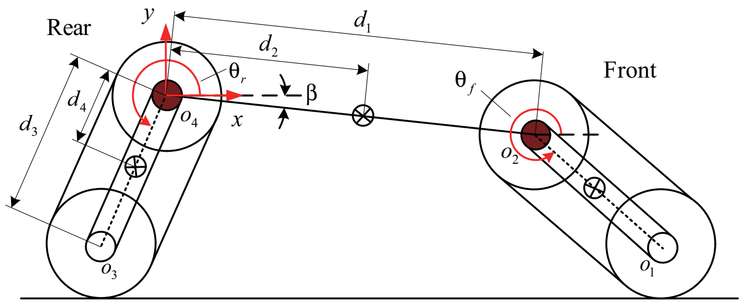

Figure 3.2. Dimensions of the dual-crawler-driven robot

front crawler unit. The action that the front unit and the rear unit keep at different positions, can produce different configurations. Thus, there are several geometrically possible postures for this dual-crawler-driven robot [77], [78].

In order to define the configurations of this robot in a two-dimensional environment, an orthogonal coordinate system (xo_4y) is established at the center of the rear active pulley, as shown in Figure 3.2. The x axis is parallel to the ground surface while the y axis is normal to the ground. The rear angle θ_r is the angle that the rear crawler unit rotates from the x axis to the connecting frame of the rear unit; the front angle θ_f is the angle that the front crawler unit rotates from x axis to the connecting frame of the front unit.

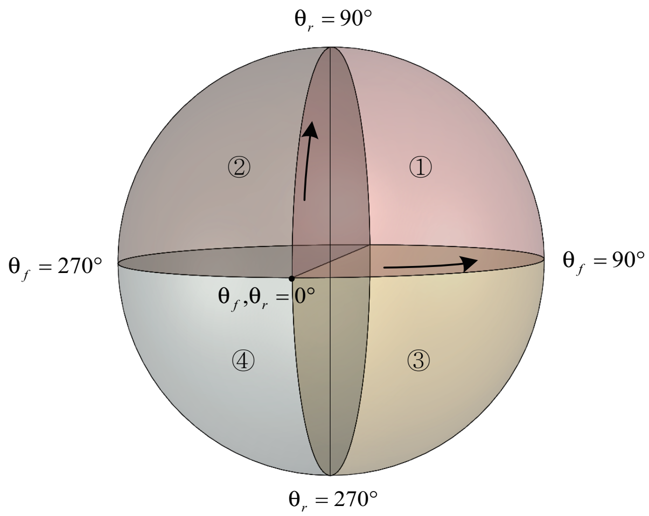

Figure 3.3. Regions of all the configurations of a dual-crawler-driven robot represented by the latitude and longitude of a sphere

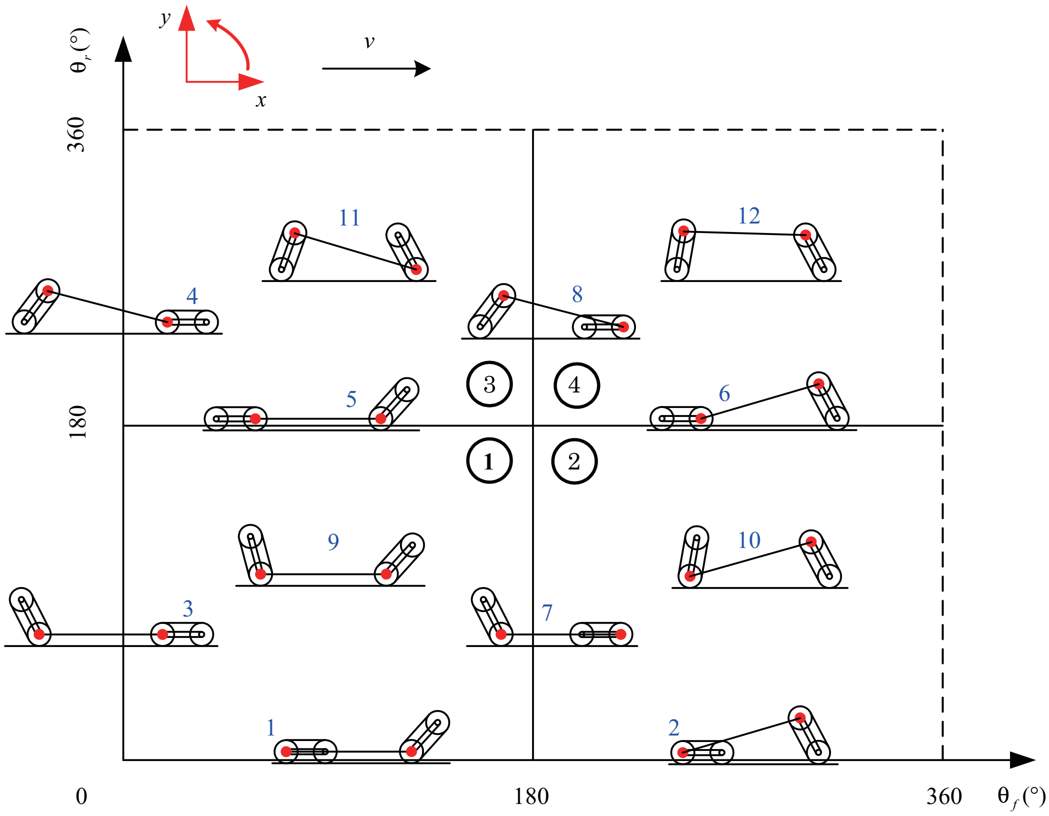

Figure 3.4. All geometrical configurations of the robot

As shown in Figure 3.3, θ_f and θ_r are selected as the latitude and longitude respectively, so that the point on the surface of the sphere can represent the corresponding configuration.

Figure 3.3 shows a sphere to represent the region of all configurations of the robot, where each corresponding configuration is on the surface of the sphere. For conveniently viewing, Figure 3.4 shows all the configurations in an unfolded plane, where different combinations of the front angle θ_f and the rear angle θ_r stand for the relevant geometric possible postures. In total, there are 12 possible typical configurations when both the front angle θ_f and the rear angle θ_r vary from $0°$ to $360°$.

In the coordinate system (xo_4y) of Figure 3.2, the coordinates of the center of the rear passive pulley o_3, the center of the front active pulley o_2, the center of the front passive pulley o_1 can be expressed as

$$
\begin{aligned}
x_{o_3} &= d_3 \cos\theta_r, & y_{o_3} &= d_3 \sin\theta_r \\
x_{o_2} &= d_1 \cos\beta, & y_{o_2} &= d_1 \sin\beta \\
x_{o_1} &= d_1 \cos\beta + d_3 \cos\theta_f, & y_{o_1} &= d_1 \sin\beta + d_3 \sin\theta_f
\end{aligned}
\tag{3.1}
$$

1) For the configurations in the *Region* ①, the incline angle of the robot body β is always kept at $0°$.

2) For the configurations in the *Region* ②, the rear active pulley maintains full contact with ground surface while the front crawler unit is lifted up. Since the centers of o_1 and o_4 have the same y coordinate element, the incline angle β can thus be described by

$$\beta = \arcsin(-d_3 \sin\theta_f / d_1) \tag{3.2}$$

3) For the configurations in the *Region* ③, the front active pulley always stays in contact with ground surface while the rear crawler unit is lifted up. The fact that centers of o_2 and o_3 have the same y coordinate element makes the incline angle β given by

$$\beta = \arcsin(d_3 \sin\theta_r / d_1) \tag{3.3}$$

4) For the configurations in the *Region* ④, both the front crawler unit and the rear crawler unit are lifted up. Because of the fact that centers of o_1 and o_3 have the same y coordinate element, the incline angle β can be described by

$$\beta = \arcsin((d_3 \sin\theta_r - d_3 \sin\theta_f)/d_1) \tag{3.4}$$

Table 3.1 summarizes the angle of incline of the robot body β for each different case of configurations.

From the above analysis, we can obviously know that the robot can realize several possible configurations. For executing some tasks in rough terrain, the posture of robot body is desired to change according to the task. For example, if a manipulator is mounted on the robot body, as the base of the manipulator, the robot body can help the end-effector to perform the desired tasks. Thus, all the controllable postures should be found to support the posture control of the robot.

Table 3.1. Incline angle β of robot body for each region of configurations

θ_r \ θ_f	[0°,180°]	[180°,360°]
[0°,180°]	$\beta = 0$	$\beta = \arcsin\frac{-d_3 \sin\theta_f}{d_1}$
[180°,360°]	$\beta = \arcsin\frac{d_3 \sin\theta_r}{d_1}$	$\beta = \arcsin\frac{d_3 \sin\theta_r - d_3 \sin\theta_f}{d_1}$

3.2 Quasi-static Analysis of All Configurations of the Robot

From the geometrical analysis of the dual-crawler-driven robot stated in the prior section, it is known that this robot could generate several configurations through cooperatively controlling the two actuators. However, this tracked robot, which makes use of two actuators to provide four outputs, could have less realizable postures than that where each output is given by only one individual actuator. In this section, we will conduct the quasi-static analysis of the robot and discuss realizable postures and their transitions.

Since there are 12 typical configurations as stated in Section 1, there should be 12 different groups of equations for the statics. In order to get a group of statics equations, which can be employed to describe each posture clearly, we will present a group of basic formulations for the statics analysis.

3.2.1 Generic Statics Formulations for All Configurations

It can be easily found that the difference of each configuration is just that for each unit of the robot, the active pulley contacts ground, the passive pulley contacts the ground, or both the active and passive pulleys contact the ground. To describe all the possible configurations in a general form, configuration 12 has been selected as a generic posture for the general form. We presume that the normal forces and friction are exerted at the rim of each pulley. Thus, this general form can be used to describe all the possible configurations. The difference is that the normal force and frictions at the rim of pulley should be regarded as zero with respect to the different configurations.

A slope, which is denoted by α, is also considered in the general form of equations, thereby this general form can describe all the possible configurations in a two-dimensional environment. Still, in the coordinate system, the directions of x axis and y axis are selected to be parallel and perpendicular to the slope, respectively.

As shown in Figure 3.5, the normal forces N_{r4} and N_{f2}, which are normal to the slope, are assumed to be exerted at the rim of the rear active and front active pulleys, respectively. Friction F_{rc4} and F_{fc2}, which are parallel to the slope, are also assumed to be exerted at the rim of the rear active and front active pulleys, respectively. Rolling resistance M_4 and M_2 are assumed to be exerted likewise at the rim of front and rear active pulleys.

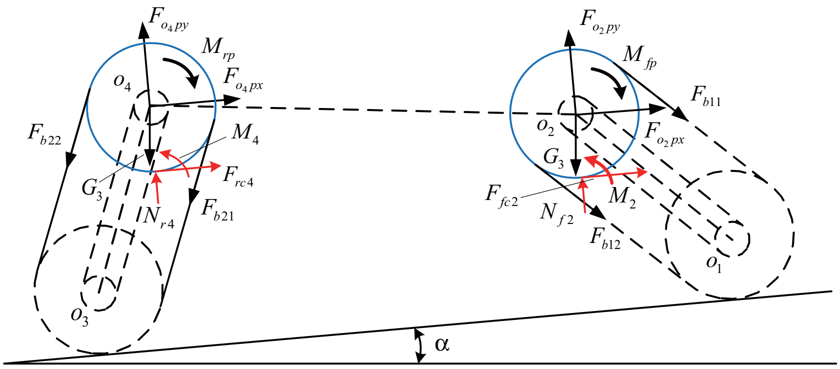

Figure 3.5. Force diagram of the rear and front active pulleys

As shown in Figure 3.5, additional forces including normal force and friction are exerted at the rim of the rear active and front active pulleys, respectively. The equilibrium of the rear active and front active pulleys can be expressed as

$$\begin{cases} \Sigma F_x = F_{o_4px} + (F_{b21} + F_{b22})\cos\theta_r + F_{rc4} - G_3 \sin\alpha = 0 \\ \Sigma F_y = F_{o_4py} + (F_{b21} + F_{b22})\sin\theta_r + N_{r4} - G_3 \cos\alpha = 0 \\ \Sigma M_{o_4} = -F_{b21}R + F_{b22}R + F_{rc4}R - M_{rp} + M_4 = 0 \end{cases} \tag{3.5}$$

$$\begin{cases} \Sigma F_x = F_{o_2px} + (F_{b11} + F_{b12})\cos\theta_f + F_{fc2} - G_3 \sin\alpha = 0 \\ \Sigma F_y = F_{o_2py} + (F_{b11} + F_{b12})\sin\theta_f + N_{f2} - G_3 \cos\alpha = 0 \\ \Sigma M_{o_2} = -F_{b11}R + F_{b12}R + F_{fc2}R - M_{fp} + M_2 = 0 \end{cases} \tag{3.6}$$

where M_{rp} and M_{fp} are the first outputs of each unit to drive the rear and front active pulleys, respectively. $F_{bij}(_{i=1,2;\ j=1,2})$ is the force of belt acted on the rim of the rear active pulley and front active pulley; F_{o_4px} and F_{o_4py} are the interaction of forces between the robot body and the rear active pulley in x and y directions; F_{o_2px} and F_{o_2py} are the interaction forces between the robot body and front active pulley in x and y directions. M_2 and M_4 are the rolling resistances, herein, $M_2 = \delta N_{f2}$, $M_4 = \delta N_{r4}$, δ is the coefficient of rolling resistance.

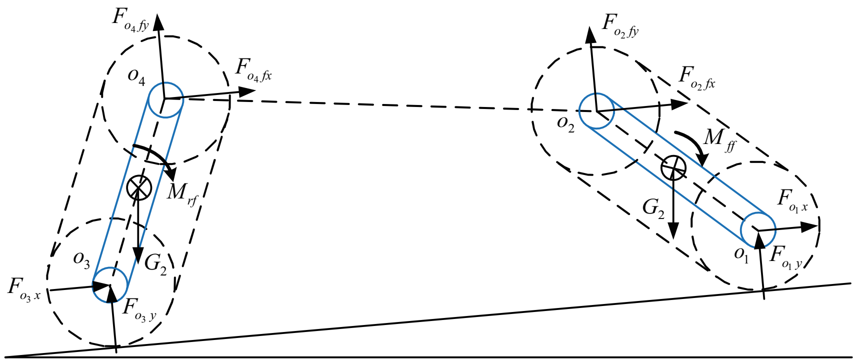

Figure 3.6. Force diagram of the rear and front frames

A force diagram relating to the front and rear frame is shown in Figure 3.6. The equilibrium of two frames can be given by

$$\begin{cases} \Sigma F_x = F_{o_4fx} + F_{o_3x} - G_2 \sin\alpha = 0 \\ \Sigma F_y = F_{o_4fy} + F_{o_3y} - G_2 \cos\alpha = 0 \\ \Sigma M_{o_4} = -F_{o_3x} d_3 \sin\theta_r + F_{o_3y} d_3 \cos\theta_r - M_{rf} \\ \qquad\qquad - G_2 d_4 \cos\alpha\cos\theta_r + G_2 d_4 \sin\alpha\sin\theta_r = 0 \end{cases} \tag{3.7}$$

$$\begin{cases} \Sigma F_x = F_{o_2fx} + F_{o_1x} - G_2 \sin\alpha = 0 \\ \Sigma F_y = F_{o_2fy} + F_{o_1y} - G_2 \cos\alpha = 0 \\ \Sigma M_{o_2} = -F_{o_1x} d_3 \sin\theta_f + F_{o_1y} d_3 \cos\theta_f - M_{ff} \\ \qquad\qquad - G_2 d_4 \cos\alpha\cos\theta_f + G_2 d_4 \sin\alpha\sin\theta_f = 0 \end{cases} \tag{3.8}$$

where M_{rf} and M_{ff} are the second outputs of each unit to drive the rear and front frame, respectively. F_{o_3x} and F_{o_3y} are the interaction forces between the rear frame and rear passive pulley in x and y directions. F_{o_4fx} and F_{o_4fy} are the interaction forces between the rear frame and robot body in x and y directions. F_{o_1x} and F_{o_1y} are the interaction forces between the front frame and front passive pulley in x and y directions. F_{o_2fx} and F_{o_2fy} are the interaction forces between the front frame and robot body in x and y directions.

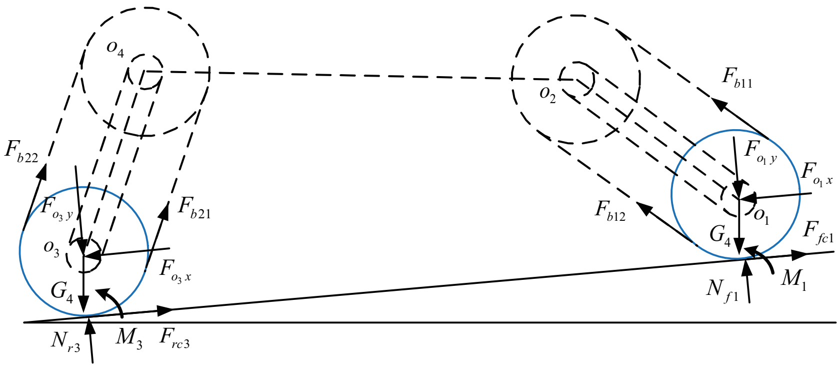

Figure 3.7. Force diagram of the rear and front passive pulleys

A force diagram concerning the front and rear passive pulley is shown in Figure 3.7. The equilibrium of the two passive pulleys can be obtained by

$$\begin{cases} \Sigma F_x = F_{rc3} - (F_{b21} + F_{b22})\cos\theta_r - F_{o3x} - G_4 \sin\alpha = 0 \\ \Sigma F_y = N_{r3} - (F_{b21} + F_{b22})\sin\theta_r - F_{o3y} - G_4 \cos\alpha = 0 \\ \Sigma M_{o_3} = F_{b21}R - F_{b22}R + F_{rc3}R + M_3 = 0 \end{cases} \tag{3.9}$$

$$\begin{cases} \Sigma F_x = F_{fc1} - (F_{b11} + F_{b12})\cos\theta_f - F_{o_1x} - G_4 \sin\alpha = 0 \\ \Sigma F_y = N_{f1} - (F_{b11} + F_{b12})\sin\theta_f - F_{o_1y} - G_4 \cos\alpha = 0 \\ \Sigma M_{o_1} = F_{b11}R - F_{b12}R + F_{fc1}R + M_1 = 0 \end{cases} \tag{3.10}$$

where N_{r3} and N_{f1} are the normal forces acted on the rear and front passive pulley from the ground; F_{rc3} and F_{fc1} are the tangential frictions exerted on the rear and front passive pulley; M_3 and M_1 are the rolling resistances on the rear passive and front passive pulleys, respectively, herein, $M_3 = \delta N_{r3}$, $M_1 = \delta N_{f1}$, δ is the coefficient of rolling resistance.

The following part is the robot body, which is shown in Figure 3.8. The following

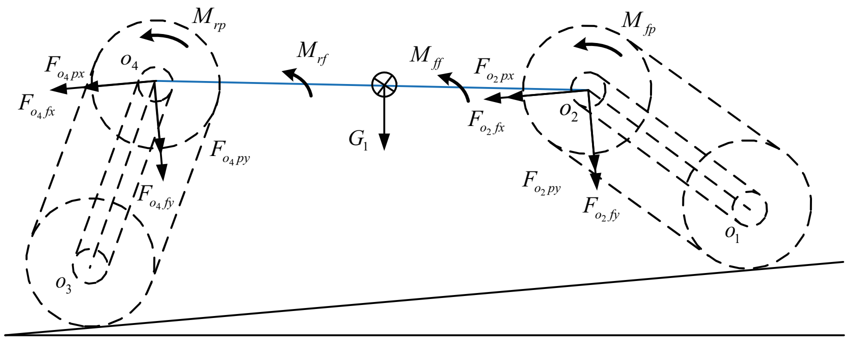

Figure 3.8. Force diagram of the robot body

equilibrium about the robot body can be given by

$$\begin{cases} \Sigma F_x = -F_{o_4px} - F_{o_4fx} - F_{o_2px} - F_{o_2fx} - G_1 \sin\alpha = 0 \\ \Sigma F_y = -F_{o_4py} - F_{o_4fy} - F_{o_2py} - F_{o_2fy} - G_1 \cos\alpha = 0 \\ \Sigma M_{o_4} = M_{rp} + M_{rf} + M_{fp} + M_{ff} - G_1 d_2 \cos(\alpha+\beta) \\ \quad + (F_{o_2fx} + F_{o_2px}) d_1 \sin\beta - (F_{o_2fy} + F_{o_2py}) d_1 \cos\beta = 0 \end{cases} \tag{3.11}$$

From the principle of mechanism design in the crawler, the output to frame keeps a proportional relation with the output to the active pulley. It can be indicated by

$$\begin{cases} M_{rf} = K M_{rp} \\ M_{ff} = K M_{fp} \end{cases} \tag{3.12}$$

where M_{rf} and M_{rp} are the outputs to the rear active pulley and frame, respectively; M_{ff} and M_{fp} are the outputs to the front active pulley and frame, respectively. K is ratio of reducer ratios and its value is 7.5.

A group of basic equations for all configurations are presented above. The differences among these configurations, are the constraints on the normal force, the tangential force and the rolling resistance. For instance, to describe the “config. 10” in the static case, the following constraints should be taken into consideration:

$$
\begin{cases}
\alpha = 0^\circ \cdots\cdots\cdots\cdots\cdots\cdots \text{Ground without incline} \\
180^\circ < \theta_f < 360^\circ \\
0^\circ < \theta_r < 180^\circ \\
\left.\begin{array}{l} N_{r3} = 0,\ N_{f2} = 0 \\ F_{rc3} = 0,\ F_{fc2} = 0 \end{array}\right\} \cdots \begin{array}{l}\text{No contact of the rear passive pulley and the} \\ \text{front active pulley with the ground}\end{array} \\
\left.\begin{array}{l} M_3 = 0,\ M_2 = 0 \\ M_1 = 0,\ M_4 = 0 \end{array}\right\} \cdots\cdots \text{No forward or backward motion}
\end{cases}
\tag{3.13}
$$

3.2.2 Realizable Postures

Based on the above equations, analysis for each configuration is conducted here. For each configuration, there are two cases: without moving velocity and with moving velocity. The case "Without Moving Velocity" is that the maximum static friction is not exceeded and there is no rolling resistance. The case "With Moving Velocity" means that pulleys are subject to sliding friction and rolling resistance concurrently. The coefficient of static friction between pulley and ground μ_s is set to 0.5 and the coefficient of rolling friction δ is considered as 2 mm.

(1) Without Moving Velocity

When the robot stays on the horizontal ground without moving velocity, rolling resistance exerted on the front and rear pulleys can be ignored. Thus, the constraints for each configuration in this static case are

$$
\begin{aligned}
&\alpha = 0^\circ \\
&M_1 = 0,\ M_2 = 0 \\
&M_3 = 0,\ M_4 = 0
\end{aligned}
\tag{3.14}
$$

From the numerical results of reaction forces shown in Figure 3.9, the normal reaction forces from ground can always be maintained larger than 0 for "config. 1" and "config. 5".

Due to the fact that “config. 1” is geometrically symmetrical to “config. 7” while “config. 5” is symmetrical to “config. 3”, we can find that “config. 1”, “config. 3”, “config. 5” and “config. 7” can be kept under the friction conditions. The results of these configurations are summarized in Figure 3.10.

As shown in Figure 3.9, for “config. 2”, the rear normal reaction force N_{r3} is larger than 0 just when the front angle θ_f is in the range ($180° \leq \theta_f \leq 282°$), otherwise N_{r3} is less than 0. Similarly, the rear normal reaction force N_{r3} is larger than 0 just when the front angle θ_f is in the range ($258° \leq \theta_f \leq 312°$) for “config. 6”. With regard to “config. 2”, “config. 4”, “config. 6”, and “config. 8”, only part of the postures can be balanced, since “config. 2” is geometrically symmetrical to “config. 8” while “config. 6” is symmetrical to “config. 4”. The controllable postures are listed for “config. 2”, “config. 4”, “config. 6” and “config. 8” in Table 3.2.

Concerning “config. 9”, “config. 10”, “config. 11”, and “config. 12”, there is only one line to show that the posture which can be balanced is that θ_f and θ_r should hold a one-one relation.

As shown in Figure 3.10, the configuration in the area where the robot cannot be balanced has the trend to change to another stable posture. The symbol “$\rightarrow$” denotes the transition through controlling the front and rear actuator outputs cooperatively. For instance, for the point in the region that ($0° < \theta_f, \theta_r < 180°$, $0° < \theta_f + \theta_r < 180°$), the robot can change posture to the posture ($0° < \theta_f < 180°,\ \theta_r = 0°$) or ($\theta_f = 0°,\ 0° < \theta_r < 180°$) in control of two actuators.

As shown in Figure 3.11, for the given angle of rear frame θ_r, there is just one angle of front frame θ_f to match it. When the rear unit is kept in the current position, a rotation torque M_{ff} is inevitably exerted on the front frame. If there is a deviation that makes the front angle become θ_{f1}, the torque M_{ff} cannot provide enough force to lift the front frame back to the equilibrium point θ_f. Also if there is a deviation that makes the front angle become θ_{f2}, the torque M_{ff} will make the front frame accelerate to go far away from the equilibrium point θ_f. In a word, the current state in “config. 11” is unstable equilibrium.

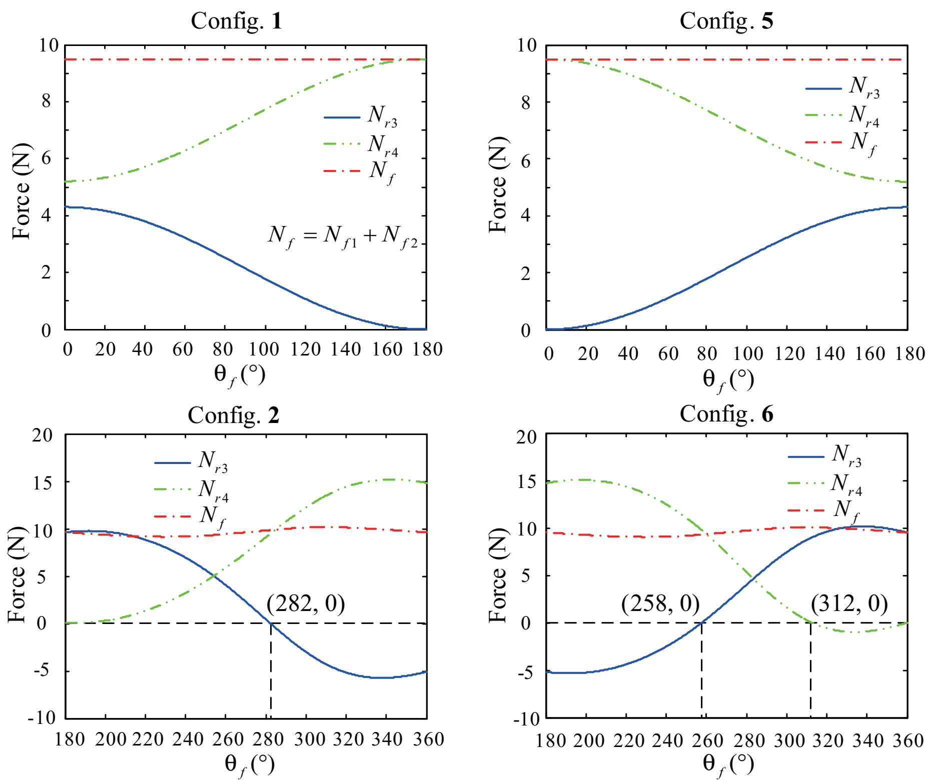

Figure 3.9. Numerical results of normal reaction forces for different config. 1, 5, 2 and 6

Using the same method, it can be easily found that the balance in "config. 9", "config. 10", "config. 11" and "config. 12" is unstable equilibrium.

The balance of "config. 1", "config. 2", "config. 3", "config. 4", "config. 5", "config. 6", "config. 7" and "config. 8" belongs to stable equilibrium while the balance of "config. 9", "config. 10", "config. 11" and "config. 12" belongs to unstable equilibrium.

(2) With Moving Velocity

If the robot moves with a velocity of v, rolling friction should be exerted at the rim of pulley which contacts the ground. Thus, the constraint for each configuration in the movement case on a horizontal plane is

$$\alpha = 0^\circ \tag{3.15}$$

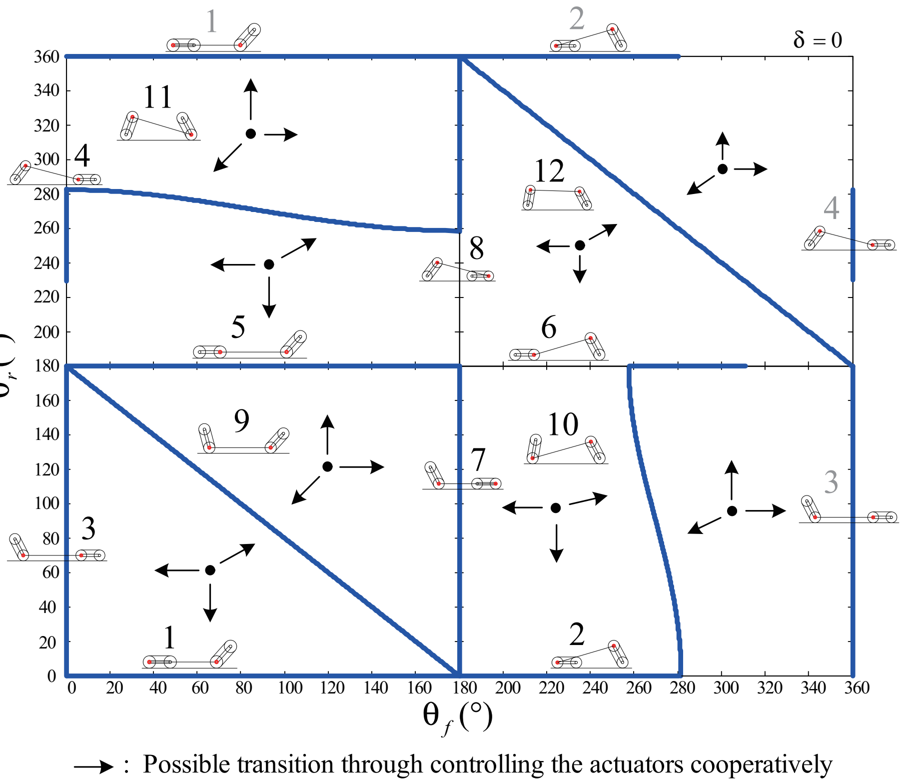

Figure 3.10. Controllable static postures of the robot

The numerical results of this static analysis are shown in Figure 3.12. “Config. 1”, can be kept under the friction conditions since all the normal reaction forces are larger than 0, as shown in Figure 3.12(a).

For “config. 2”, “config. 3”, “config. 4”, “config. 6”, and “config. 8”, just part of the postures can be balanced to keep the normal reaction forces on the active and passive pulleys larger than 0, as shown in Figure 3.12(b), (c), (d), (f), and (h), respectively. The corresponding ranges are listed in Table 3.2.

Regarding to “config. 5” and “config. 7”, since the rear normal reaction force N_{r3} for “config. 5” and the front normal reaction force N_{f1} for “config. 7” are always less than 0, there does not exist any suitable posture for the robot to be generated. Concerning “config. 9”, the robot cannot perform the posture since the configuration is impossible to keep balance.

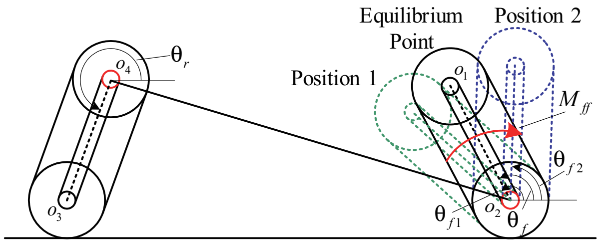

Figure 3.11. Stability analysis for "config. 11"

For "config. 10", "config. 11", and "config. 12", there are postures that can be generated for one-one relation between θ_f and θ_r.

As shown in Figure 3.13, the posture in the region where the robot cannot be balanced has the trend to change to another stable posture. The symbol "$\longrightarrow$" stands for the transition through controlling the front and rear actuator outputs cooperatively. For instance, for the point in the area that ($0° < \theta_f, \theta_r < 180°$), it can make transition to the postures ($0° < \theta_f < 180°,\ \theta_r = 0°$) or ($\theta_f = 0°,\ 54° < \theta_r < 180°$) through effective control.

Table 3.2. Controllable range of θ_f and θ_r of the robot in two cases

Config.	Controllable Range of θ_f and θ_r			
	Without Moving Velocity		With Moving Velocity	
	θ_f	θ_r	θ_f	θ_r
1	$0° \sim 180°$	$0°$	$0° \sim 180°$	$0°$
2	$180° \sim 282°$	$0°$	$222° \sim 360°$	$0°$
3	$0°$	$0° \sim 180°$	$0°$	$54° \sim 180°$
4	$0°$	$228° \sim 282°$	$0°$	$272° \sim 310°$
5	$0° \sim 180°$	$180°$	$---$	$---$
6	$258° \sim 312°$	$180°$	$292° \sim 360°$	$180°$
7	$180°$	$0° \sim 180°$	$---$	$---$
8	$180°$	$258° \sim 360°$	$180°$	$285° \sim 360°$
9	$\theta_f + \theta_r = 180°$		$---$	
10	$^\star g_1(\theta_f, \theta_r) = 0$		$^\star g_2(\theta_f, \theta_r) = 0$	
11	$^\star g_3(\theta_f, \theta_r) = 0$		$^\star g_4(\theta_f, \theta_r) = 0$	
12	$^\star g_5(\theta_f, \theta_r) = 0$		$^\star g_6(\theta_f, \theta_r) = 0$	

$^\star g_i(\theta_f, \theta_r)(i = 1, 2, ..6)$ describes a function of their variables.

The balance of "config. 1", "config. 2", "config. 3", "config. 4", "config. 6" and

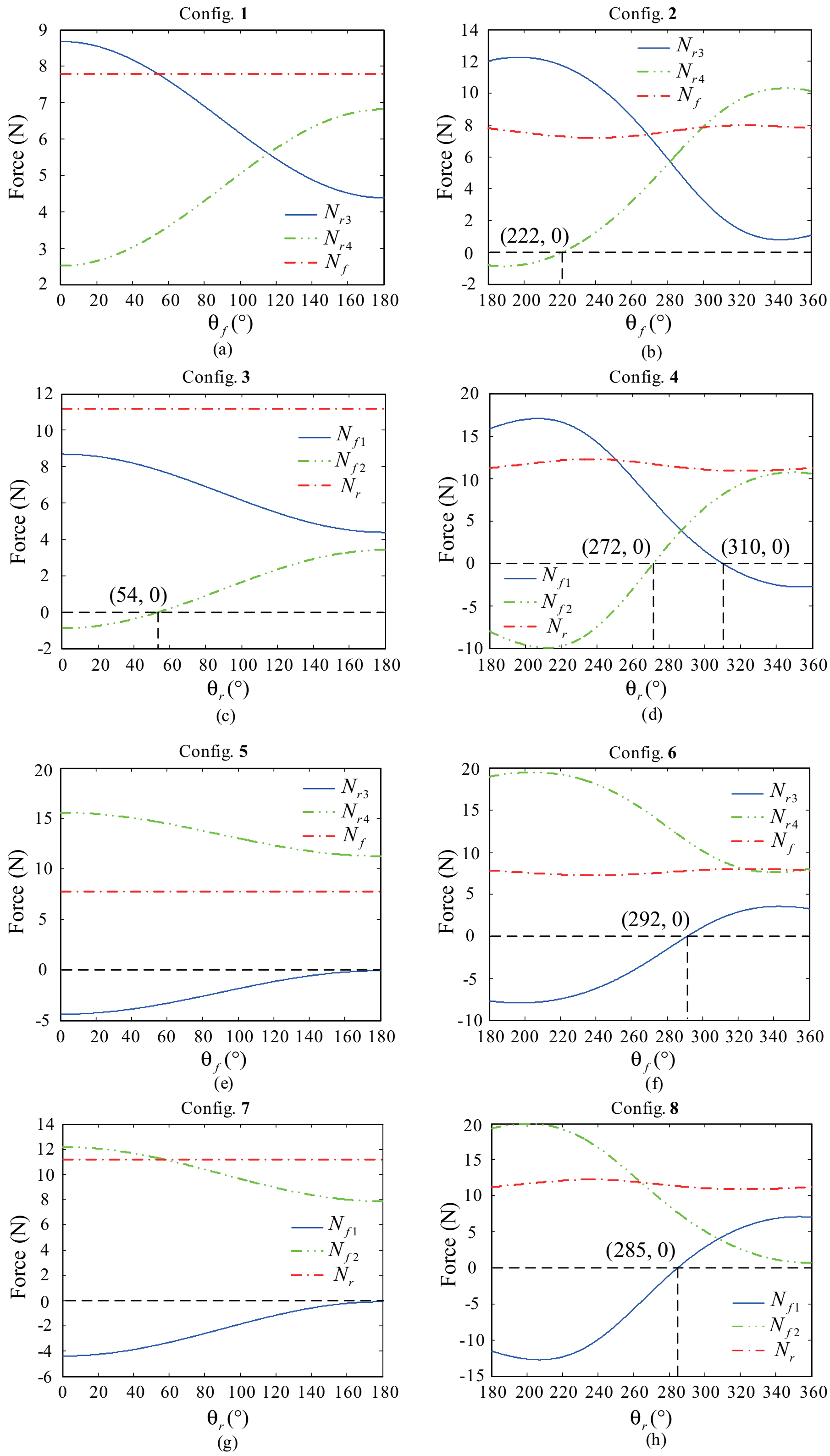

Figure 3.12. Numerical results of normal reaction forces for different config. 1, 2, 3, 4, 5, 6, 7 and 8 considering rolling resistance

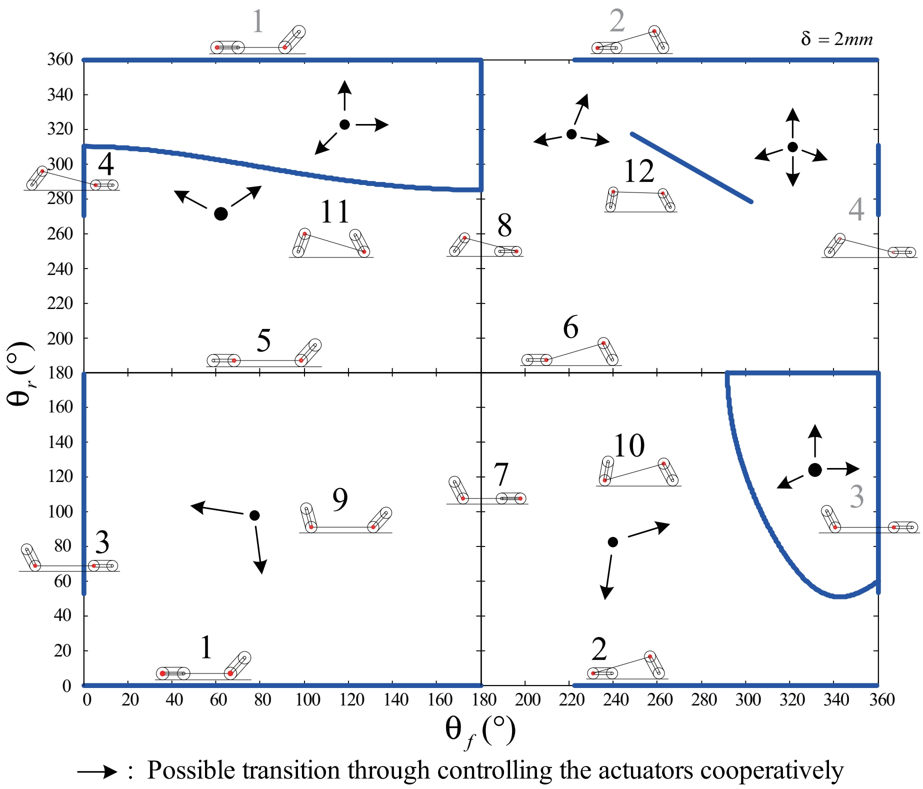

Figure 3.13. Controllable postures of the robot with movement

"config. 8" belongs to stable equilibrium while the balance of "config. 10", "config. 11" and "config. 12" belongs to unstable equilibrium.

3.2.3 Posture Transition

In Figure 3.10, we see that the robot can change from one stable posture to another continuously. On the other hand, when the robot moves forwards with a certain velocity, the stable posture sometimes cannot be changed from one to another continuously since the range of stable postures is strictly limited, as shown in Figure 3.13. However, the robot can overcome the blind area through the static posture transition, as shown in Figure 3.14. For example, the robot with a certain moving velocity, can overcome the blind area from P_1 to P_2, through stopping the forward motion to perform posture transition statically. Note that, the posture transition discussed here can be executed without proper control of the interaction between the front and rear crawler units. To perform the discontinuous posture transition like that from "config. 12" to "config. 2", the interaction between two crawler units must be effectively controlled. We will discuss this in our future studies.

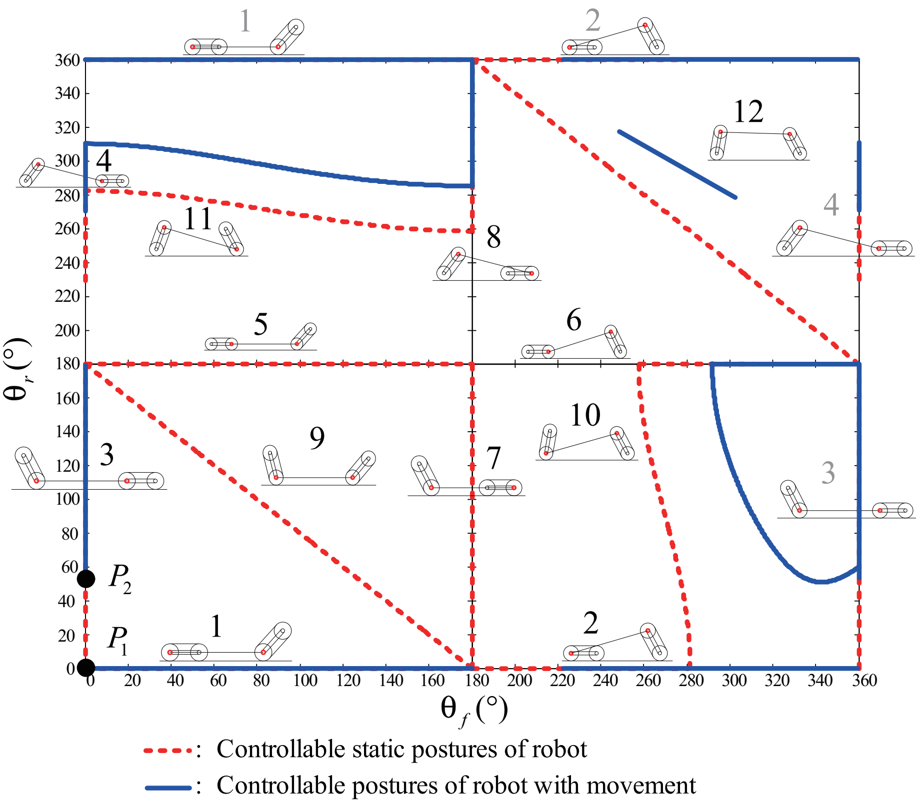

Figure 3.14. Posture transition of the robot

3.3 Experimental Validation

In order to verify the quasi-static analysis above, experiments were conducted to control the robot to perform the postures for each configuration. The velocities of two actuators were controlled manually by using two potentiometers. The internal interaction between the two crawler mechanism units causes the robot to perform several postures.

3.3.1 Experiments Without Moving Velocity

When the robot stays on the horizontal ground without moving velocity, rolling resistance exerted on the front and rear pulleys can be neglected.

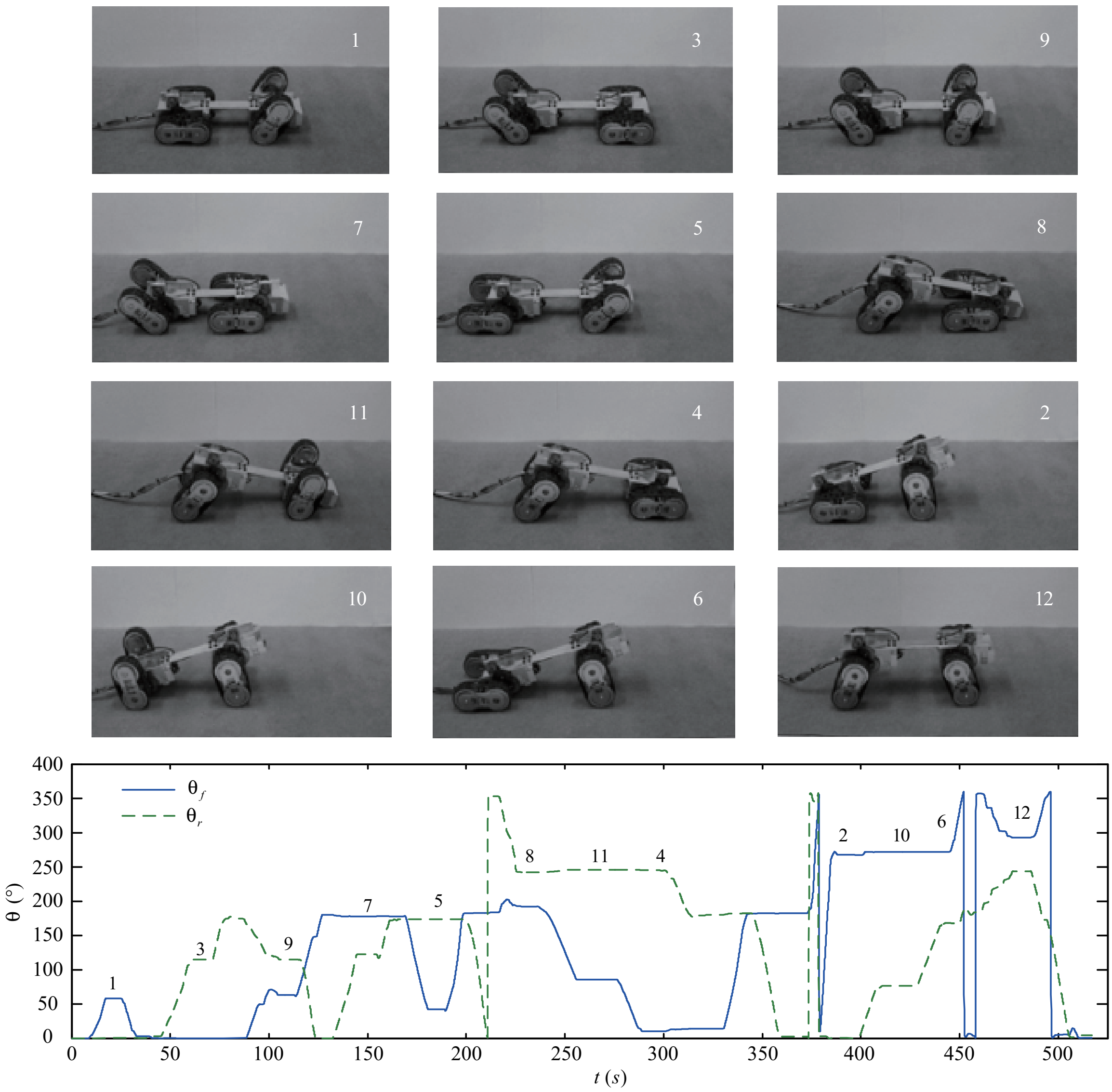

Figure 3.15. Experiment scenes and angle relation when the robot performs posture transition without moving velocity

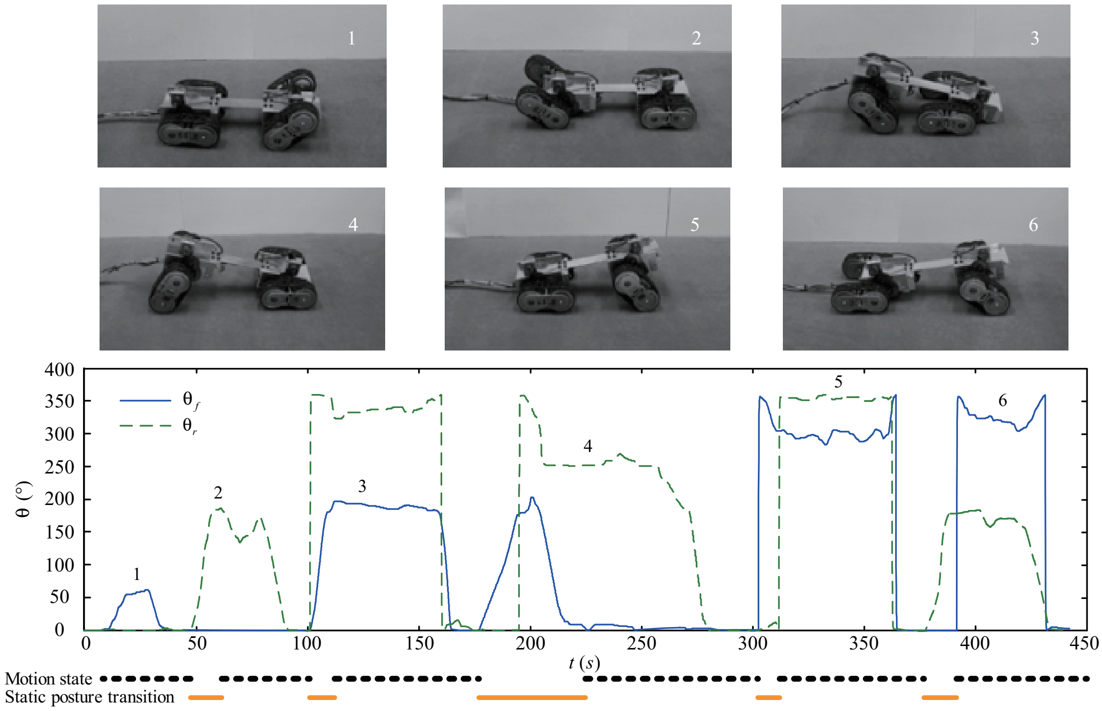

Figure 3.16. Experiment scenes when the robot moves forwards

As shown in Figure 3.15, postures are consecutively performed from “config. 1” to “config. 12”. Same as the numerical results of simulation, “config. 1”, “config. 3”, “config. 5” and “config. 7” are stable equilibrium and thus can be achieved continuously. Regarding to “config. 9” and “config. 12”, the robot should be kept symmetrically otherwise it will make a posture transition to another posture, breaking the balance. For “config. 4”, “config. 6” and “config. 8”, the angle θ_f or θ_r just can be kept in part of the range from 0° to 360°. Once the angle θ_f or θ_r is beyond the related range, the balance is broken so as to cause the posture transition of the robot. For “config. 10” and “config. 11”, the one-one relation should be kept strictly to perform the posture.

3.3.2 Experiments With Moving Velocity

If the robot moves with a certain velocity of v, rolling friction should be exerted at the rim of pulley that contacts the ground.

As shown in Figure 3.16, six postures including “config. 1”, “config. 3”, “config. 8”, “config. 4”, “config. 2” and “config. 6” can be realized in the case that the robot moves forward, since other postures are unstable equilibrium stated in Section 2. As with the analysis in Section 2, experiments also show that the robot can keep the front frame at any position in the range $0° < \theta_f < 180°$ in “config. 1”. In order to realize posture 3, a static transition is deployed necessarily, where the rear frame of the robot first rotates from 0° to 180°, then the robot moves with the rear frame lifted at the angle θ_r through the internal interaction between the two crawler units. Like “config. 3”, it is inevitable that the robot adopts a static transition for “config. 2”, “config. 4”, “config. 6”, and “config. 8”.

3.4 Summary

Since this dual-crawler-driven robot is an under-actuated system, quasi-static analysis has been conducted to find out all the realizable postures. From the presented results, it is known that the robot can perform less postures than that of fully-driven robot and the robot moving forward at a certain velocity realizes less postures than that in static case. Static posture transition can be employed for the robot maintaining forward motion to overcome the blind spot of the posture transition.

Chapter 4

Posture Control of a Dual-crawler-driven Robot

A tracked robot with polymorphic locomotion has been realized by use of two units of the proposed crawler mechanism. Controllable postures of the crawler-driven robot have been obtained through the quasi-static analysis numerically. How to control the robot to realize the corresponding possible postures is still a great challenge to overcome.

As stated in Chapter 3, the configurations of the dual-crawler-driven robot can be divided into two classes: stable equilibrium and unstable equilibrium. Until now, we have just got the method to control the stable equilibrium postures and the unstable equilibrium postures will be investigated in the future research. As a typical stable equilibrium, the "config. 1" is selected as the object to perform posture control.

For this tracked robot, there are usually two typical methods to negotiate an obstacle. As shown in Figure 4.1(a), the robot can overcome the obstacle autonomously due to our design concept. Figure 4.1(b) shows another method to traverse rugged terrains, in which the front unit is controlled to lift up actively. Herein, we will discuss how to control the posture that the front unit is lifted up [79].

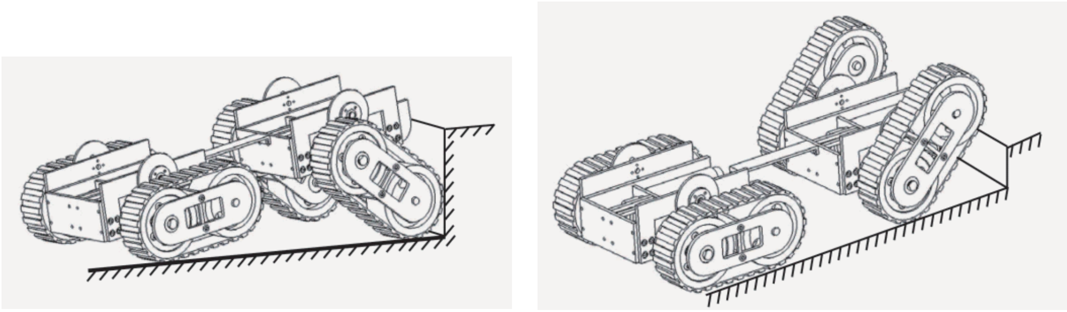

(a) (b)

Figure 4.1. Two methods for negotiating obstacles. (a)without control (b)with control

4.1 Static Analysis of the Posture

In order to negotiate rugged terrains, the front unit sometimes should be lifted up to increase the contact angle with obstacle. In this posture, the front crawler unit lifts up for an angle θ_f while the rear crawler unit keeps totally contact to the ground. This posture makes the robot climb actively and easily over an obstacle. We have analyzed the statics of this posture and thus herein the interaction relationship between the front and rear crawler units will be figured out to attempt to find the control method.

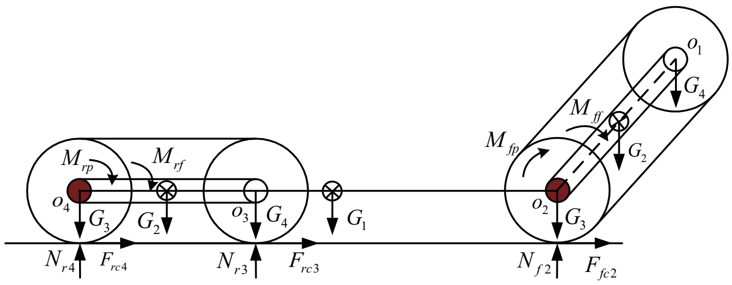

Figure 4.2. Force diagram of robot for the posture

The total reaction forces of rear and front crawler units can be given by

$$N_f = N_{f1} + N_{f2}, \qquad N_r = N_{r3} + N_{r4} \tag{4.1}$$

When the robot moves forwards with velocity of v while keeping a frame posture, the power of front and rear crawler units can be calculated by

$$P_f = F_{fc}\, v, \qquad P_r = F_{rc}\, v \tag{4.2}$$

where F_{fc} $(= F_{fc1} + F_{fc2})$ is the friction force acting on the front crawler and F_{rc} $(= F_{rc3} + F_{rc4})$ is that on the rear crawler.

Figure 4.3 shows the numerical results where (a) is about reaction forces on pulleys, N_{fi} and N_{ri}, with respect to θ_f, (b) is the required power of rear and front crawler units [67].

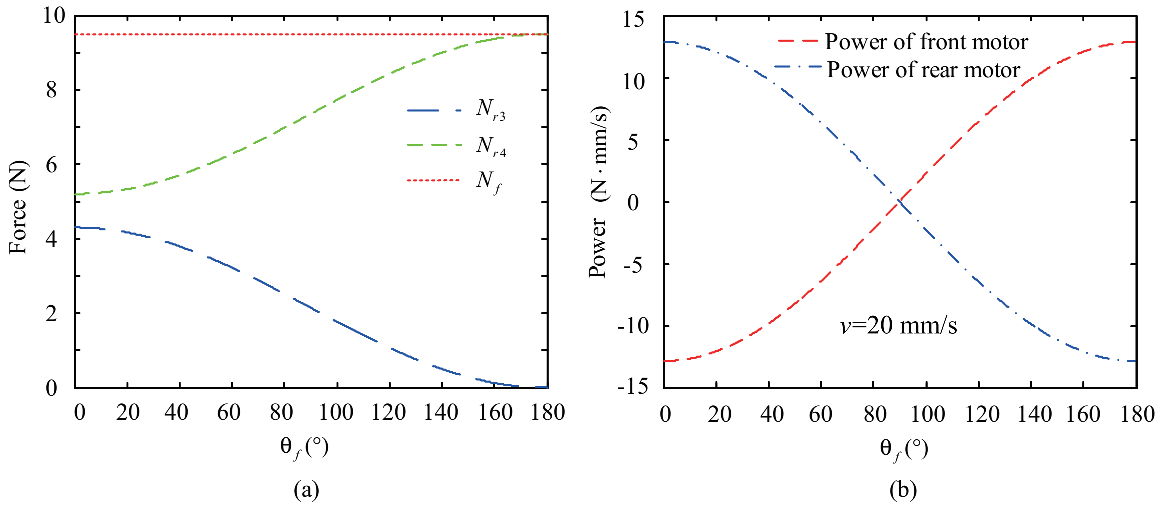

Figure 4.3. Numerical results for the posture

In Figure 4.3(a), it is clearly shown that the reaction forces on rear active pulley and passive pulley are always larger than 0 [N]. It means that the rear unit always keeps contact with the ground, and does not need any posture control. Thus, this posture, where θ_f changes from 0° to 180°, can be kept if there is enough friction from the ground. When θ_f is larger than 90°, the power transfers from front crawler unit to rear crawler unit, as shown in Figure 4.3(b). This power is used by the rear crawler unit to keep its posture. However, the power transfers from rear crawler unit to front crawler unit when θ_f is less than 90°, and it is used by front crawler unit to keep its posture.

Herein, we discuss that the robot is required to change posture from current angle θ_f to a desired goal angle θ_{fd}. If $\theta_f > \theta_{fd}$, the front motor should increase power output to rotate in clockwise direction to realize the posture change. In this process, the front unit pulls the rear unit. If $\theta_f < \theta_{fd}$, the rear motor should increase power output to make the front frame rotate in anticlockwise direction to realize the posture alternation. The front unit is pushed by the rear unit during this process.

4.2 Posture Control Approaches

From the numerical results of static analysis for the posture, we know that the posture that the front unit is lifted up can be controlled theoretically. To control the robot to move forwards while keeping the posture, velocity relations of each component of the robot are discussed first and then the control methods: direct control and indirect control, and cooperative control are presented based on these velocity relations.

4.2.1 Velocity Relationship

To get the velocity relations of each component of the front and rear units, we should analyze the internal planetary gear reducer first because it is the main transmission component inside the robot. Firstly we presume that the planetary gear reducer works in a general state shown in Figure 4.4. Using the simultaneous center method for the planetary gear, we have

$$\omega_1 r_1 + \omega_3 r_3 = 2\omega_2(r_1 + r_2) \tag{4.3}$$

where ω_1, ω_2, ω_3 are the angular velocities of the sun gear, the carrier and the ring gear, respectively; r_1, r_2, r_3 are the radii of the sun gear, the planetary gear and the ring gear, respectively. Herein, the rotational direction of those components is defined according to the direction of robot motion, and shows in Figure 4.4.

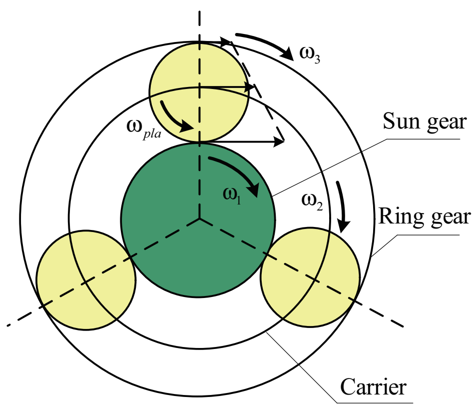

Figure 4.4. A general state of planetary gear reducer

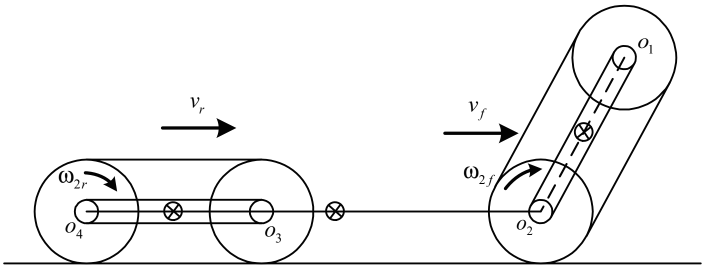

Figure 4.5. Velocity relations between the front and rear units

By solving Equation (4.3), we can get

$$\omega_2 = \omega_1 r_1/(2(r_1 + r_2)) + \omega_3 r_3/(2(r_1 + r_2)) \tag{4.4}$$

$$\omega_3 = \omega_2(2(r_1 + r_2))/r_3 - \omega_1 r_1/r_3 \tag{4.5}$$

Due to the fact that the reducer ratio from the sun gear to the carrier is $i_1 = 2(r_1+r_2)/r_1$, the reducer ratio from the sun gear to the ring gear is $i_{21} = -r_3/r_1$, for the planetary gear reducer in the front unit, the velocity relations can be expressed as

$$\omega_{2f} = 1/i_1\omega_{1f} - i_{21}/i_1\omega_{3f} \tag{4.6}$$

$$\omega_{3f} = 1/i_{21}\omega_{1f} - i_1/i_{21}\omega_{2f} \tag{4.7}$$

for the planetary gear reducer in the rear unit, the velocity relations can be given by

$$\omega_{2r} = 1/i_1\omega_{1r} - i_{21}/i_1\omega_{3r} \tag{4.8}$$

$$\omega_{3r} = 1/i_{21}\omega_{1r} - i_1/i_{21}\omega_{2r} \tag{4.9}$$

As shown in Figure 4.5, the front carrier output ω_{2f} drives the front active pulley while the rear carrier output ω_{2r} drives the rear active pulley. v_f and v_r are the linear moving velocities of the front unit and rear unit, respectively.

If there is no slip for the front and rear pulley on ground, the linear moving velocities of the two mechanism units can be given by

$$v_f = \omega_{2f} R \tag{4.10}$$

$$v_r = \omega_{2r} R \tag{4.11}$$

where R is the radius of the active pulley. Since the front and rear units are connected through a rigid body, we can get

$$v_f = v_r \tag{4.12}$$

When robot moves with the posture stably, the angular velocities of the front and rear actuators should be the same.

The velocity relation between the front unit and the rear unit is shown in Figure 4.6. The front motor inputs to the sun gear of the front planetary gear reducer with velocity of ω_{1f} and transmits separately to the front frame and the front pulley. The rear motor inputs to the sun gear of the rear planetary gear reducer with velocity of ω_{1r} and transmits to the rear frame and the rear pulley.

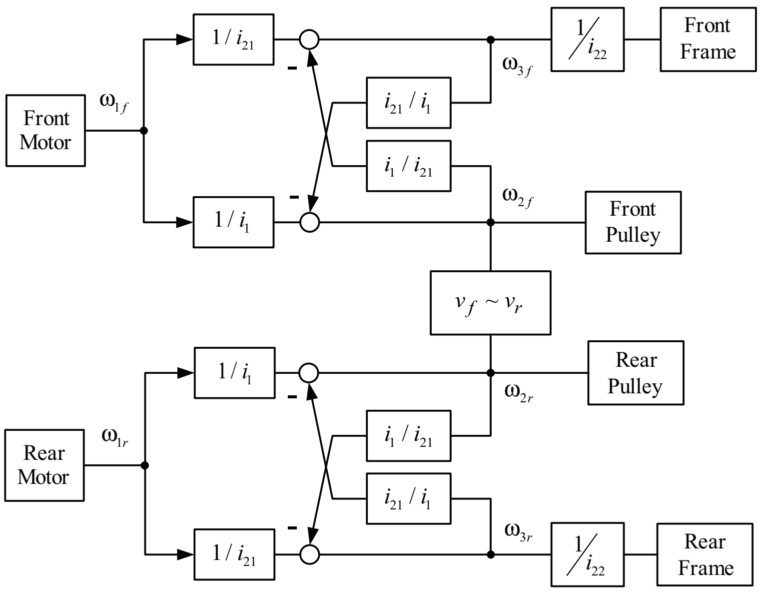

Figure 4.6. Velocity transference diagram between the front and rear units

Owing to the fact that the front and rear units are linked by the robot body, the linear velocity of the front unit v_f should be the same as that of the rear unit v_r.

The dual-crawler-driven robot is an under-actuated system, in which there is a kinematic redundancy. The internal interaction between the front unit and the rear unit can be used to realize the robot posture control.

θ_{fd} is the desired front frame angle of the posture. As shown in Figure 4.7, the current frame angle is larger than the desired frame angle θ_{fd}. The front frame should rotate in clockwise direction so as to reach the desired goal angle. At this moment, the front unit pulls the rear unit.

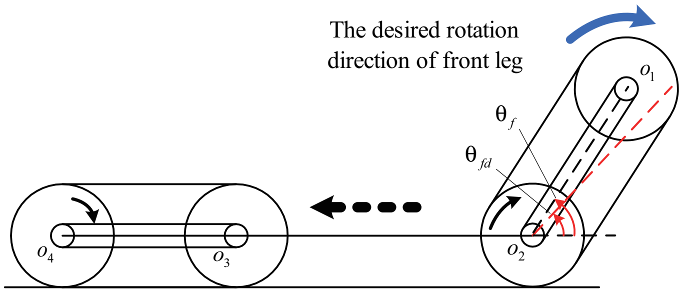

Figure 4.7. Control concept when $\theta_f > \theta_{fd}$

As shown in Figure 4.8, the current frame angle is smaller than the desired frame angle θ_{fd}. The front frame should rotate in anticlockwise direction so as to reach the desired goal angle. At this moment, the front unit is pushed by the rear unit.

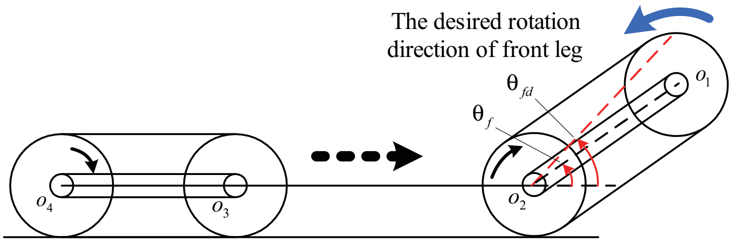

Figure 4.8. Control concept when $\theta_f < \theta_{fd}$

Velocity analysis gives the velocity relations between the front unit and rear unit clearly and control strategy using internal interaction explains the control principle. There are three ways to realize the posture control: direct, indirect, and cooperative control.

Direct and indirect control methods are the ways that keep the actuator of one unit in a constant velocity while controls the actuator of another unit to perform the posture. Cooperative control makes the front and rear actuators cooperate to perform the desired posture.

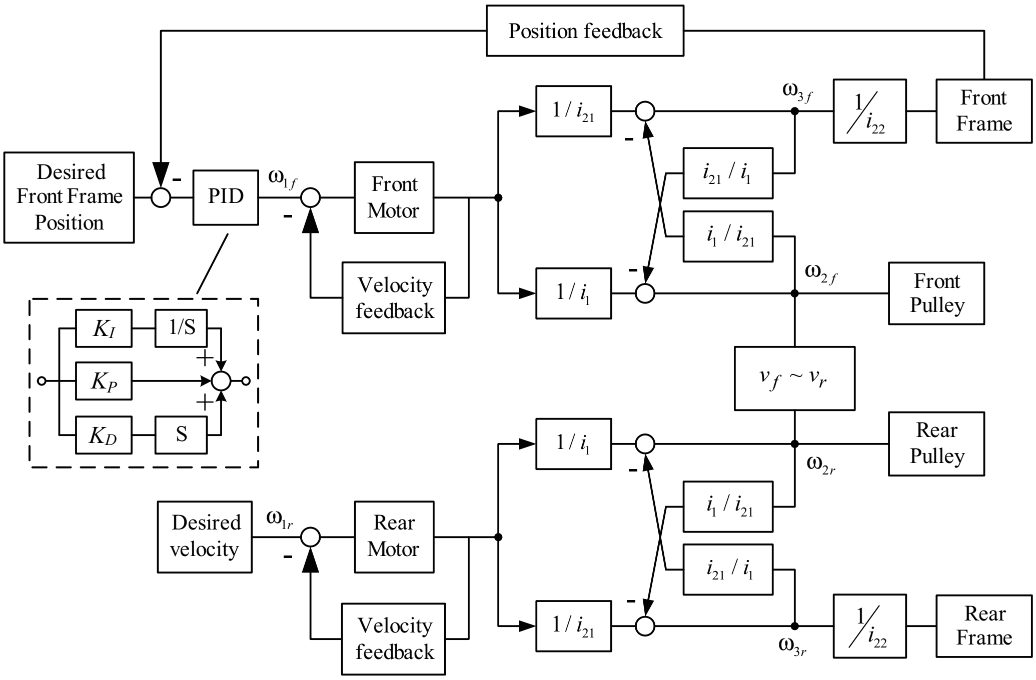

Figure 4.9. Posture realization through direct control

4.2.2 Direct Control Method

As shown in Figure 4.9, the actuator in the rear unit keeps a constant velocity while the actuator in the front unit is controlled through the position feedback from the front frame. The rear actuator is controlled to keep a desired constant velocity through its own velocity feedback. The front actuator is controlled to keep the front frame at a desired angle with the position feedback. Here, we call this control method "Direct control".

4.2.3 Indirect Control Method

As shown in Figure 4.10, the actuator in the front unit keeps a constant velocity while the actuator in the rear unit is controlled through the position feedback from the front frame. Here, this control method is called "Indirect control".

The two control methods including direct control and indirect control actually just control one actuator as main device to keep or change the posture while another actuator is just controlled in a constant velocity to move its own unit.

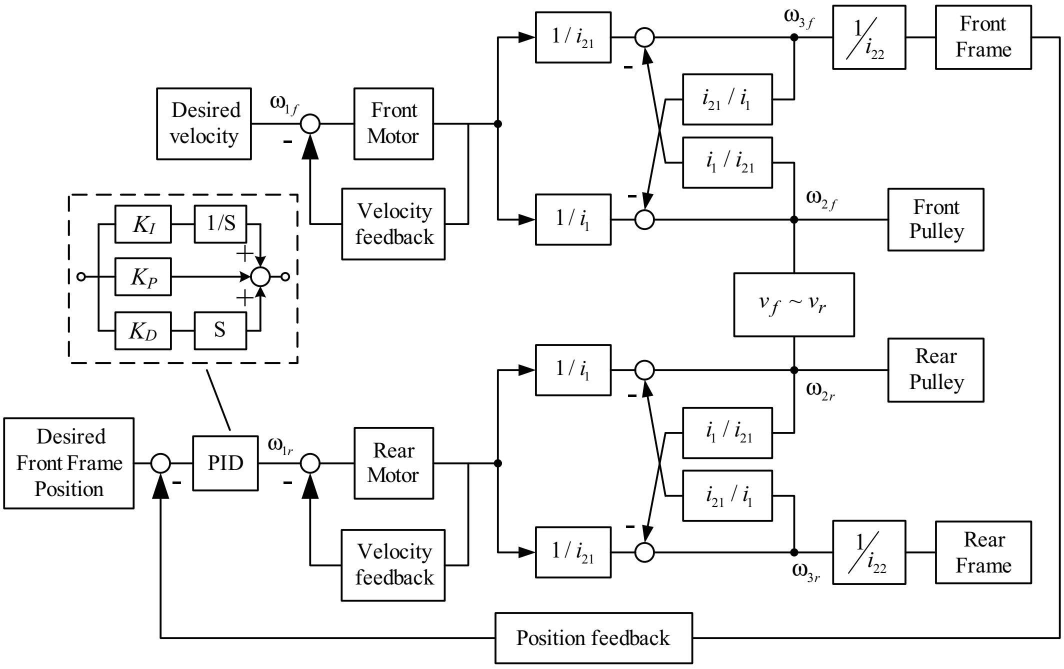

Figure 4.10. Posture realization through indirect control

4.2.4 Cooperative Control Method

On the contrary, cooperative control method is the way to control two actuators of the front and rear units concurrently to realize posture control. There is a cooperation between the two actuators of front and rear units. As shown in Figure 4.11, cooperative control is a way that controls both the front actuator and rear actuator to keep the posture. The position feedback of front frame is used to control the front and rear actuators at the same time. Here, we call this kind of control method “Cooperative control”.

4.3 Experimental Validation

Experiments using different control methods including direct, indirect, and cooperative control, are conducted to verify the posture control.

The desired control input is shown in Figure 4.12. At the time $t = 0$ s, there is a step input signal of angle from 0° to 60°; at the time $t = 20$ s, input angle signal decreases

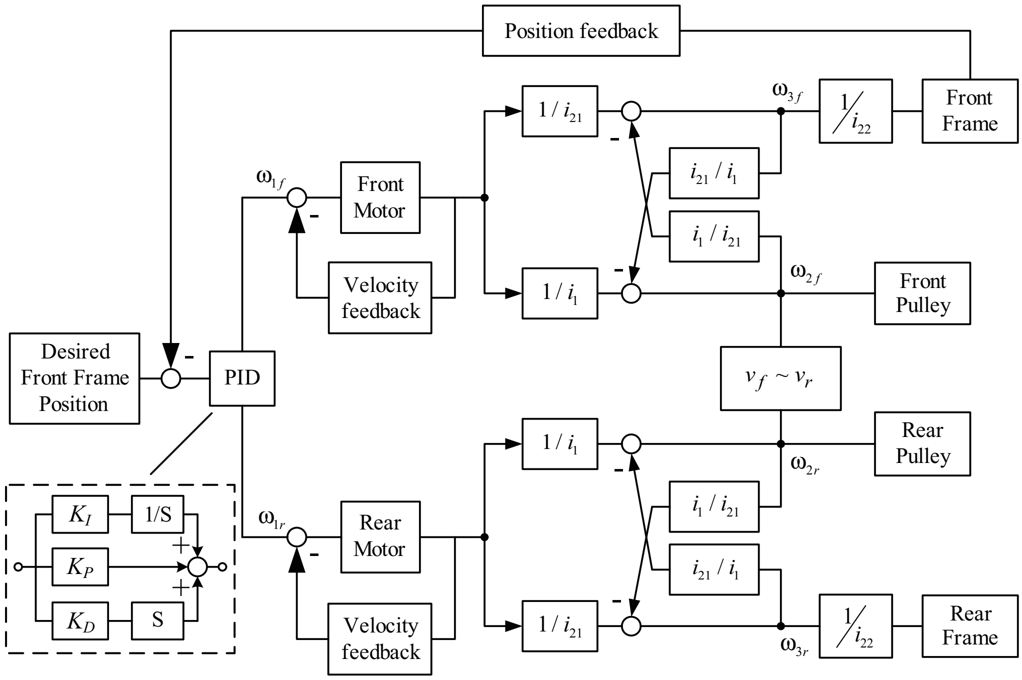

Figure 4.11. Posture realization through cooperative control

from 60° to 30°. In different control methods, for comparison, the same PID parameters ($K_P = 0.08$, $K_I = 0.03$ and $K_D = 0.01$ are tuned in this study) are used for the experiments.

4.3.1 Experiments with Direct Control

Figure 4.13 shows the experiment results using the direct control method. The rear actuator keeps a constant velocity of 65 rad/s while the front actuator is controlled to realize the posture change. As shown in Figure 4.13, when robot moves stably with the desired posture, the velocities of the front actuator and the rear actuator are the same, as stated in velocity analysis. Figure 4.14 shows the running states of the robot when time $t = 0\ s$, $15\ s$, $30\ s$.

4.3.2 Experiments using Indirect Control

The experiment results using the indirect control method are shown in Figure 4.15. The front actuator keeps a constant velocity of 65 rad/s while the rear actuator is controlled to

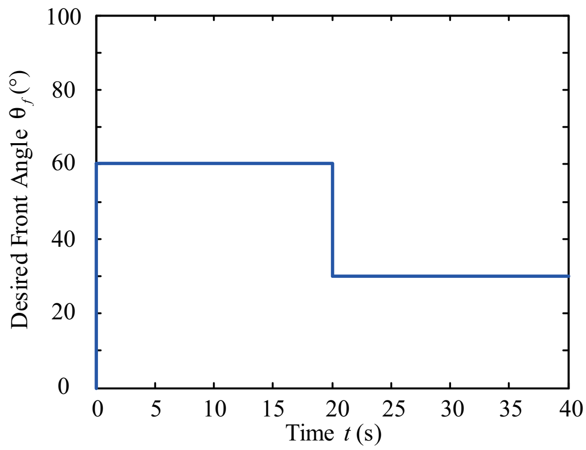

Figure 4.12. The desired control angle of the front frame

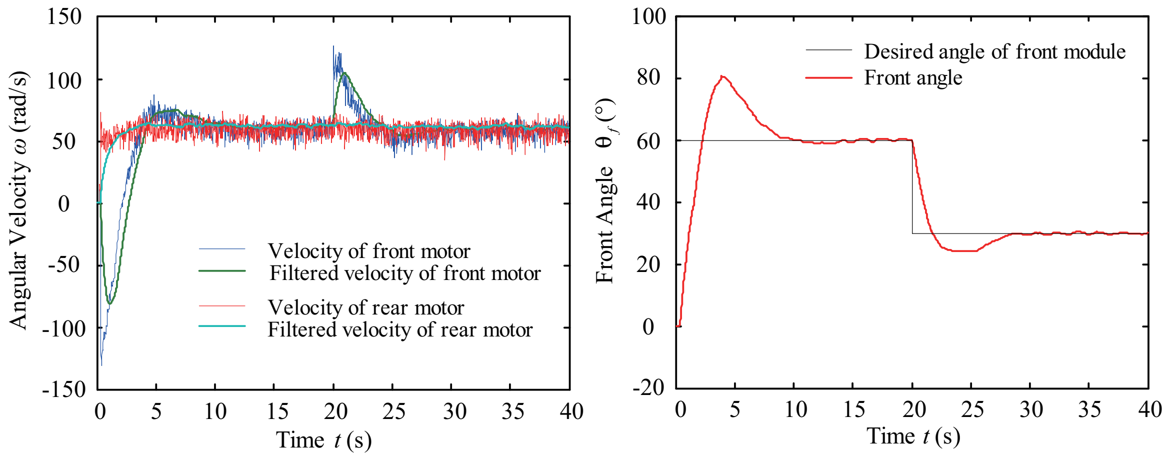

Figure 4.13. Experiment results using direct control method

realize the posture change. Compared with the results in direct control, the overshot of front angle response in this indirect control is much larger and the rising time is also much longer. When robot moves stably with the desired posture, the velocity of the front actuator and that of the rear actuator are also nearly the same, but are little roughly changed, compared with that in direct control. Figure 4.16 shows the running states of the robot when time $t = 0\ s$, $15\ s$, $30\ s$.

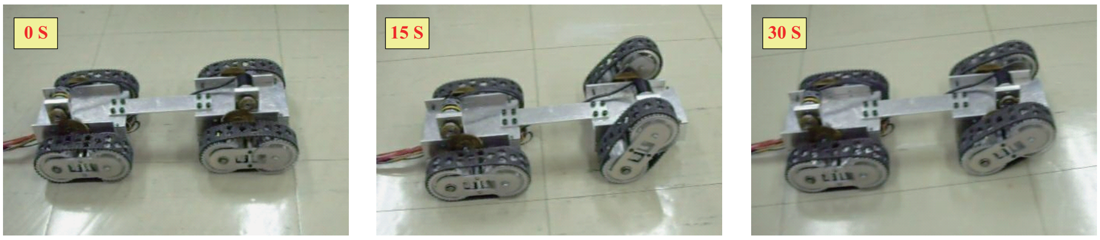

Figure 4.14. Experiment scenes using direct control method

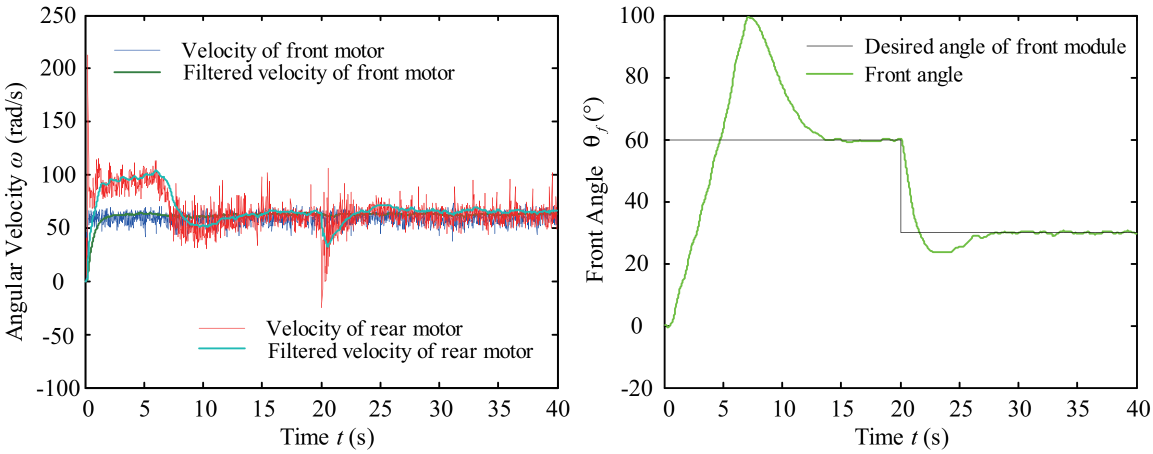

Figure 4.15. Experiment results using indirect control method

4.3.3 Experiments with Cooperative Control

The experiment results using the cooperative control method are shown in Figure 4.17. The feedback of posture angle of the front frame is used to control both the front actuator and the rear actuator at the same time. From results shown in Figure 4.17, the velocity outputs of the front and rear motors are adjusted by control program in the opposite directions. The response performance in cooperative control is very close to that in direct

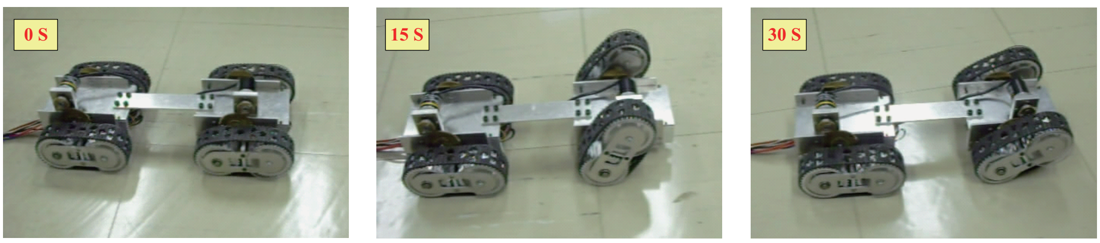

Figure 4.16. Experiment scenes using indirect control method

control. When robot moves stably, the velocity of the front actuator and that of the rear actuator are almost the same and keep the more steady change. Figure 4.17 shows the running states of the robot when time $t = 0$ s, 15 s, 30 s.

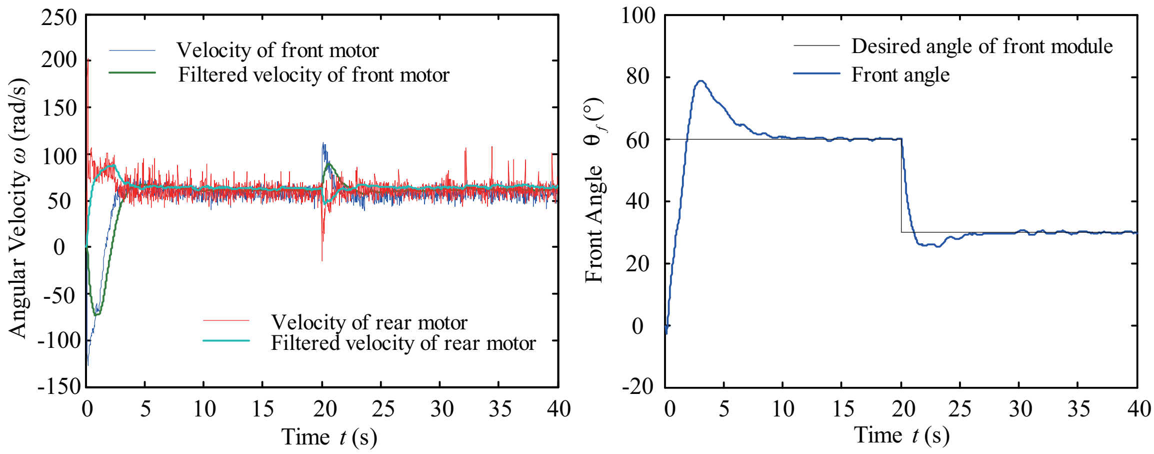

Figure 4.17. Experiment results using cooperative control method

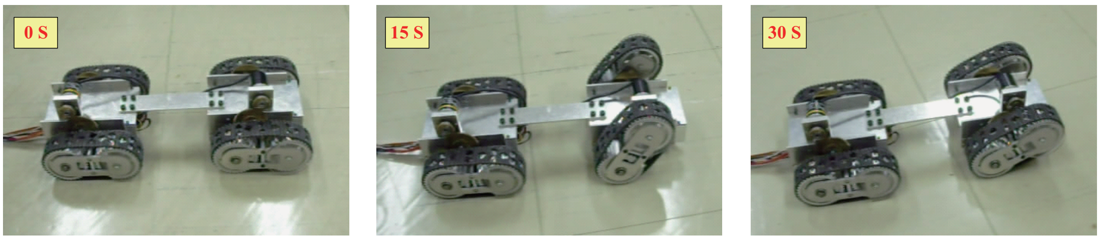

Figure 4.18. Experiment scenes using cooperative control method

4.3.4 Comparison of Responses among Different Control Methods

The front angle responses of direct control, indirect control and cooperative control are illustrated in Figure 4.19. From the results, it is known that the rising time of response using indirect control is much longer than that using direct control and cooperative control. Also the overshot of response using indirect control is much larger than that using direct control and cooperative control. The indirect control method which adjusts the angular velocity of rear actuator to change the linear velocity of robot and then to control the posture. In this process, the velocity of robot is relatively not easy to change since the whole robot has a big inertia. That is the reason why experiment using indirect control has relatively low response performance.

As shown in Figure 4.19, the responses using direct control and cooperative control have relatively close performance. However, the performance of response using cooperative control is superior to that using direct control.

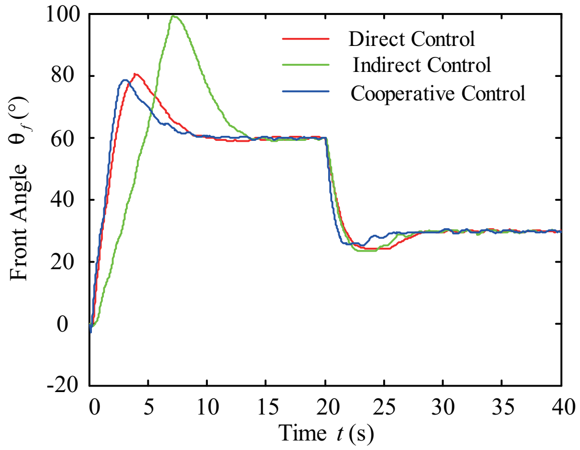

Figure 4.19. Comparison among different control methods

4.4 Summary

This chapter deals with the control issue of a tracked robot composed of two units of the developed crawler mechanism. On occasion, the front unit is required to be lifted up for overcoming obstacle actively and easily. We have introduced static analysis to demonstrate a possibly controlled posture and given the velocity analysis to verify the velocity distribution of each component in two crawler units. Different methods have been proposed to realize the posture that robot moves with the front unit lifted up. Using different control methods, experiments proved the static analysis and velocity analysis, and demonstrated that cooperative control shows better performance in the posture control than direct and indirect control.

Among the twelve different configurations of the dual-crawler-driven robot, controllable postures in config. 1 through 8 are stable equilibrium while other controllable postures in config. 9 through 12 are unstable equilibrium. Regarding the controllable postures in config. 1 through 8, similar control methods can be used to control the postures referring to the proposed methods for config. 1. Concerning the controllable postures with the properties of unstable equilibrium, new control methods should be further investigated to achieve the desired goal.

Chapter 5

Modular Design of the Crawler-driven Mechanism

Since there are several advantages of our proposed crawler mechanism, in order to extend the application of this mechanism, we attempt to design the mechanism as a modular unit. The basic idea underlying modular design is to organize the crawler mechanism unit as a set of distinct components that can be developed independently and then plugged together [80]. Therefore, the crawler module could be integrated into the anticipated robot system conveniently. As the applications of the modular design, a single-module robot and a four-module robot are accomplished by use of the module connection situated at the interface.

5.1 Modular Design for the Crawler Mechanism

5.1.1 Basic Requirements Under Consideration

We have proposed a crawler mechanism with a planetary gear reducer and the triangular reducer. The part power of motor is transmitted to the first output through the main shaft directly while another part of power is transmitted to the second output via the routine main shaft, shaft 2, shaft 3. Apparently, three shafts are deployed to distribute the power between two outputs. As a result, the frame unit of the crawler (see Figure 5.1(b)) must be

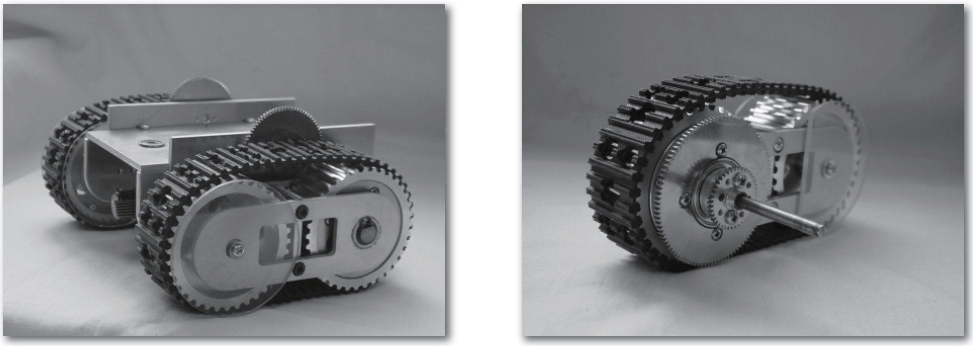

(a) The crawler mechanism unit (b) The frame unit of the crawler

Figure 5.1. Prototype of one crawler unit

connected with engaged gear pairs. This complex connection between the frame unit and crawler body spoils the process of modularity for the crawler mechanism.

We want to address this difficulty through a dedicated interface which is able to provide the mechanical and electrical information. As shown in Figure 5.2, the crawler module is capable of connecting to the anticipated robot body through the specially-designed interface.

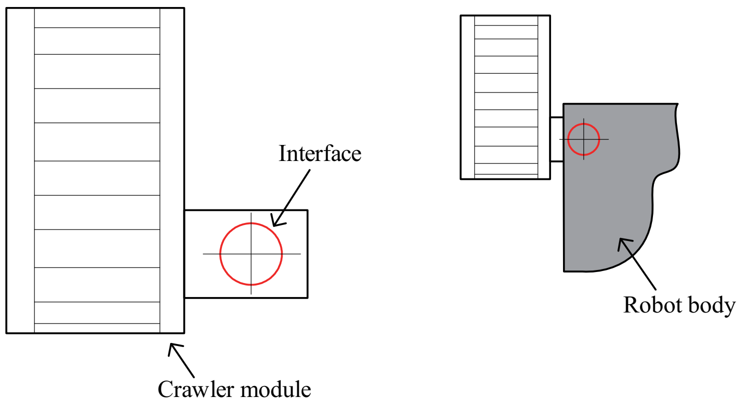

Figure 5.2. An idea for the modularity of crawler mechanism

Based on this principle, a possible mechanical transmission scheme for modular crawler is proposed first. Subsequently, the mechanical design of a modular crawler is conducted, based on the proposed transmission scheme. Waterproof and dust-proof qualities are also considered in this design process [81].

5.1.2 Transmission Scheme of a Modular Crawler

A transmission scheme of a modular crawler is shown in Figure 5.3. Only one motor is deployed to give two outputs in this modular crawler. This motor is included inside the crawler module.

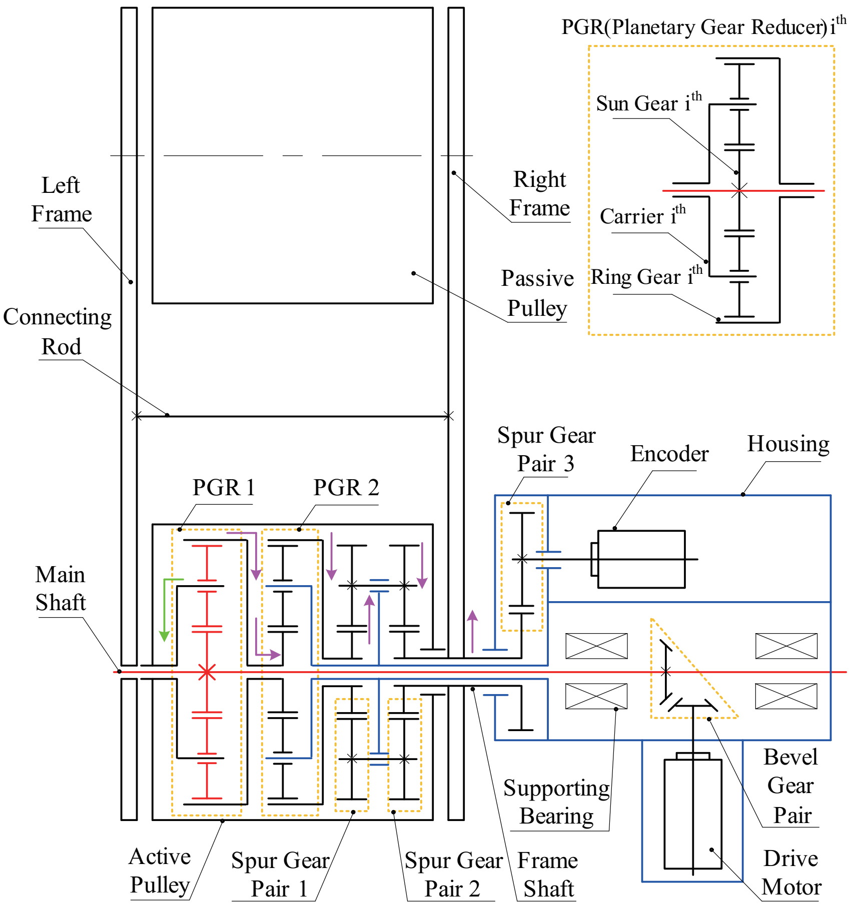

Figure 5.3. Transmission scheme of a modular crawler

As shown in Figure 5.3, power is transmitted to the "main shaft" from "drive motor" via a pair of bevel gear. Since the "main shaft" is fixed with "sun gear 1" of the "planetary gear reducer (PGR) 1", the power is transmitted to the first planetary gear reducer and then separately to the "carrier 1" and "ring gear 1", respectively. Due to the truth that "carrier 1" is fixed to the "active pulley", the output of "carrier 1" is transmitted to the active pulley to drive the crawler to move forwards as the first output. As another output of the "planetary gear reducer 1", the power of "ring gear 1" is transmitted to the "sun gear 2" of the "planetary gear reducer 2". Since the "carrier 2" is fixed with "Housing", without any movement, the output power from "ring gear 2" is transmitted to the "spur gear pair 1", and then to the "spur gear pair 2", finally to the "right frame" as the second output.

The transmission components are arranged inside the active pulley. The "left frame" and "right frame" are fixed via a part named "connecting rod". A timing belt adopted as the crawler track, connects the "active pulley" and "passive pulley" to propel the crawler. The "right frame" is connected to an encoder through "spur gear 3". The rotation angle of the frame is measured by the encoder.

5.1.3 Mechanism Design of a Modular Crawler

Based on the scheme proposed above, the detailed design of a modular crawler robot is developed while considering waterproof and dust-proof characteristics. The mechanical model of a new modular crawler is shown in Figure 5.4.

(1) Distribution of Reducer Ratios

The design of two reducer ratios for the two outputs from one input is pretty crucial in that it must meet the second and third terms stated in Chapter 2. From the static analysis of three locomotion modes, the first reducer ratio i_1 from "main shaft" to the "active pulley" and the second reducer ratio i_2 from "main shaft" to the "frame" are selected to be 4 and 27, respectively.

The reducer ratio from "sun gear 1" to "carrier 1" in the "PGR 1" is adopted as the reducer ratio of the first output i_1, the value of which is 4. Thus, according to the basics of planetary gear reducer, the reducer ratio from "sun gear 1" to "ring gear 1", named i_{21}, is -3. Due to the fact that the "ring gear 1" is connected with the "sun gear 2" using serration and the "carrier 2" is fixed with the housing statically, the reducer ratio of the second planetary gear reducer from "sun gear 2" to "ring gear 2" named i_{22} is selected to be -3. The "ring gear 2" transmits power to the frame through the "spur gear pair 1" (reducer

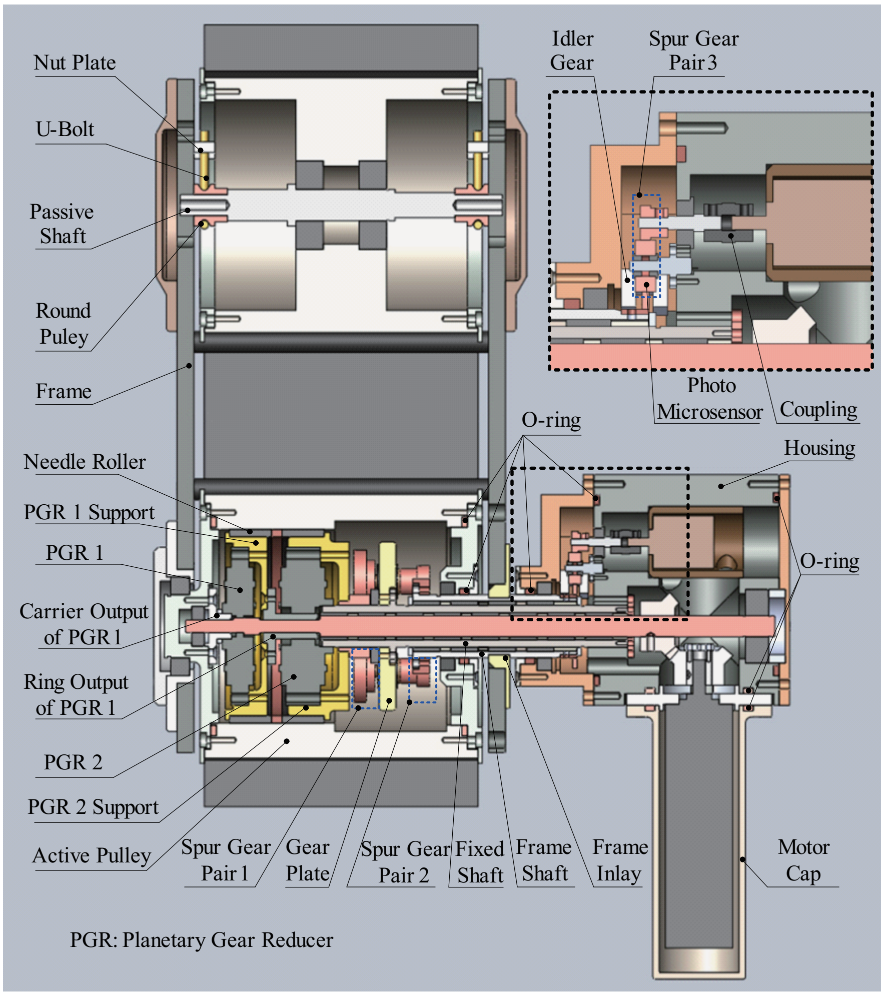

Figure 5.4. Mechanical model of a modular crawler

ratio $i_{23} = -1$) and "spur gear pair 2" (reducer ratio $i_{24} = -3$). Thus the reducer ratio from the "main shaft" to the "frame" i_2 can be calculated by

$$i_2 = i_{21} \times i_{22} \times i_{23} \times i_{24} = (-3) \times (-3) \times (-1) \times (-3) = 27 \tag{5.1}$$

Since both the reducer ratios i_1 and i_2 are positive, the two outputs certainly run in the same direction.

The "carrier 1" is connected with "carrier output of PGR 1" which is fixed to the "active pulley". Thus, output of "carrier 1" is deployed as the first output to the active pulley. The "ring gear 1" of the "planetary gear reducer 1" is fixed with "PGR 1 support" which is supported by a "needle roller" in the active pulley. The "PGR 1 support" is also fixed to “ring output of PGR 1” which is connected to “sun gear 2” by serration. The “PGR 2 support” also supported by a needle roller in the active pulley is fixed to the “ring gear 2” and the first gear of “spur gear pair 1”, respectively. Since the “carrier 2” is fastened with “fixed shaft” which is fixed with the “housing”, the single output of “PGR 2” from the “ring gear 2” is transmitted to “spur gear pair 1”. The output gear of “spur gear pair 1” and input gear of “spur gear pair 2” are fixed on a shaft which is supported by rolling bearing inside the hole of “gear plate”. The “gear plate” is fastened with “fixed shaft” with screws as a static part. The output gear of “spur gear 2” is fixed to “frame shaft” on the left side which is supported on “fixed shaft” with needle rollers. The middle of “frame shaft” is fixed to the “frame inlay” which is also fixed to the “frame” through screws. The right side of “frame shaft” is connected to the input gear of “spur gear pair 3” for encoding the rotation angle of the frame. Lastly, the power is transmitted from the “spur gear pair 2” to the “frame” as the second output.

(2) Setup of the Encoder and Zero Positioning of the Frame

To obtain a high resolution of the rotation angle of the frame, the mechanism of “spur gear pair 3” should be designed with a larger reducer ratio. If two gears are adopted here, the size of input gear should be designed much bigger to get a high reducer ratio. This will inevitably cause the outer housing to become much larger. Thus, to prevent this undesirable effect on the outer dimension of the housing, an idler gear is deployed in the transmission of “spur gear pair 3” shown in Figure 5.5. Consequently, this reducer ratio from the frame to the encoder is selected to be 4 considering other related dimensions.

Since an incremental encoder is adopted to obtain the rotation angle of the frame, it is extremely crucial to decide the zero position for the incremental encoder. As shown in Figure 5.5, a photo micro-sensor is fixed on the housing statically with the input gear of “spur gear pair 3” penetrating its U slot. A small hole drilled near the edge of the input gear turns the photo sensor light on while the other area prevents the light penetrating so as to turn the photo sensor light off. This on/off signal is used to judge whether the zero

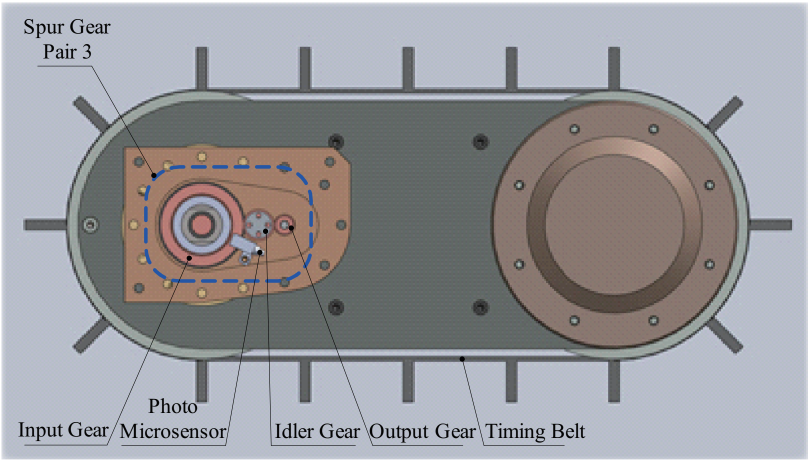

Figure 5.5. Zero positioning for the frame

position of the frame is reached. The current position in Figure 5.5 is considered as the zero position of the frame.

(3) Tension Mechanism for the Belt

As shown in Figure 5.5, the timing belt is deployed as the track which connects the active pulley and passive pulley. There are several cogs exposed on the exterior side of the timing belt. The cogs can increase the friction effectively to improve the locomotion of crawler in rough terrain. Tension mechanism is a necessary part to keep the belt always tight. As shown in Figure 5.4, "passive shaft" is located in the U-shaped hole of the frame which enables the passive shaft to move freely in the tension direction of timing belt. "Nut plate" fixed with the frame cooperates with the "U-bolt" to change the distance between passive pulley and active pulley so as to keep the timing belt always tight.

(4) Sealing of Transmission System

In this modular crawler, both waterproof and dust proof are considered in the design process. As shown in Figure 5.4, "motor cap" is used to prevent water and dust to damage the motor. The interior transmission devices of active pulley and housing adopt closed mechanism. At the connecting interface, "O-rings" are deployed to keep the inside sealed.

Table 5.1. Major parameters of the modular crawler

Weight	11.5 [Kg]
Size(L× W× H)	453 [mm], 302 [mm], 169 [mm]
Reducer Ratio	4 (Output 1), 27 (Output 2)
Torque	5.1 [Nm], 34.4 [Nm]
Speed	0.5 [m/s], 8.6 [rpm]

(5) Design of Module Interface

As a modular crawler, the crawler should provide a convenient connection interface to robot system. As shown in Figure 5.7, the top surface of the housing with eight screw holes is used as the mechanical interface and an air plug is adopted as the electrical interface. The mechanical interface makes the modular crawler easily attachable to the anticipated robot body by screw fastening. The internal electrical signals including encoder of the drive motor, photo micro-sensor, encoder of the frame can be provided through the electrical interface (air plug).

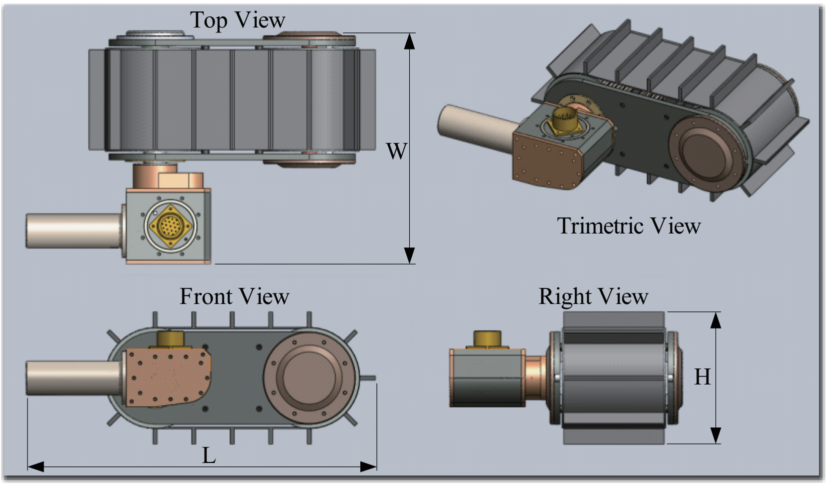

Figure 5.6. CAD views of the modular crawler

CAD views of the modular crawler in front, top, right, and trimetric perspectives are shown in Figure 5.6, and the real prototype is shown in Figure 5.7. The outer dimensions of this modular crawler are listed in Table 5.1.

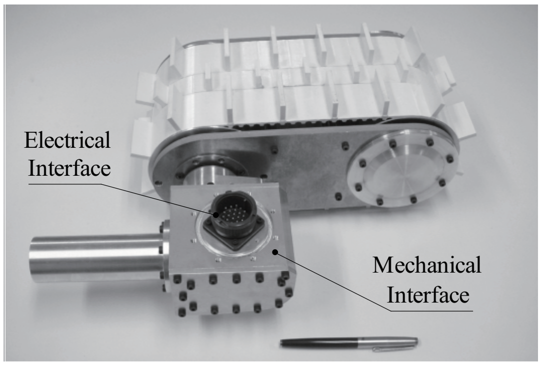

Figure 5.7. Prototype of a modular crawler

5.1.4 Experimental Validation for the Single Modular Crawler

As stated in Chapter 2, the under-actuated system in which one motor input gives two different outputs makes it impossible to treat as an individual mobile system. Thus, in the following experiments the housing of the modular crawler is held horizontally by hand.

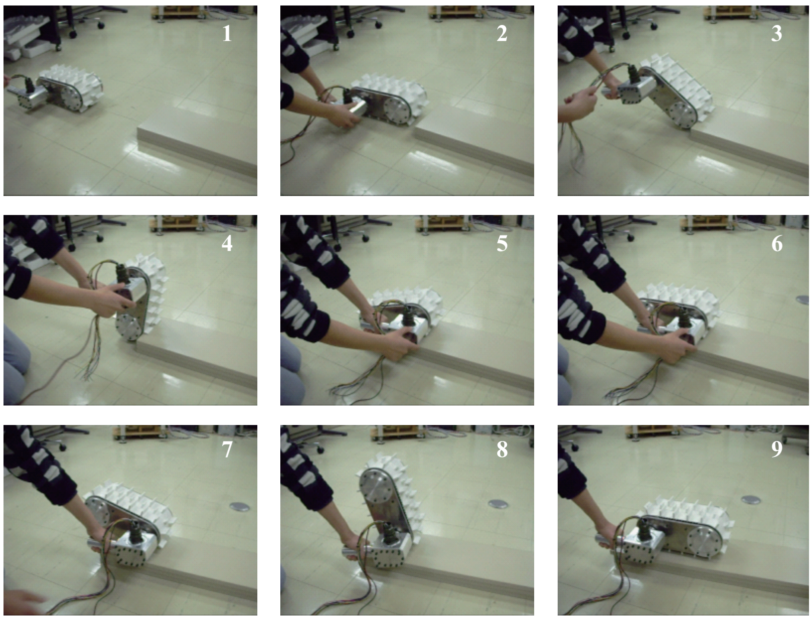

Figure 5.8. Experiment scenes of a single-module crawler

First, the air plug is connected and then the power is turned on. The experiment scenes of the housing of the modular crawler held by hand are shown in Figure 5.8. From scene 1 to 2, the crawler moves forwards as the normal tracked robot (moving mode). When

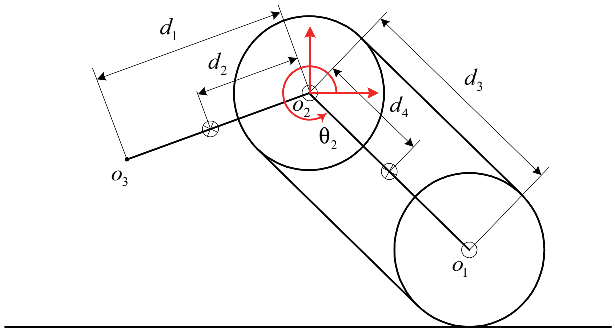

Figure 5.9. Simplified diagram of the crawler module

the crawler encounters an obstacle, the first output for driving the track is limited and the second output for driving the frame plays a role in negotiating the obstacle, as shown in scenes 3, 4, 5, and 6. After overcoming the obstacle, the modular crawler begins to recover to the initial position, as shown in scenes 7, 8, and 9.

From the experiment shown in Figure 5.8, we know that the proposed three locomotion modes of a single modular crawler can be well realized in this modular design.

The simplified diagram of the modular robot is demonstrated in Figure 5.9. The interface is located at point "o_3", through which the crawler module can be integrated into the desired robot systems. Using the proposed new crawler module, several kinds of robots can be constituted, such as one-crawler-module, four-crawler-module. The two new crawler-driven robots will be discussed in the following contents.

5.2 A Robot with One Crawler Module

5.2.1 Compositions of the Robot

A one-crawler-module robot can be composed of a crawler module, a robot body, and one wheel. For instance, the crawler module connected with a robot body and a rear pulley, constitutes a mobile system. The chief dimensions of the robot are illustrated in Figure 5.10.

When the front angle θ_2 varies from 0° to 360°, there are two typical configurations for

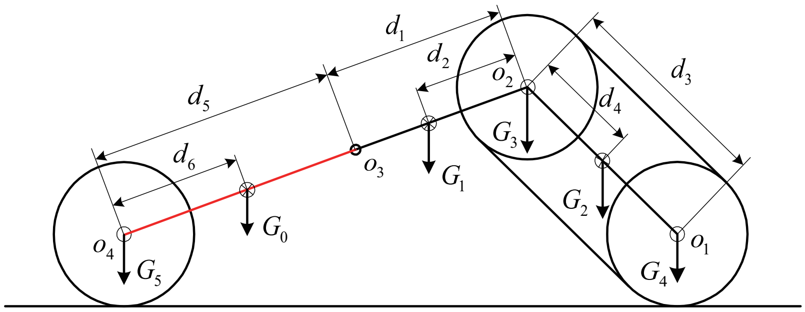

Figure 5.10. A robot with the crawler module

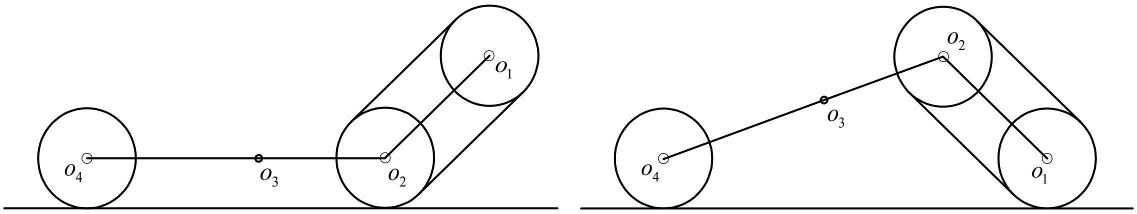

(a) Configuration 1 ($0° < \theta_2 < 180°$) (b) Configuration 2 ($180° < \theta_2 < 360°$)

Figure 5.11. Two typical configurations of the robot

this crawler-driven robot. The first one is the case that the front frame is lifted up with $0° < \theta_2 < 180°$ while the other is that the front frame rotates down with $180° < \theta_2 < 360°$ as shown in Figure 5.11.

5.2.2 Modular Mechanic Model for the Crawler Robot

To model this modular crawler correctly, statics for describing the modular mechanism is discussed in this section. An example consisting of one modular crawler mechanism, one pulley and robot body is presented as the object for study [82].

(1) Basic Equilibrium for the Crawler Mechanism

In two-dimensional environment, two forces F_x, F_y and one torque M_z are considered into the quasi-static model when the robot body is disconnected from the interface, as shown in Figure 5.12. The equilibrium of the interface can be expressed by

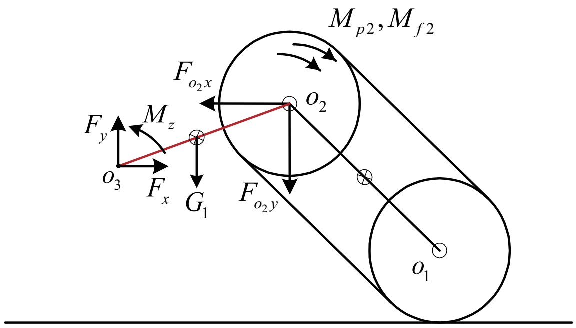

Figure 5.12. Force diagram of the connecting interface

$$\begin{cases} \Sigma F_x = -F_{o_2x} + F_x = 0 \\ \Sigma F_y = -F_{o_2y} + F_y - G_1 = 0 \\ \Sigma M_z = -M_{p2} - M_{f2} + M_z - F_y d_1 \cos\beta \\ \qquad + G_1 d_2 \cos\beta + F_x d_1 \sin\beta = 0 \end{cases} \tag{5.2}$$

where F_x, F_y and M_z are the reaction forces exerted at the point "o_3" on the connecting interface; F_{o_2x} and F_{o_2y} are the reaction forces acting at the point "o_2" on the interface; M_{p2} and M_{f2} are reaction torques from the front active pulley and frame, respectively, herein, $M_{f2} = KM_{p2}$.

Concerning the active pulley, frame, and the passive pulley, Figure 5.13 shows the possible forces exerted on each part. To describe all the cases for the front crawler unit, normal forces N_1, N_2, tangential forces F_{f1x}, F_{f2x} and rolling resistance M_{rol1}, M_{rol2} are deemed to exist at all times, as shown in Figure 5.13.

Specially, two extra parameters are used to describe the contact status between the front crawler unit and ground.

$$\begin{cases} e_1 = 0,\ e_2 = 1 \quad when\ \sin\theta_2 > 0 \\ e_1 = 1,\ e_2 = 1 \quad when\ \sin\theta_2 = 0 \\ e_1 = 1,\ e_2 = 0 \quad when\ \sin\theta_2 < 0 \end{cases} \tag{5.3}$$

When only the front active pulley contacts ground with the property $\sin\theta_2 > 0$ ($0° < \theta_2 < 180°$), the coefficients $e_1 = 0, e_2 = 1$ stand for this case; the coefficients $e_1 = 1, e_2 = 1$ are used to denote the case where both the front active and passive pulleys contact ground

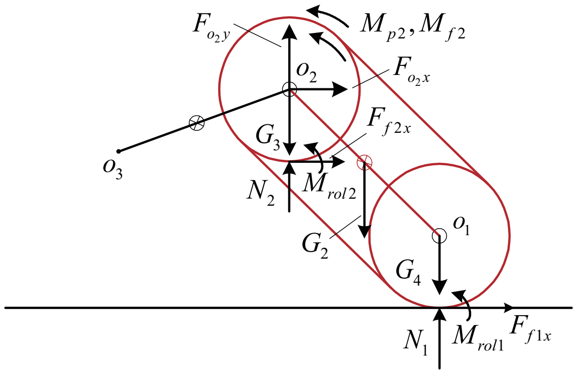

Figure 5.13. Force diagram of the front crawler unit

concurrently; when only the front passive pulley contacts ground with attribute $\sin\theta_2 < 0$ ($180° < \theta_2 < 360°$), the coefficients $e_1 = 1, e_2 = 0$ are used to stand for this case.

Subsequently, through using the presumed coefficients e_1, e_2 for describing the status of the front crawler, the balance of the front crawler unit can be expressed by

$$\begin{cases} \Sigma F_x = F_{o_2x} + e_1 F_{f1x} + e_2 F_{f2x} = 0 \\ \Sigma F_y = F_{o_2y} + e_1 N_1 + e_2 N_2 - G_2 - G_3 - G_4 = 0 \\ \Sigma M_z = M_{p2} + M_{f2} + (e_1 F_{f1x} + e_2 F_{f2x})R \\ \qquad - G_2 d_4 \cos\theta_2 - e_1 F_{f1x} d_3 \sin\theta_2 - G_4 d_3 \cos\theta_2 \\ \qquad + e_1 N_1 d_3 \cos\theta_2 + e_1 M_{rol1} + e_2 M_{rol2} = 0 \end{cases} \tag{5.4}$$

where F_{f1x}, F_{f2x} are the tangential forces at the rim of the passive and active pulleys, respectively; N_1, N_2 are the normal forces at the rim of the passive and active pulleys, respectively; M_{rol1} and M_{rol2} are the rolling resistance exerted at the rim of the passive and active pulleys. The coefficients e_1, e_2 in the equations are used to describe different postures while the angle θ_2 varies from 0° to 360°.

Herein, the rolling resistance can be calculated by

$$M_{rol1} = \delta N_1$$
$$M_{rol2} = \delta N_2$$

where δ is the coefficient of rolling resistance.

Excluding the front crawler module, the rear body and pulley should also be appended

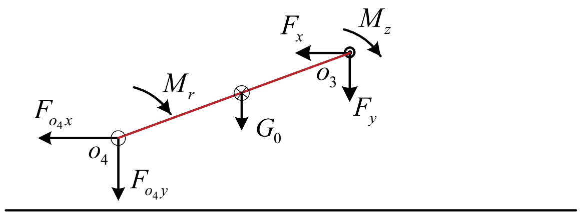

Figure 5.14. Force diagram of the robot body

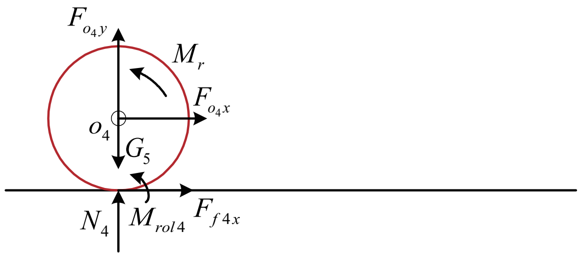

Figure 5.15. Force diagram of the rear pulley

to the mechanic model. Regarding the robot body outlined in red line, the forces illustrated in Figure 5.14 should comply with the equations as follows:

$$\begin{cases} \Sigma F_x = -F_{o_4x} - F_x = 0 \\ \Sigma F_y = -F_{o_4y} - F_y - G_0 = 0 \\ \Sigma M_z = -M_r - M_z + F_x d_5 \sin\beta \\ \qquad\qquad - F_y d_5 \cos\beta - G_0 d_6 \cos\beta = 0 \end{cases} \tag{5.5}$$

where F_{o_4x}, F_{o_4y} and M_r are the interaction forces between the rear pulley and robot body; F_x, F_y and M_z are the interaction forces between the connecting interface and robot body.

With regard to the rear active pulley, the forces illustrated in Figure 5.15 should conform to the following equations:

$$\begin{cases} \Sigma F_x = F_{o_4x} - F_{f4x} = 0 \\ \Sigma F_y = F_{o_4y} + N_4 - G_5 = 0 \\ \Sigma M_z = M_r + F_{f4x} R + M_{rol4} = 0 \end{cases} \tag{5.6}$$

where F_{f4x}, N_4 and M_{rol4} are the tangential, normal forces and rolling resistance exerted on the rear pulley, respectively.

(2) Analysis Results

Solving the equations listed above, we can get the required torques and the relevant contact forces for the robot to keep equilibrium.

For "Configuration 1", the driving torque for the front active pulley can be obtained by

$$M_{p2} = (G_2 d_4 \cos\theta_2 + G_4 d_3 \cos\theta_2)/K \tag{5.7}$$

The coefficients of friction can be determined by

$$\mu_2 = F_{f2x}/N_2 \tag{5.8}$$

$$\mu_4 = F_{f4x}/N_4 \tag{5.9}$$

For "Configuration 2", the driving torque for the front active pulley can be obtained by

$$M_{p2} = (D \cdot P - E - T \cdot L)/(Q + T \cdot H) \tag{5.10}$$

where

$C = (d_1 + d_5)\sin\beta/K$

$D = (d_1 + d_5)\cos\beta/K$

$E = [G_1 d_2 \cos\beta - G_0 d_6 \cos\beta + \delta(G_0 + P + G_5)]/K$

$H = -(KR + d_3 \sin\theta_2)/[d_3 \cos\theta_2 (R + \delta\tan\theta_2)]$

$L = (G_2 R d_4/d_3 + G_4 R)/(R + \delta\tan\theta_2)$

$P = G_1 + G_2 + G_3 + G_4$

$Q = C/R - 1$

$T = C\delta/R + D$

The coefficients of friction can be determined by

$$\mu_1 = F_{f1x}/N_1 \tag{5.11}$$

$$\mu_4 = F_{f4x}/N_4 \tag{5.12}$$

Table 5.2. A group of robot parameters for simulation

m_0	9.8 [Kg]	d_1	0 [mm]
m_1	2.5 [Kg]	d_2	0 [mm]
m_2	2.9 [Kg]	d_3	200 [mm]
m_3	4.1 [Kg]	d_4	100 [mm]
m_4	2.0 [Kg]	d_5	756 [mm]
m_5	2.0 [Kg]	d_6	378 [mm]

5.2.3 Simulation Results

This section will give the numerical results for the modular mechanic model. A group of parameters for the robot with one crawler module is listed in Table 5.2. Several physical parameters play an important role in the performance of the robot and thus the effects of the parameter on the mobility will be discussed in the following contents.

(1) Simulation Results of One Group of Parameters

Figure 5.16(a) shows the normal reaction forces of the active and passive pulleys from ground considering the rolling resistance. When the front angle θ_2 varies from 0° to 180°, the normal force N_2 decreases while the normal force N_4 increases correspondingly. When the front angle θ_2 varies from 180° to 360°, the normal force N_1 decreases while the normal force N_4 increases correspondingly. It is obviously viewed that N_2 is shaped symmetrically with N_4 regarding the horizontal line $N = G/2$; N_1 and N_4 are also in the same manner. This phenomenon is a consequence of the following equations:

$$\begin{cases} N_2 + N_4 = G \ \ (\theta_2 \in [0^\circ, 180^\circ]) \\ N_1 + N_4 = G \ \ (\theta_2 \in [180^\circ, 360^\circ]) \end{cases} \tag{5.13}$$

where the total weight of robot $G = G_0 + G_1 + G_2 + G_3 + G_4 + G_5$.

Also, for two configurations, there is a large step at the angle $\theta_2 = 180°$. When the front crawler mechanism rotates for one round, the posture shifting process can be divided

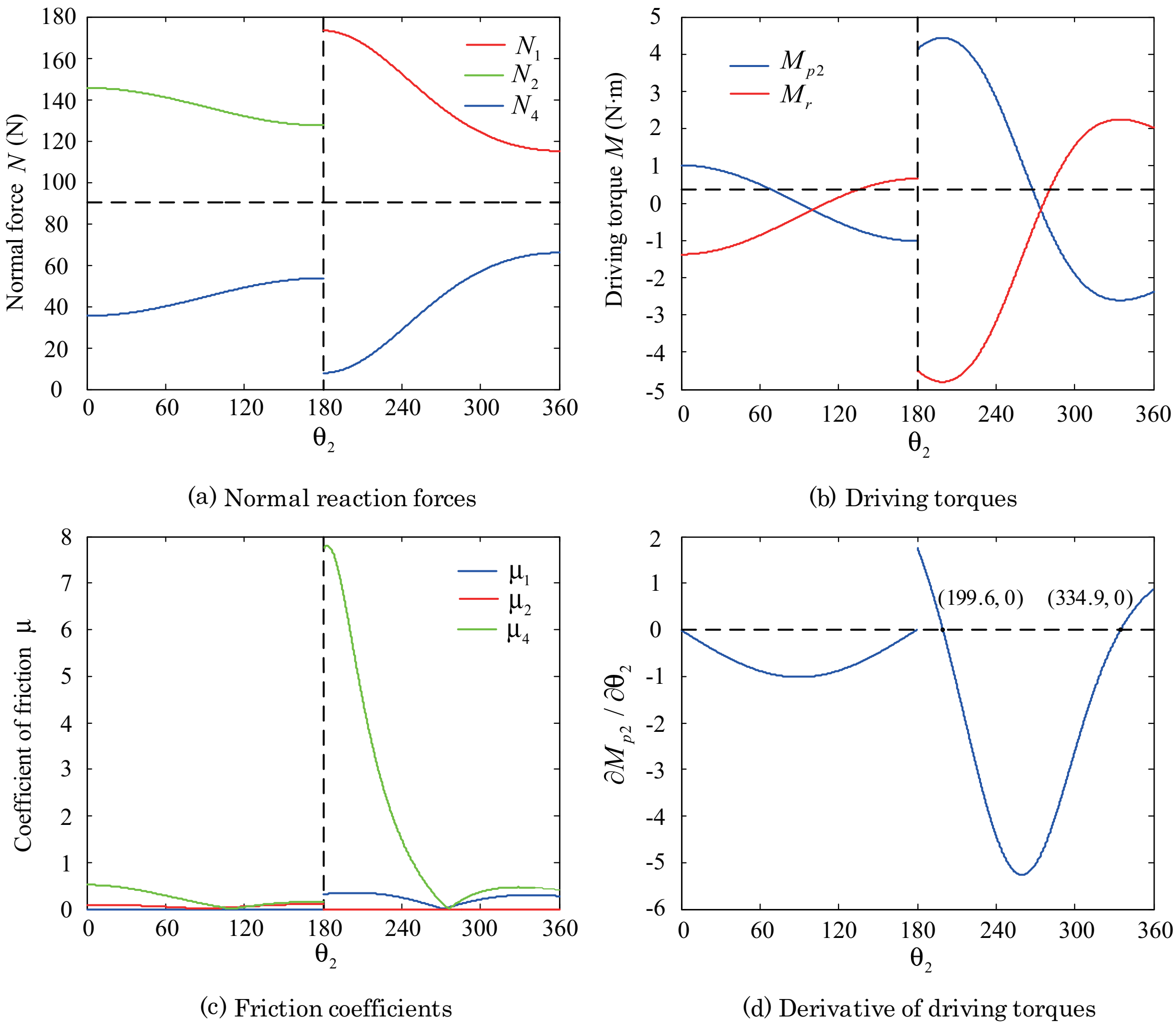

(a) Normal reaction forces

(b) Driving torques

(c) Friction coefficients

(d) Derivative of driving torques

Figure 5.16. Numerical results with the group of robot parameters

into several steps as shown in Figure 5.17. For the front angle θ_2 at 180°, there are two states for the front crawler mechanism: state I and state II.

In state I, only the front active pulley contacts ground while only the front passive pulley contacts ground in state II. For state I, the front output to the frame is provided to lift the front crawler arm up only, while both the front crawler arm and the robot body are lifted up by the output to the frame in state II. Therefore, there is a discontinuous step for the driving toques and normal forces from state I to state II.

The driving toques of the front and rear units are obtained as shown in Figure 5.16(b). When the front angle θ_2 varies from 0° to 180°, the driving torque of front pulley M_{p2}

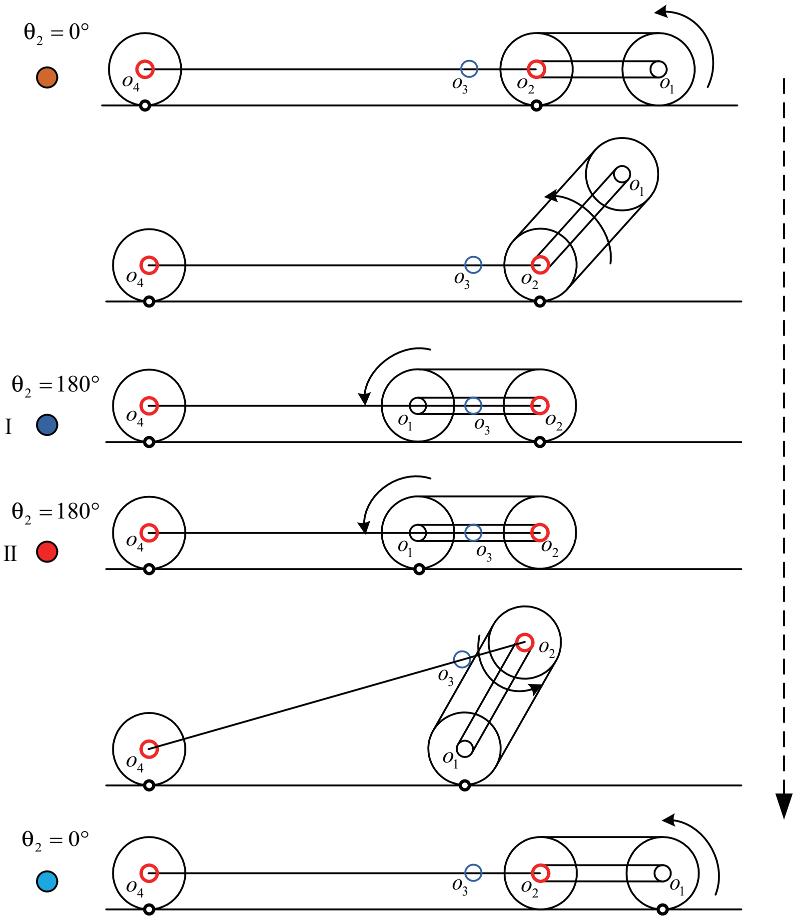

Figure 5.17. Configuration shifting process of the robot

decreases while the driving torque of rear pulley M_r increases correspondingly. When the front angle θ_2 varies from 180° to 360°, the driving torque of front pulley M_{p2} firstly increases and then decreases while driving torque of rear pulley M_r firstly decreases and subsequently increases correspondingly. Also, for two configurations, there is a large step at the angle $\theta_2 = 180°$. As shown in Figure 5.16(d), the derivatives of driving torques demonstrate that the inflection points are located at (199.6°, 0) and (334.9°, 0), respectively. It appears that M_{p2} is shaped symmetrically with M_r corresponding to the horizontal line $M = -M_{rol}/2$. This is because of the equation as follows:

$$M_{p2} + M_r + M_{rol} = 0 \ \ (\theta_2 \in [0°, 360°])$$

where the total rolling resistance $M_{rol} = M_{rol2} + M_{rol4}$.

Figure 5.16(c) shows the friction conditions of the active and passive pulleys from ground. When the front angle θ_2 varies from $0°$ to $180°$, just the front active pulley and the rear pulley contact ground. The friction conditions of the front active pulley and rear pulley are denoted by μ_2, μ_4, respectively. We can find that the coefficient μ_4 is relatively larger than μ_2. When the front angle θ_2 varies from $180°$ to $360°$, just the front passive pulley and the rear pulley contact ground. The friction conditions of the front active pulley and rear pulley are denoted by μ_1, μ_4, respectively. It is easily found that the coefficient μ_4 varies dramatically from the state I to state II at the angle $\theta_2 = 180°$. In the current status of robot parameters, this robot is almost impossible to transfer the posture from state I to state II.

The major parameters constituting the robot affect the performance of the robot dramatically. Thus, the effects of some structural parameters on the performance of the robot will be studied as follows.

(2) Effects of Each Major Parameter

We will discuss the effects of each parameter on the normal contact force and driving torques. Herein, simulation results are compared when only one parameter is selected to change from smaller to larger value in series and other parameters are kept as the constants. In the following parts, the effects of the parameters d_5, G_0, G_5 are investigated individually.

Parameter d_5

As shown in Figure 5.18, when the parameter d_5 changes in series $d_5/2$, d_5, $2d_5$, $4d_5$, the normal reaction forces and the driving torques alter correspondingly. When the parameter d_5 changes from $d_5/2$ to $4d_5$, the force N_1 decreases and the force N_4 increases correspondingly.

The torque M_{p2} decreases and M_r increases when the front angle θ_2 belongs to the range $[180°, 360°]$. However, the the driving torques do not perform any change when the front angle is in the range $[0°, 180°]$ due to the fact that there is no any relation between the driving torque and the parameter d_5 in configuration 1 according to Equation (5.7).

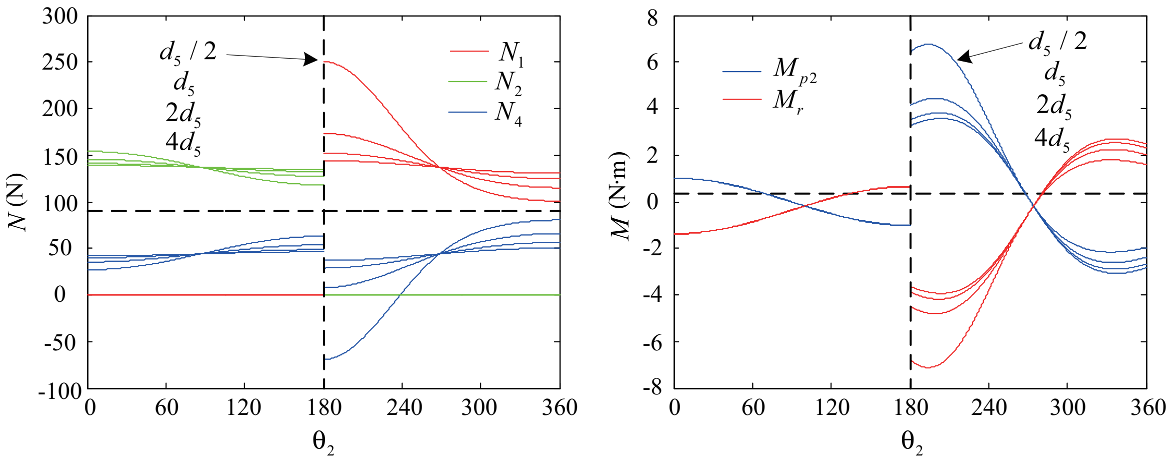

Figure 5.18. Effects of the parameter d_5

Parameter G_0

As illustrated in Figure 5.19, when the parameter G_0 changes in series $G_0/2$, G_0, $2G_0$, $4G_0$, the normal reaction forces and the driving torques vary correspondingly. When the parameter G_0 changes from $G_0/2$ to $4G_0$, the forces N_1, N_2 and N_4 increase correspondingly due to Equation (5.13) with respect to the distribution of normal contact forces.

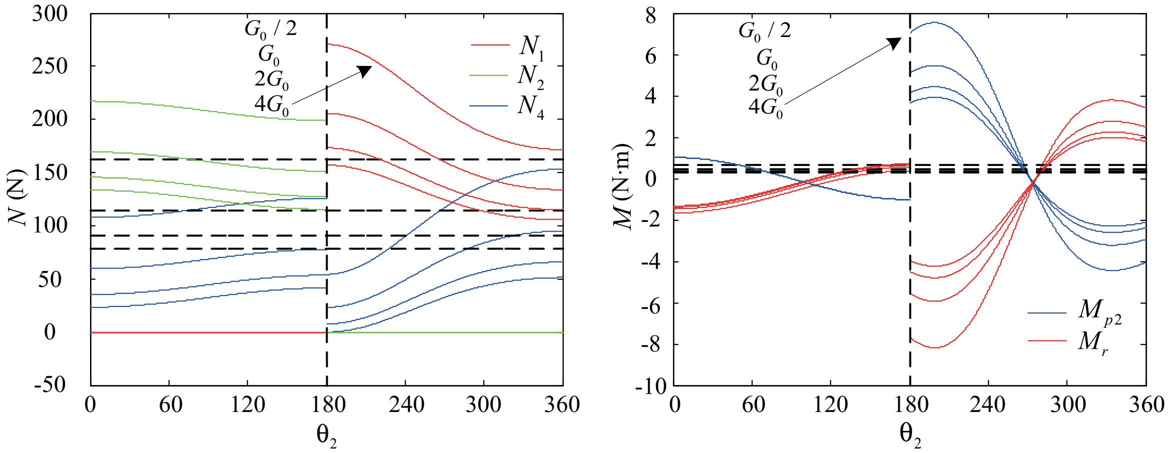

Figure 5.19. Effects of the parameter G_0

The torque M_{p2} decreases and M_r increases when the front angle θ_2 is in the range within $[180°, 360°]$. However, the driving torques do not vary at all when the front angle is in the range $[0°, 180°]$ due to the fact that there is no any relation between the driving torque and the parameter G_0 in configuration 1 according to Equation (5.7).

Parameter G_5

As shown in Figure 5.20, when the parameter G_5 changes in series $G_5/2$, G_5, $2G_5$, $4G_5$, the forces N_1 and N_4 increase correspondingly.

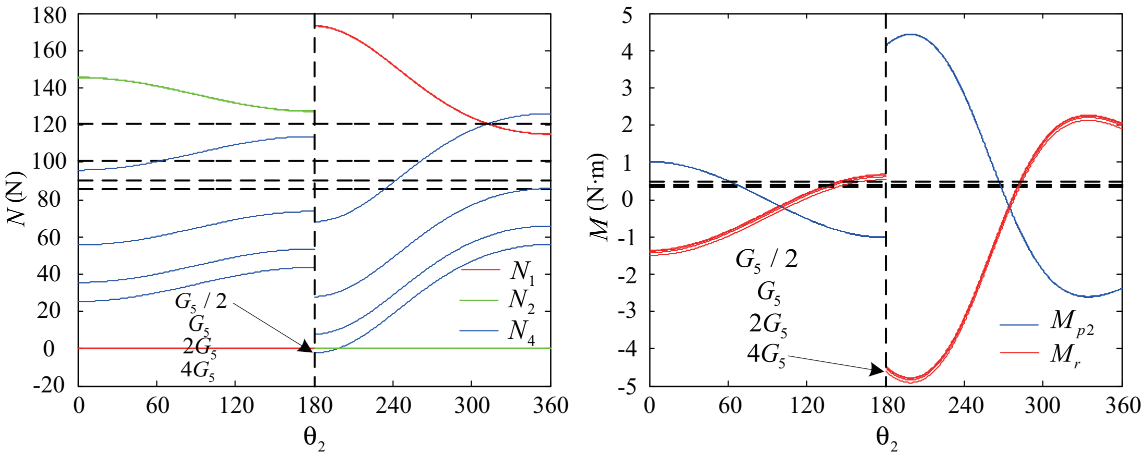

Figure 5.20. Effects of the parameter G_5

However, the the driving torques do not perform any change due to the fact that there is no any relation between the driving torque and the parameter G_0 in configuration 1 according to Equation (5.7) and Equation (5.10).

5.2.4 Experiment of Negotiating a Step

Experiments are conducted to confirm the mobility of the proposed modular crawler. With regard to one crawler module, the experiment is used to verify the three locomotion modes in a real prototype.

As stated in Chapter 2, this under-actuated system in which one motor input gives two different outputs makes it impossible to treat just one modular crawler as an individual mobile system. Therefore, in the following experiments, an assistant rod is connected to the interface of the crawler module to provide necessary support as shown in Figure 5.21.

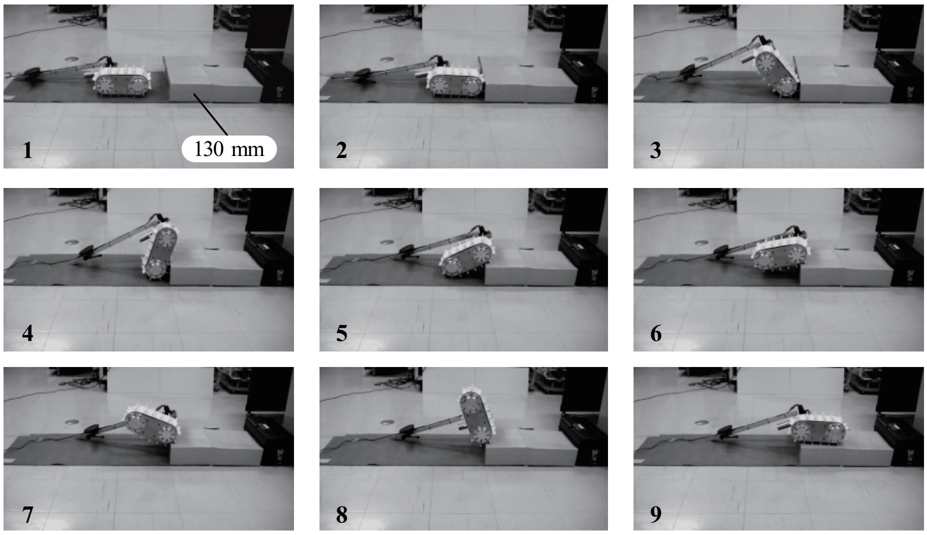

Figure 5.21. Scenes of a single modular crawler negotiating a step of 130 mm

From scenes 1 to 2, the crawler moves forwards like a normal tracked robot (moving mode). When the crawler encounters a step, the first output for driving the track is constrained and the second output for driving the frame plays a role in negotiating the obstacle, as shown in scenes 3, 4, 5, and 6. After overcoming the obstacle, the modular crawler begins to recover to the initial posture, as shown in scenes 7, 8, and 9.

From the experiment shown in Figure 5.21, it is known that the proposed three locomotion modes of single modular crawler can be achieved in this modular crawler.

5.3 A Robot with Four Crawler Modules

5.3.1 Profile of the Robot Structure

As an example of the possible applications of the proposed modular crawler, a four-crawler-driven robot has been built as shown in Figure 5.22. Four crawler modules are connected to the robot body through their interfaces. An effect view of the four-crawler-module robot is depicted in Appendix B.

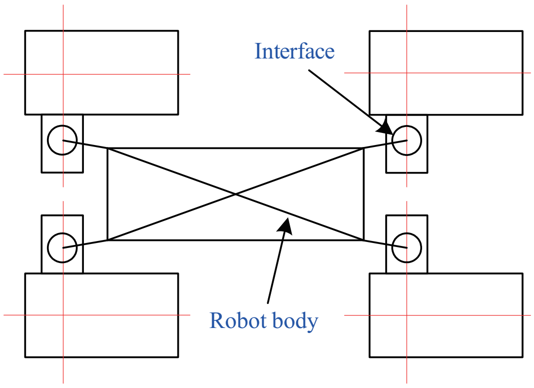

(a) Assembly

(b) Prototype

Figure 5.22. A four-crawler-module robot

5.3.2 Control System of the Four-crawler-module Robot

A centralized control system is developed to perform the posture control. Control computers are separated from the mechanical system of the robot. The control computers containing a master computer and a target computer are employed to constitute xPC target hardware. A D/A converter and a counter board are installed in the target computer through PCI slots. The output voltage of D/A converter is transmitted to the port of reference voltage input of motor driver as the speed command. The counter board can get the pulses of both motor encoders and frame encoders to control speed of the motors and position of the rotating frames.

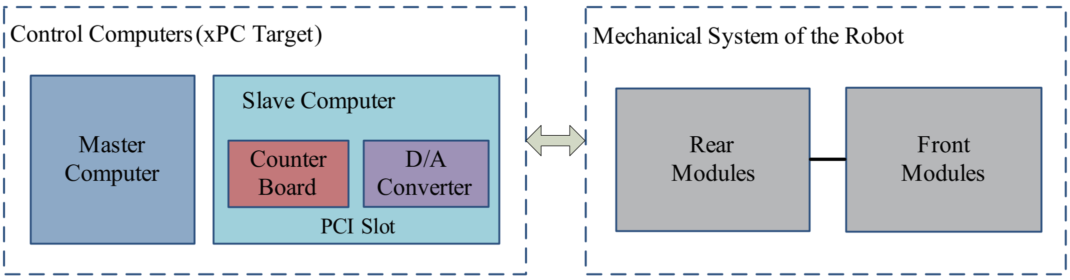

Figure 5.23. The centralized system for the posture control

In the Appendix C, we have developed a wireless decentralized control system, in which an onboard computer is employed to execute the control tasks in the robot body and a laptop is selected as the control station to send the command signal and receive the state information of the robot.

5.3.3 Experiments with a Four-crawler-module Robot

Experiments were conducted to confirm the mobility of the proposed modular crawler mechanism. A four-crawler-driven robot which consists of four modular crawler mechanisms is also adopted as the object to do experiments in an obstacle environment.

A four-crawler-driven robot equipped with four modular crawlers could perform good adaptability over rough terrain. This four-crawler-driven robot can overcome obstacles passively without any control as shown in Figure 5.24(a). In addition, the posture in which the front crawler modules are lifted up can be deployed to move over relatively rough obstacles, as shown in Figure 5.24(b). Thus this robot can also negotiate obstacles actively with effective control.

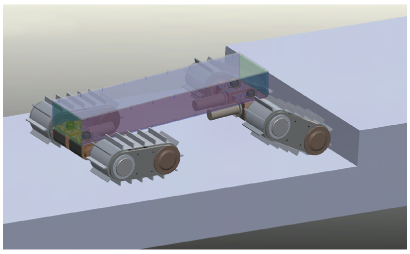

(a) Passively

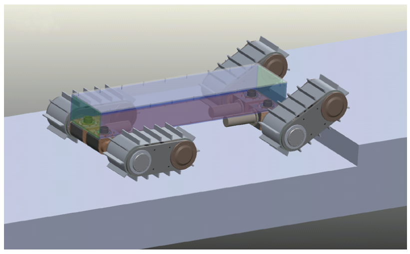

(b) Actively

Figure 5.24. Different ways for the robot to overcome an obstacle

(1) The Crawler Robot Overcoming Obstacles Passively

When this crawler robot encounters an obstacle, the front modules overcome the obstacle passively and subsequently the rear modules overcome the obstacle passively. In this process of negotiating obstacles, it is not necessary to provide any control to the robot.

As shown in Figure 5.25, the robot moves forwards on a flat surface (moving mode) in scene 1. When there is an obstacle stopping the timing belts of the front crawler modules,

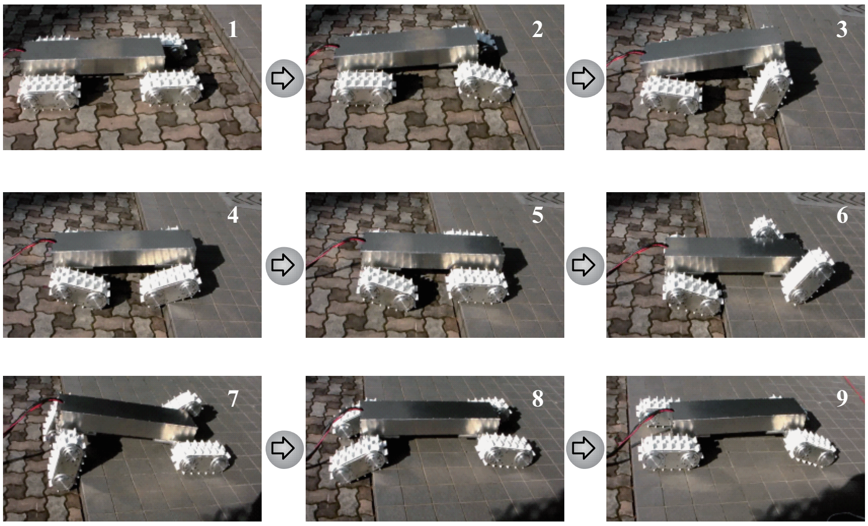

Figure 5.25. Experiment scenes when the robot overcomes an obstacle passively

the front crawler modules switch into rotating mode to overcome the obstacle from scenes 2 to 5. In this process the rear crawler modules continue to move forwards, pushing the front modules, since the front rotation velocity is much smaller than the rear moving speed. After climbing up the obstacle, the front modules begin to return to the initial motion mode in scenes 6, 7, and 8. When the rear modules touch the obstacle surface, they also begin to overcome the obstacle in the same manner as the front modules. After climbing over the obstacle, the rear modules also begin to return to the original position in scene 9. The experimental video can be found on the homepage of Ma Laboratory [83].

(2) The Crawler Robot Overcoming Obstacles Actively

The four-crawler-driven robot is an under-actuated system, in which there is a kinematic redundancy. The internal interaction between the front module and the rear module can be used to realize the robot posture control [79]. The posture in which the front module is lifted up can be used to negotiate obstacles, as shown in Figure 5.24(b). The fact that the posture can be kept has been proved through numerical method.

θ_{fd} is the desired front frame angle of the posture. As shown in Figure 5.26(a), the current frame angle is larger than the desired frame angle θ_{fd}. The front frame should rotate in clockwise direction so as to reach the desired goal angle. At this point, the front module is pulled by the rear module. As shown in Figure 5.26(b), the current frame angle is smaller than the desired frame angle θ_{fd}. The front frame should rotate in anticlockwise direction so as to reach the desired goal angle. At this point, the front module is pushed by the rear module.

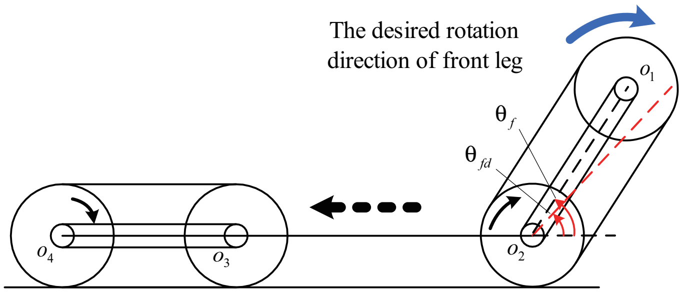

(a) When $\theta_f > \theta_{fd}$

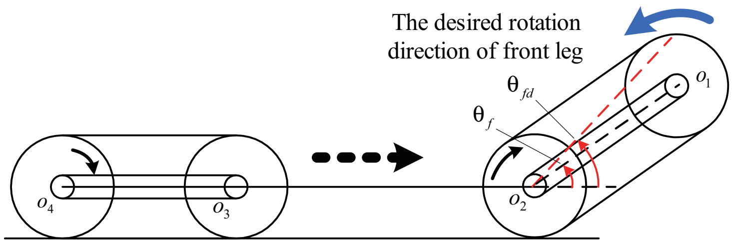

(b) when $\theta_f < \theta_{fd}$

Figure 5.26. Control concept for negotiating an obstacle actively

Based on the principle discussed above, the front modules are controlled to be lifted up 30° using direct control method and proceed to overcome the obstacle. The experiment scenes using the centralized control system are shown in Figure 5.27. In scene 1, the crawler robot moves forwards in motion mode. In scene 2, the front modules of the crawler robot are controlled to be lifted up at the angle of 30°. The crawler robot overcomes the obstacle with the front modules lifted up in scenes 3, 4, and 5. After the front modules climb over the obstacle, the rear modules begin to overcome the obstacle as that in the case of the passive experiment in scenes 6, 7, and 8. Consequently, the crawler robot successfully overcomes the obstacle in scene 9. The experimental video can be found on the homepage of Ma Laboratory [83].

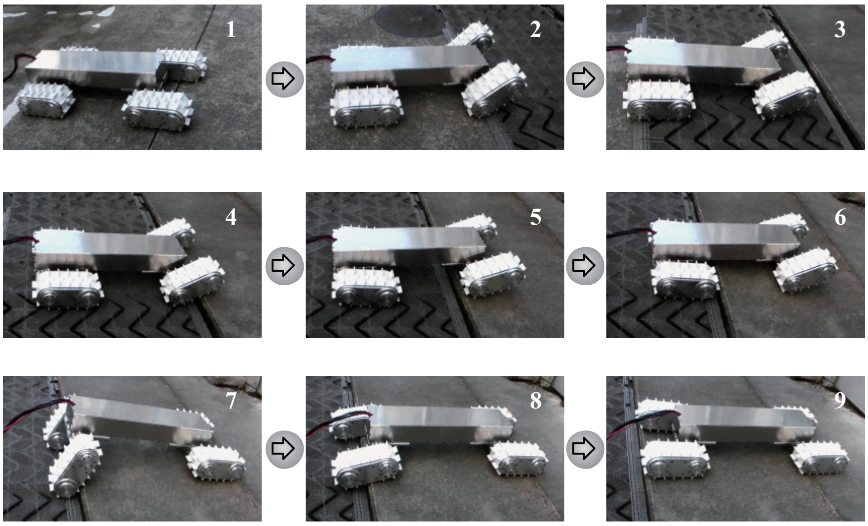

Figure 5.27. Experiment scenes when the robot overcomes an obstacle actively

(3) Some Experiment Tests of the Robot

In order to figure out the adaptability of the four-crawler-module robot, we continue to conduct some experimental tests for the robot. Figure 5.28(a) and Figure 5.28(b) depict the cases that the robot climbs up and down a ramp, respectively.

Figure 5.29 depicts an encountering condition where the left crawler modules should overcome the step and the right crawler modules move on the flat surface. In scene 2, the front left crawler module firstly climbs up the step and subsequently the robot body is lifted up by the front left and right modules as shown in scene 3. When the rear left module contacts the step, the module begins to overcome the obstacle through the proposed three locomotion modes as depicted in scenes 4, 5, 6, 7 and 8. Consequently, the crawler robot recovers to the initial state and continues to move forwards as shown in scenes 9 and 10.

As shown in Figure 5.30, the crawler robot is negotiating a two-step obstacle. In scene 2 the front two crawler modules transmit the power to the rotating frames since the pulley is stopped by the first step. When the front modules begin climbing up the first step, the propulsion of the rear two modules makes the robot body raised up in scene 3. Subsequently, after the front modules negotiate the first step, the rear two modules start to overcome the first step and the front modules begin to traverse the second step as shown in scenes 4, 5, 6,

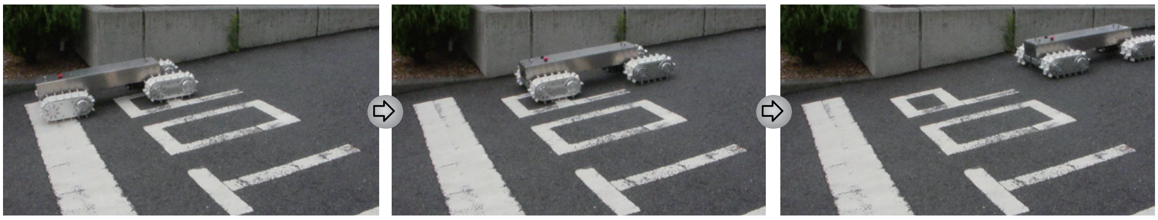

(a) Climbing up a slope

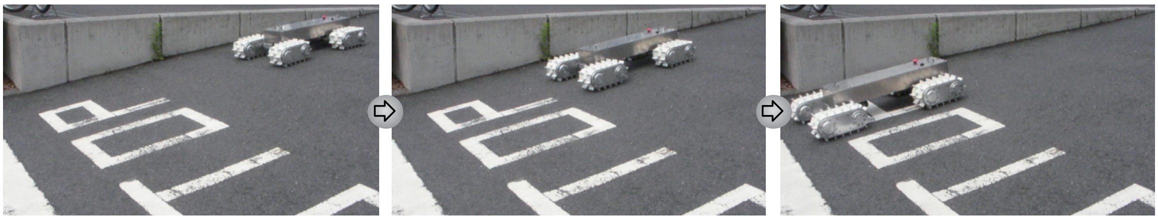

(b) Climbing down a slope

Figure 5.28. The robot working on a ramp of 9°

and 7. Once the front modules overcome the second step successfully, the remaining task of the rear two modules is to negotiate the second step using the locomotion modes in scenes 8, 9, 10, and 11. Finally, the robot successfully traverses the two-step obstacle in scene 12. The experimental video can be found on the homepage of Ma Laboratory [83].

5.4 Summary

A modular concept was proposed and the mechanical design has been achieved considering waterproof and dust-proof qualities. As examples, a one-crawler-module robot and a four-crawler-module robot have been constructed using the proposed crawler module. The posture analysis of the one-crawler-module has been conducted in quasi-static method numerically. The four-crawler-module robot can overcome an obstacle using both the active and passive methods. The experimental tests including slope, one-side-step and two-step obstacles, show that the robot has good passive environmentally-adapted mobility.

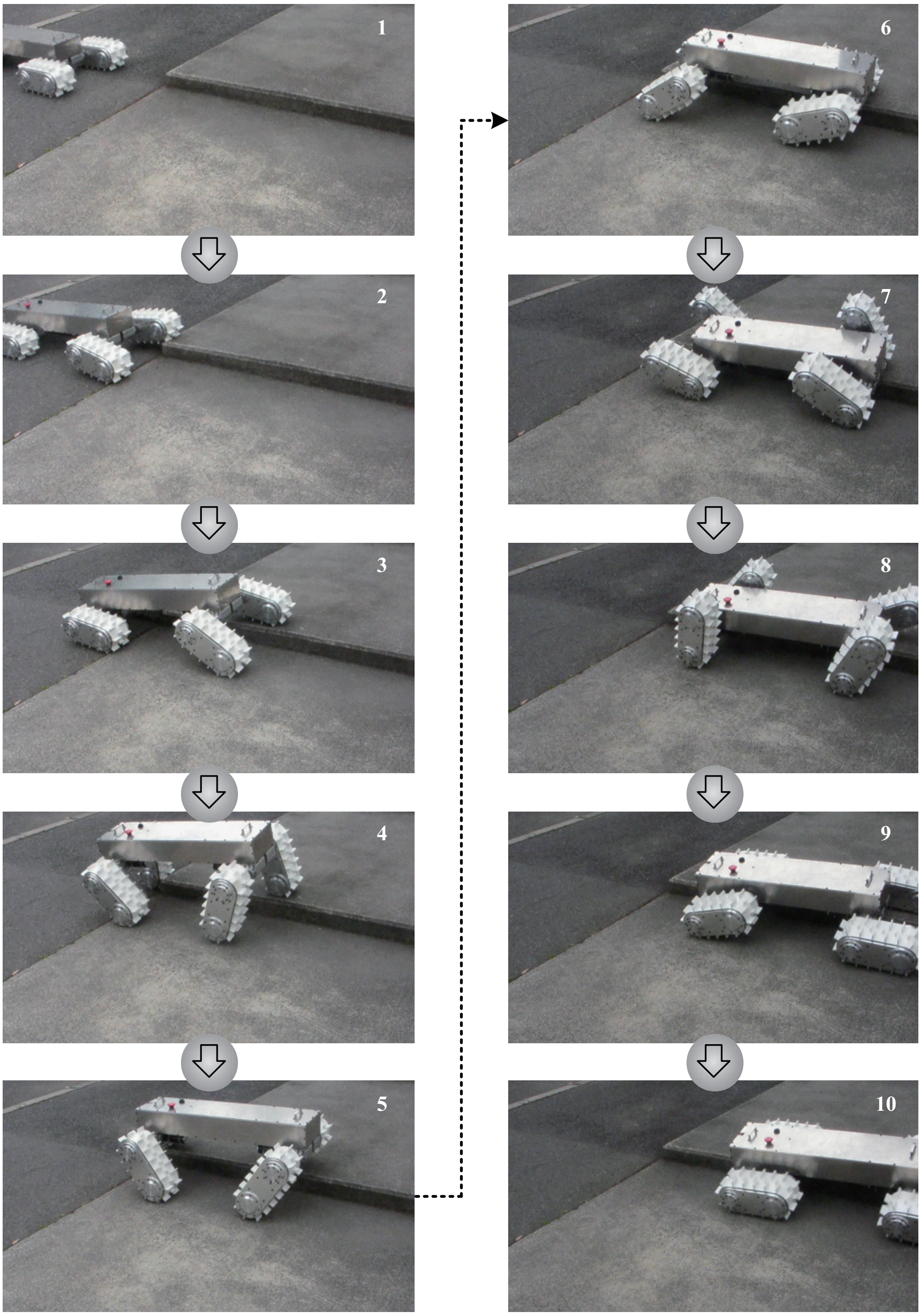

Figure 5.29. Experiment scenes when the robot overcomes a one-side-step obstacle

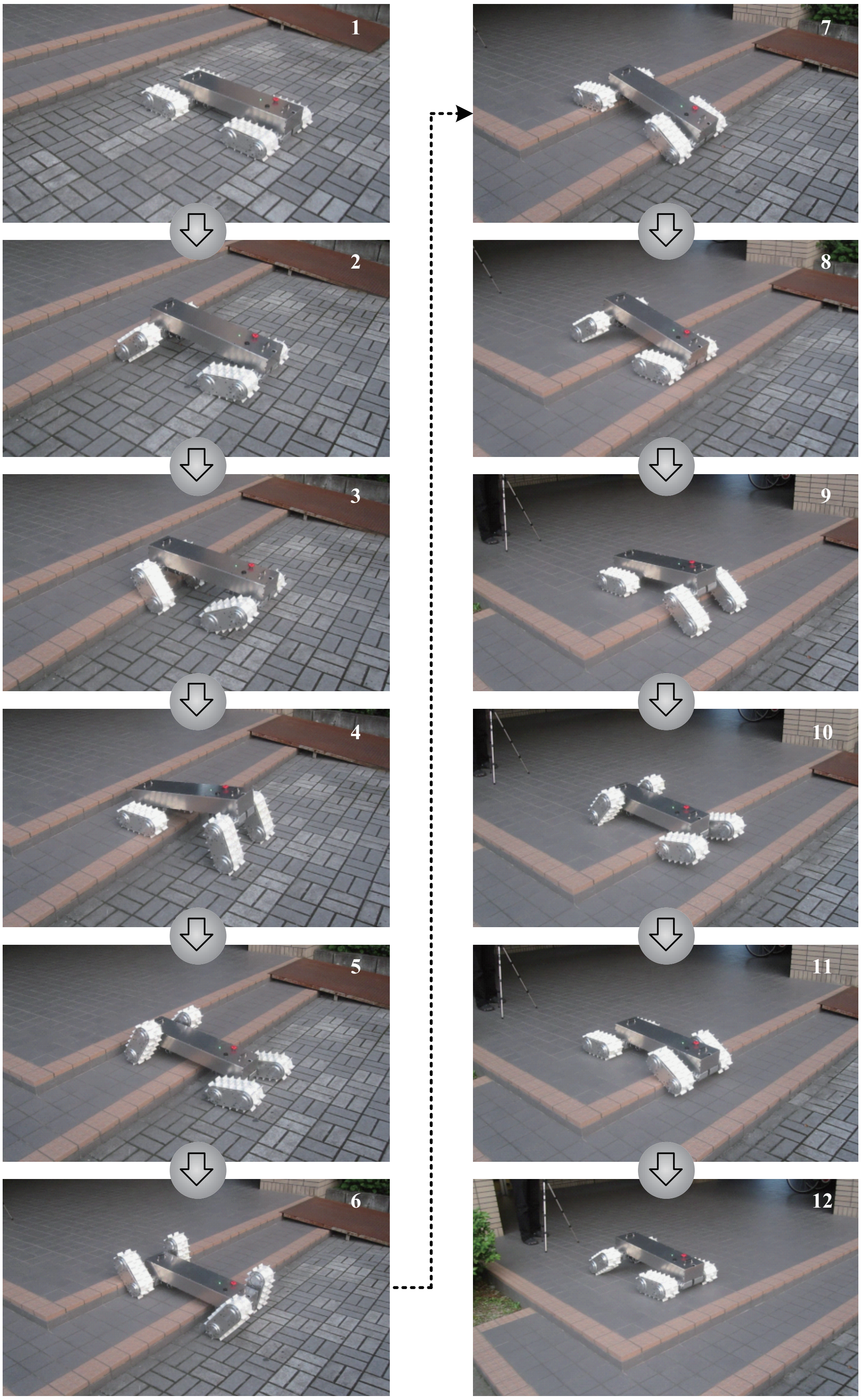

Figure 5.30. Experiment sequence when the robot climbs a two-step obstacle

Chapter 6

Conclusion and Future Work

6.1 Conclusion

In order to develop a kind of efficient mobile robot for exploring and rescuing tasks, we have proposed a novel tracked crawler mechanism, in which a planetary gear reducer is employed as a transmission device and provides two outputs in different forms with only one actuator.

Since there are two outputs in only one crawler mechanism, one crawler mechanism cannot move as an individual unit. One-crawler robot is composed of the proposed crawler mechanism and an assistant leg while a dual-crawler-driven robot is constituted through connecting two crawler mechanisms rigidly. Both the one-crawler robot and the dual-crawler-driven robot show good adaptability to terrains, overcoming obstacles autonomously without any control algorithm. Another crucial characteristic is the impact absorption of our crawler mechanism when collision inevitably happens. To figure out what the advantage of our mechanism to the impact absorption is, impact analysis of the robot is conducted from the external components of the robot to its internal transmission parts while the robot encounters the collision with obstacles. The results of impact effect to actuators in our mechanism are correspondingly derived in comparison with that in the conventional mechanism where each output is provided by one actuator. Numerical results demonstrate the advantage of our mechanism on impact absorption. The under-actuated mechanism can release the impact energy caused by collision and protect the actuator.

As an under-actuated system, a dual-crawler-driven robot can generate several configurations through cooperatively controlling the two actuators. This tracked robot, which uses two actuators to give four outputs, however have less realizable postures than that where each output is provided by one actuator exactly. To figure out what postures can be generated by the dual-crawler-driven robot, quasi-static analysis of the robot has been conducted while taking the rolling resistance into consideration and its realizable postures have been obtained numerically. The posture transition of the robot provides a way for the robot to overcome the blind area of postures. Three control methods are proposed to control the postures in configuration 1.

A modular concept for the crawler is proposed for enlarging its use in robot systems and mechanical design of a modular crawler is conducted. Using this crawler module, a four-crawler-driven robot is realized by easily assembling. Experiments are conducted to verify the proposed concept and mechanical design. A single crawler module can well perform the proposed three locomotion modes. The four-crawler-driven robot which can get over obstacles both passively and actively has good adaptability to the environment.

6.2 Future Work

To control the under-actuated crawler system smoothly, many aspects are necessary to be further studied.

- In the aforementioned contents, just quasi-static analysis of the postures was conducted. Dynamics of the robot system should be considered to find some new results based on the current quasi-static analysis.

- We have already pointed out the possible controllable postures of the robot, however, there are no effective control methods for some postures. New control methods should be investigated to control the unstable equilibrium of the robot posture.

Bibliography

[1] H. van de Groenendaal, “Search and rescue robot - lessons from 9/11,” *J. EngineerIT Online*, 2010. [Online]. Available: http://www.eepublishers.co.za/view.php?sid=19940

[2] R. M. DeSantis, “Modeling and path-tracking control of a mobile wheeled robot with a differential drive,” *Robotica*, vol. 13, pp. 401—410, 1995.

[3] S. Hirose, “Mechanical design of a mobile robot for external environments,” *J. Robotics Soc. Japan*, vol. 18, no. 7, pp. 2—6, 2000.

[4] J. C. Alexander and J. H. Maddocks, “On the kinematics of wheeled mobile robots,” *Intl. J. Robotics Research*, vol. 23, no. 7-8, pp. 763—781, 2004.

[5] V. B. Larin, “Motion planning for a wheeled robot (kinematic approximation),” *International Applied Mechanics*, vol. 41, no. 2, pp. 187—196, 2005.

[6] M. D. Berkemeier, E. Poulson, and T. Groethe, “Elementary mechanical analysis of obstacle crossing for wheeled vehicles,” in *Proc. 2008 Intl. Conf. on Robotics and Automation*, Pasadena, CA, USA, 2008, pp. 2319—2324.

[7] [Online]. Available: http://www.nasa.gov/mission_pages/mer/spirit-update.html

[8] S. Hirose, “A study of design and control of a quadruped walking vehicle,” *Intl. J. Robotics Research*, vol. 3, no. 2, pp. 113—133, 1984.

[9] S. Hirose, Y. Fukuda, and H. Kikuchi, “The gait control system of a quadruped walking vehicle,” *Intl. J. Advanced Robotics*, vol. 1, no. 4, pp. 289—323, 1986.

[10] E. Celaya and J. M. Porta, “A control structure for the locomotion of a legged robot on difficult terrain,” *IEEE Robotics and Automation Magazine*, vol. 5, no. 2, pp. 43—51, 1998.

[11] K. Yoneda, Y. Ota, F. Ito, and S. Hirose, “Quadruped walking robot with reduced degrees of freedom,” *J. Robotics and Mechatronics*, vol. 13, no. 2, pp. 190—197, 2001.

[12] S. Hirose, K. Yoneda, R. Furuya, and T. Takagi, “Dynamic and static fusion control of quadruped walking vehicle,” in *Proc. IEEE/RSJ Intl. Workshop on Intelligent Robots and Systems*, Tsukuba, Japan, 1989, pp. 199—204.

[13] C. Ridderstrom, “Stability of statically balanced stances for legged robots with compliance,” in *Proc. 2002 IEEE Intl. Conf. on Robotics and Automation*, Washington, DC, 2002, pp. 2240—2245.

[14] J. Foret, O. Bruneau, and J. G. Fontaine, “Unified approach for m-stability analysis and control of legged robots,” in *Proc. 2003 IEEE/RSJ Intl. Conf. on Intelligent Robots and Systems*, Las Vegas, Nevada, 2003, pp. 106—111.

[15] D. M. Helmick, S. I. Roumeliotis, M. C. McHentry, and L. Matthies, “Multi-sensor, high speed autonomous stair climbing,” in *Proc. 2002 IEEE/RSJ Intl. Conf. on Intelligent Robotic and System*, Lausanne, Switzerland, 2002, pp. 733—742.

[16] S. Ma, T. Tomiyama, and H. Wada, “Omni-directional static walking of a quadruped robot,” *IEEE Trans. on Robotics*, vol. 21, no. 2, pp. 152—161, 2005.

[17] [Online]. Available: http://en.wikipedia.org/wiki/Continuous_track

[18] A. T. Le, “Modeling and control of tracked vehicles,” Ph.D. dissertation, Department of Mechanical and Mechatronic Engineering, The University of Sydney, 1999.

[19] O. Jahanian and G. Karimi, “Locomotion systems in robotic application,” in *Proc. 2006 IEEE Intl. Conf. on Robotics and Biomimetics*, Kunming, China, 2006, pp. 689—696.

[20] M. Guarnieri, P. Debenest, T. Inoh, E. Fukushima, and S. Hirose, “Helios vii: a new vehicle for disaster reponse—mechanical design and basic experiments,” *Intl. J. Advanced Robotics*, vol. 19, no. 8, pp. 901—927, 2005.

[21] T. Takayama and S. Hirose, “Development of souryu-i connected crawler vehicle for inspection of narrow and winding space,” in *Proc. 2000 Intl. Conf. on Industrial Electronics, Control and Instrumentation*, 2000, pp. 143—148.

[22] ——, “Development of souryu i, ii-connected crawler vehicle for inspection of narrow and winding space,” *J. Robotics and Mechatronics*, vol. 15, no. 1, pp. 61—69, 2003.

[23] A. Masayuki, T. Takayama, and S. Hirose, “Development of ”souryu-iii”: Connected crawler vehicle for inspection inside narrow and winding spaces,” in *Proc. 2004 Intl. Conf. on Intelligent Robots and Systems*, Sendai, Japan, 2004, pp. 52—57.

[24] M. Arai, Y. Tanaka, S. Hirose, H. Kuwahara, and S. Tsukui, “Development of ”souryu-iv” and ”souryu-v:” serially connected crawler vehicles for in-rubble searching operations,” *J. Field Robotics*, vol. 25, no. 1, pp. 31—65, 2008.

[25] M. Arai, Y. Tanaka, S. Hirose, S. Tsukui, and H. Kuwahara, “Improved driving mechanism for connected crawler vehicle souryu-iv for in rubble searching operations,” in *Proc. IEEE Intl. Workshop on Safety, Security and Rescue Robotics National Institute of Standards and Technology (NIST), SSRR2006*, Gaithersburg, MD, USA, 2006.

[26] Y. Tanaka, M. Arai, S. Hirose, and S. Tsukui, “Development of souryu-v with mono-tread-crawlers and elastic-rods joint,” in *Proc. 2006 IEEE Intl. Workshop on Safety, Security and Rescue Robotics National Institute of Standards and Technology (NIST), SSRR2006*, Gaithersburg, MD, USA, 2006.

[27] S. Hirose and H. Yamada, “Snake-like robots machine design of biologically inspired robots,” *IEEE Robotics and Automation Magazine*, vol. 16, no. 1, pp. 88—98, 2009.

[28] S. Hirose, E. F. Fukushima, R. Damoto, and H. Nakamoto, “Design of terrain adaptive versatile crawler vehicle helios-vi,” in *Proc. 2001 IEEE/RSJ Intl. Conf. on Intelligent Robots and Systems*, Maui, Hawaii, USA, 2001, pp. 1540—1545.

[29] M. Guarnieri, I. Takao, E. F. Fukushima, and S. Hirose, “Helios viii search and rescue robot: Design of an adaptive gripper and system improvements,” in *Proc. 2007 IEEE/RSJ Intl. Conf. on Intelligent Robots and Systems*, San Diego, CA, USA, 2007, pp. 1775—1780.

[30] M. Guarnieri, R. Kurazume, H. Masuda, T. Inoh, K. Takita, P. Debenest, R. Hodoshima, E. Fukushima, and S. Hirose, “Helios system: A team of tracked robots for special urban search and rescue operations,” in *Proc. 2009 IEEE/RSJ Intl. Conf. on Intelligent Robots and Systems*, St. Louis, USA, 2009, pp. 2795—2800.

[31] [Online]. Available: http://www.irobot.com/

[32] P. Ben-Tzvi, S. Ito, and A. A. Goldenberg, “Autonomous stair climbing with reconfigurable tracked mobile robot,” in *Proc. IEEE Workshop on Robotics and Sensors Environments*, Ottawa, Canada, 2007, pp. 1—6.

[33] P. Ben-Tzvi, A. A. Goldenberg, and J. W. Zu, “Design, simulations and optimization of a tracked mobile robot manipulator with hybrid locomotion and manipulator capabilities,” in *Proc. 2008 Intl. Conf. on Robotics and Automation*, Pasadena, CA, USA, 2008, pp. 2307—2312.

[34] ——, “Design and analysis of a hybrid mobile robot mechanism with compounded locomotion and manipulation capability,” *J. Mechanical Design*, vol. 130, iss. 7, pp. 1—13, 2008.

[35] ——, “A novel control architecture and design of hybrid locomotion and manipulation tracked mobile robot,” in *Proc. 2007 IEEE Intl. Conf. on Mechatronics and Automation*, Harbin, China, 2007, pp. 1374—1381.

[36] K. Nagatani, A. Yamasaki, K. Yoshida, T. Yoshida, and E. Koyanagi, “Improvement of the operability of a tracked vehicle on uneven terrain using autonomous control of active flippers,” in *Proc. 2008 IEEE/RSJ Intl. Conf. on Intelligent Robots and Systems*, Nice, France, 2008, pp. 2717—2718.

[37] Y. Okada, K. Nagatani, and K. Yoshida, “Semi-autonomous operation of tracked vehicles on rough terrain using autonomous control of active flippers,” in *Proc. 2009 IEEE/RSJ Intl. Conf. on Intelligent Robots and Systems*, St. Louis, USA, 2009, pp. 2815—2820.

[38] K. Ohno, S. Morimura, S. Tadokoro, E. Koyanagi, and T. Yoshida, “Semi-autonomous control system of rescue crawler robot having flippers for getting over unknown-steps,” in *Proc. 2007 IEEE/RSJ Intl. Conf. on Intelligent Robots and Systems*, San Diego, CA, USA, 2007, pp. 3012—3018.

[39] ——, “Semi-autonomous control of 6-dof crawler robot having flippers for getting over unknown-steps,” in *Proc. 2007 IEEE/RSJ Intl. Conf. on Intelligent Robots and Systems*, San Diego, CA, USA, 2007, pp. 2559—2560.

[40] D. Calisi, D. Nardi, K. Ohno, and S. Tadokoro, “A semi-autonomous tracked robot system for rescue missions,” in *SICE Annual Conference 2008*, The University Electro-Communications, Japan, 2008, pp. 2066—2069.

[41] Q. H. Vu, B. S. Kim, and J. B. Song, "Autonomous stair climbing algorithm for a small four-tracked robot," in *Proc. Intl. Conf. on Control, Automation and Systems 2008*, COEX, Seoul, Korea, 2008, pp. 2356—2360.

[42] B. S. Kim, Q. H. Vu, J. B. Song, and C. H. Yim, "Novel design of a small field robot with multi-active crawlers capable of autonomous stair climbing," *J. Mechanical Science and Technology*, vol. 24, no. 1, pp. 343—350, 2010.

[43] C. H. Lee, S. H. Kim, S. C. Kang, M. S. Kim, and Y. K. Kwak, "Double-track mobile robot for hazardous environment applications," *Intl. J. Advanced Robotics*, vol. 17, no. 5, pp. 447—459, 2003.

[44] M. Lauria, I. Nadeau, P. Lepage, Y. Morin, P. Giguere, F. Gagnon, D. Letourneau, and F. Michaud, "Design and control of a four steered wheeled mobile robot," in *Proc. IEEE Industrial Electronics, IECON2006 - 32nd Annual Conference*, 2006, pp. 4020—4025.

[45] M. Lauria, F. Michaud, M. A. Legault, D. Letourneau, P. Retornaz, I. Nadeau, P. Lepage, Y. Morin, F. Gagnon, P. Giguere, J. Fremy, and L. Clavien, "Elastic locomotion of a four steered mobile robot," in *Proc. 2008 IEEE/RSJ Intl. Conf. on Intelligent Robots and Systems*, Nice, France, 2008, pp. 2721—2722.

[46] F. Michaud, D. Letourneau, M. Arsenault, Y. Bergeron, R. Cadrin, F. Gagnon, M. A. Legault, M. Millette, J. F. Pare, M. C. Tremblay, P. Lepage, Y. Morin, J. Bisson, and S. Caron, "Azimut, a leg-track-wheel robot," in *Proc. 2003 IEEE/RSJ Intl. Conf. on Intelligent Robots and Systems*, Las Vegas, Nevada, 2003, pp. 2553—2558.

[47] M. Lauria, I. Nadeau, P. Lepage, Y. Morin, P. Giguere, F. Gagnon, D. Letourneau, and F. Michaud, "Kinematical analysis of a four steered wheeled mobile robot," in *IEEE ISIE 2006*, Montreal, Quebec, Canada, 2006, pp. 3090—3095.

[48] [Online]. Available: http://www.is.northropgrumman.com/by_solution/remote_platforms/product/f6a/index.html

[49] X. Duan, Q. Huang, N. Rahman, J. Li, and J. Li, "Mobit, a small wheel-track-leg mobile robot," in *Proc. 6th World Congress on Intelligent Control and Automation*, Dalian, China, 2006, pp. 9159—9163.

[50] X. Duan, Q. Huang, N. Rahman, J. Li, and Q. Du, "Kinematic modeling of a small mobiel robot with multi-locomotion modes," in *Proc. 2006 IEEE/RSJ Intl. Conf. on Intelligent Robots and Systems*, Beijing, China, 2006, pp. 5582—5587.

[51] ——, "Modeling and control of a small mobile robot with multi-locomotion modes," in *Proc. 6th Intl. Conf. on Systems Design and Applications (ISDA'06)*, 2006, pp. 592—597.

[52] X. Duan, G. Bian, Z. Jiang, and Q. Huang, "Planning and control of mobit's obstacle negotiating," in *Proc. 2008 IEEE Intl. Conf. on Automation and Logistics*, Qingdao, China, 2008, pp. 580—586.

[53] N. Rahman, K. Li, X. Duan, J. Li, J. Li, and Q. Huang, "Supervised semi-autonomous controls for mobit," in *Proc. 2006 IEEE Intl. Conf. on Mechatronics and Automation*, Luoyang, China, 2006, pp. 429—434.

[54] Y. Liu and G. Liu, "Mobile manipulation using tracks of a tracked mobile robot," in *Proc. 2009 IEEE/RSJ Intl. Conf. on Intelligent Robots and Systems*, St. Louis, USA, 2009, pp. 948—953.

[55] ——, "Track-stair interaction analysis and online tipover prediction for a self-reconfigurable tracked mobile robot climbing stairs," *IEEE/ASME Trans. on Mechatronics*, vol. 14, no. 5, pp. 1—11, 2009.

[56] J. Liu, Y. Wang, B. Li, S. Ma, J. Wang, and H. Cao, "Transformation technique research of the improved link-type shape shifting modular robot," in *Proc. 2006 IEEE Intl. Conf. on Mechatronics and Automation*, Luoyang, China, 2006, pp. 295—300.

[57] J. Liu, Y. Wang, B. Li, and S. Ma, "Transmutation mechanisms and its realization of a chain-type reconfigurable modular robot," *Transactions of the Chinese Society of Agricultural Machinery*, vol. 36, no. 9, pp. 101—105, 2005.

[58] J. Liu, Y. Wang, S. Ma, and B. Li, "Analysis of stairs-climbing ability for a tracked reconfigurable modular robot," in *Proc. 2005 IEEE Intl. Workshop on Safety, Security, and Rescue Robotics*, Kobe, Japan, 2005, pp. 36—41.

[59] A. Kamimura and H. Kurokawa, "High-step climbing by a crawler robot dir-2 realization of automatic climbing motion," in *Proc. 2009 IEEE/RSJ Intl. Conf. on Intelligent Robots and Systems*, St. Louis, USA, 2009, pp. 618—624.

[60] S. Hirose, N. Ootsukasa, T. Shirasu, H. Kuwahara, and K. Yoneda, "Fundamental considerations for the design of a planetary rover," in *Proc. 1995 IEEE Intl. Conf. on Robotics and Automation*, Nagoya, Japan, 1995, pp. 1934—1944.

[61] P. Li, "Design and control of adaptive mobile mechanisms for in-pipe inspection robots," Ph.D. dissertation, Graduate School of Chinese Academy of Sciences, 2009.

[62] G. Lan, "Study on a snake-like rescue robot," Ph.D. dissertation, Graduate School of Science and Engineering, Ibaraki University, 2007.

[63] G. Lan and S. Ma, "Quasi-static analysis of a novel crawler-driven robot motion," *J. Robotics and Mechatronics*, vol. 18, no. 5, pp. 556—563, 2006.

[64] ——, "Step-climbing analysis of a novel tracked robot," in *Proc.2005 IEEE Intl. Conf. on Robotics and Biomimetics*, Hong Kong and Macau, 2005, pp. 544—549.

[65] G. Lan, S. Ma, and K. Inoue, "Development of a novel crawler for irregular terrain access," in *Proc. 2005 IEEE Intl. Workshop on Safety, Security and Rescue Robotics*, Kobe, Japan, 2005, pp. 42—47.

[66] G. Lan, S. Ma, K. Inoue, and Y. Hamamatsu, "Development of a novel crawler mechanism with polymorphic locomotion," *Intl. J. Advanced Robotics*, vol. 21, no. 3-4, pp. 421—440, 2007.

[67] S. Ma, Q. Quan, and R. Liu, "Posture analysis of a dual-crawler-driven robot," in *Proc. 2008 IEEE/ASME Intl. Conf. on Advanced Intelligent Mechatronics*, Xi'an, China, 2008, pp. 365—370.

[68] T. Matsumoto and K. Kosuge, "Collision detection of manipulator based on adaptive control law," in *Proc. 2001 IEEE/ASME Intl. Conf. on Advanced Mechatronics*, Como, Italy, 2001, pp. 177—182.

[69] S. Morinaga and K. Kosuge, "Collision detection system for manipulator based on adaptive impedance control law," in *Proc. 2003 IEEE Intl. Conf. on Robotics and Automation*, Taipei, Taiwan, 2003, pp. 1080—1085.

[70] K. Osuka and H. Kitajima, "Series elastic actuator development for a biomimetic walking robot," in *Proc. IEEE/ASME Intl. Conf. on Advanced Intelligent Mechantronics*, Atlanta, Georgia USA, 1999, pp. 561—568.

[71] D. W. Robinson and G. A. Pratt, "Force controllable hydro-elastic actuator," in *Proc. 2000 IEEE Intl. Conf. on Robotics and Automation*, 2000, pp. 1321—1327.

[72] K. Osuka and H. Kitajima, "Series elastic actuators for legged robots," in *Proc. of the SPIE*, 2004, pp. 135—144.

[73] M. Lauria, M. A. Legault, M. A. Lavoie, and F. Michaud, "Differential elastic actuator for robotic interaction tasks," in *Proc. 2008 IEEE Intl. Conf. on Robotics and Automation*, 2008, pp. 3606—3611.

[74] Q. Quan, S. Ma, R. Liu, and B. Li, "Impact absorption of a dual-crawler-driven robot," in *Proc. 2008 IEEE Intl. Conf. on Robotics and Biomimetics*, Bangkok, Thailand, 2008, pp. 800—805.

[75] Q. Quan, S. Ma, and Z. Deng, "Impact analysis of a dual-crawler-driven robot," *Intl. J. Advanced Robotics*, vol. 23, no. 12-13, pp. 1779—1797, 2009.

[76] R. M. Brach, *Mechanical impact dynamics.* John Wiley, 1991.

[77] Q. Quan, S. Ma, and R. Liu, "Controllable postures of a dual-crawler-driven robot," in *Proc. 9th Intl. Symposium on Robot Control (SYROCO'09) The International Federation of Automatic Control*, Nagaragawa Convention Center, Gifu, Japan, 2009, pp. 319—324.

[78] Q. Quan and S. Ma, "Controllable postures of a dual-crawler-driven robot," *Mechatronics*, vol. 20, iss. 2, pp. 281—292, 2010.

[79] Q. Quan, S. Ma, B. Li, and R. Liu, "Posture control of a dual-crawler-driven robot," in *Proc. 2009 IEEE Intl. Conf. on Robotics and Automation*, Kobe, Japan, 2009, pp. 2977—2982.

[80] G. Erixon, A. von Yxkull, and A. Arnstrom, "Modularity – the basis for product and factory reengineering," *CIRP Annals - Manufacturing Technology*, vol. 45, iss. 1, pp. 1—6, 1996.

[81] Q. Quan and S. Ma, "A modular crawler-driven robot: Mechanical design and preliminary experiments," in *Proc. 2009 IEEE Intl. Conf. on Intelligent Robots and Systems*, St. Louis, USA, 2009, pp. 639—644.

[82] ——, "Modular mechanic analysis of a crawler-driven module," in *Proc. 2010 Intl. Conf. on Advanced Mechatronics*, Osaka University, Suita Campus, Osaka, Japan, 4-6 October, 2010.

[83] [Online]. Available: http://www.malab.se.ritsumei.ac.jp/english/index.html

[84] [Online]. Available: http://en.wikipedia.org/wiki/PC104

[85] [Online]. Available: http://www.mathworks.com/products/xpctarget/description1.html

Appendix A

Two-dimensional Drawing of the Modular Crawler

Figure A.1 shows a section view of the crawler module, cut from the center axis of the main shaft. The two-dimensional drawing is a detailed description of the crawler module with accurate dimensions in the working environment of AutoCAD.

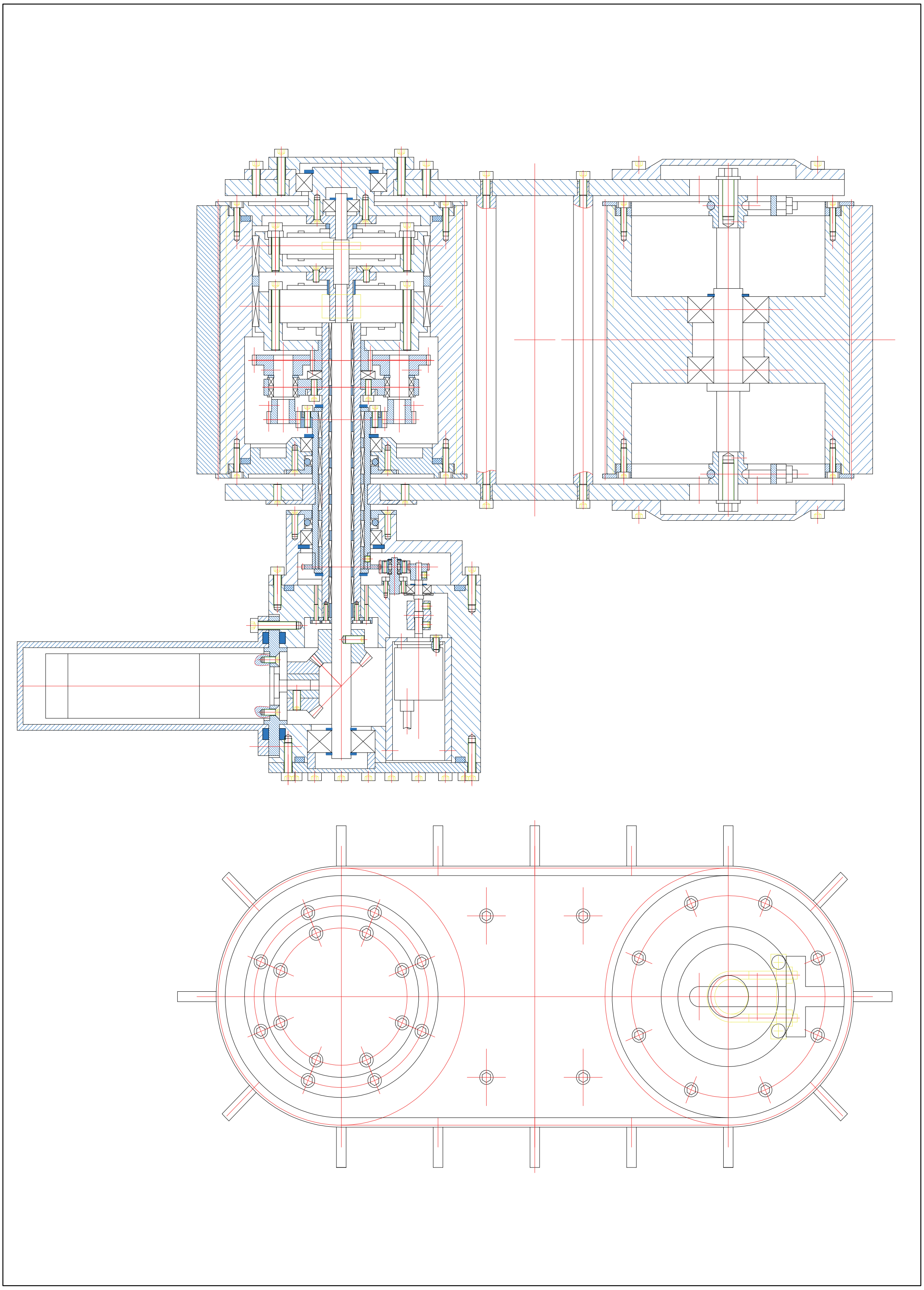

Figure A.1. Two-dimensional drawing of a crawler module

Appendix B

Three-dimensional View of the Four-crawler-module Robot

Figure B.1 shows an effect view of the four-crawler-module robot. Each module is assembled at the corner of the robot body through the connecting interface (eight screws and one air plug).

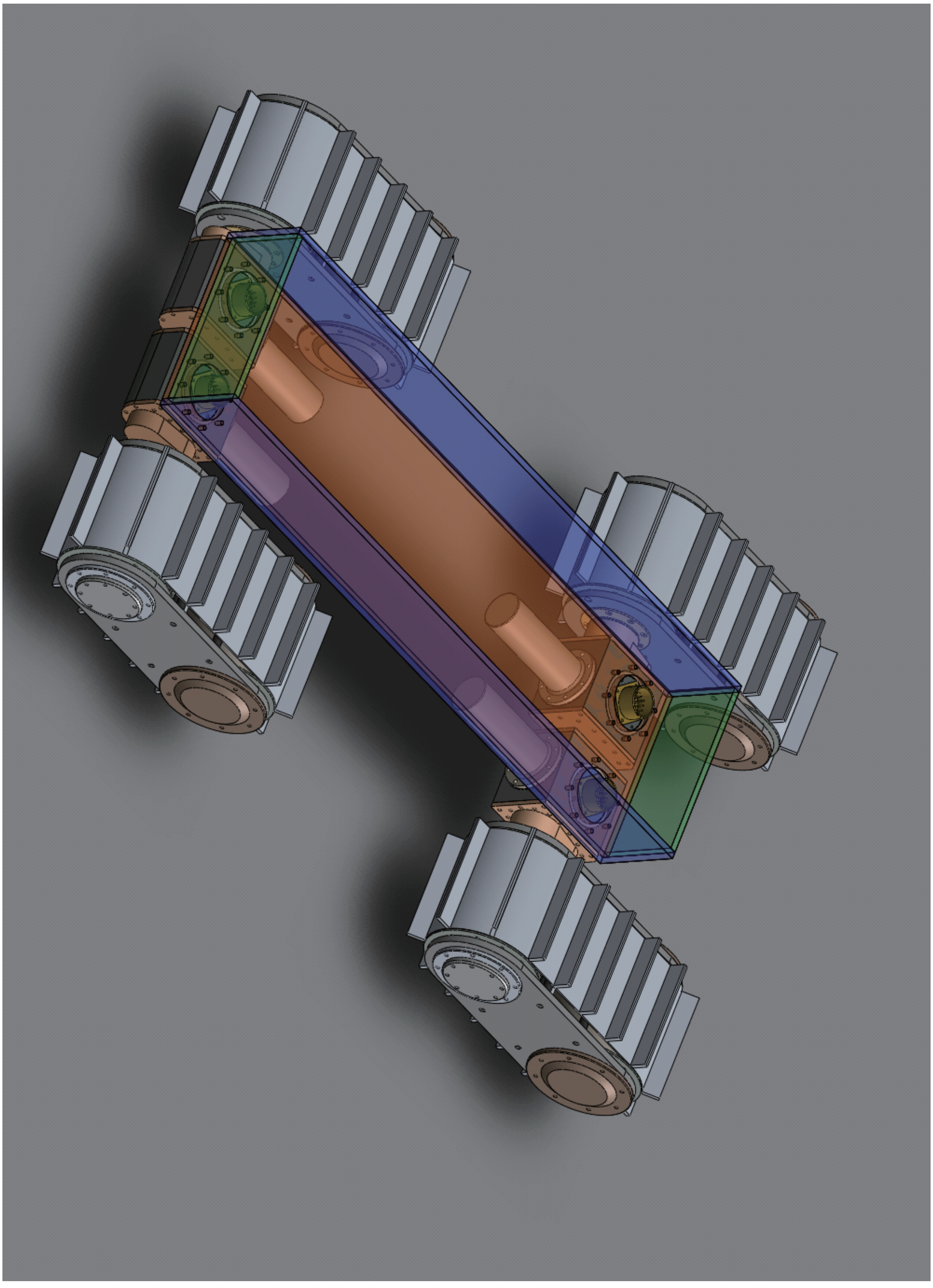

Figure B.1. Three-dimensional view of the four-crawler-module robot

Appendix C

Teleoperated Control System for Four-crawler-module Robot

(1) Hardware

As shown in Figure C.1, we have developed a control system for the four-crawler-module robot. To control the four-module-driven robot effectively, we develop a robust hierarchical control system in which there are three levels to perform different tasks.

Module-level: For each crawler module, there is a layer which is implemented to realize the basic posture control of the module using Micro-controller Unit (MCU). The MCU receives command signal from the central control computer through Controller Area Network (CAN) bus and returns the state information of crawler module to the central computer.

On board Computer-level: An on-board computer as the central control of the four-module-driven robot distributes control task for each crawler module through internal calculation. The central computer communicates with each module through CAN bus. This on-board computer receives instruction signal from a host computer in a control station using wireless communication, and returns the state information of the whole robot.

Control Station-level: The computer in control station sends the desired posture information of the commander and receives the state information of robot.

Regarding the PC104 industrial onboard computer system, PC104 (or PC/104) is an embedded computer standard controlled by the PC104 Consortium which defines both a form factor and computer bus [84]. PC104 is intended for specialized embedded computing environments where applications depend on reliable data acquisition despite an often extreme environment. The form factor benefits many consumers who want a customized rugged system without committing months of design and paperwork. The PC/104 computer bus (first released in 1992) utilizes 104 pins. These pins include all the normal lines used in the ISA bus, with additional ground pins added to ensure bus integrity. Signal timing and voltage levels are identical to the ISA bus, with lower current requirements.

As shown in Figure C.1, a SBC (Single Board Computer) of CPU-1233 made by Eurotech, a CAN communication board of CAN-AC1-104 made by Softing and a power board of PCM-P50 made by AAEON are stacked together. A solid-lead battery of RE12-12 with

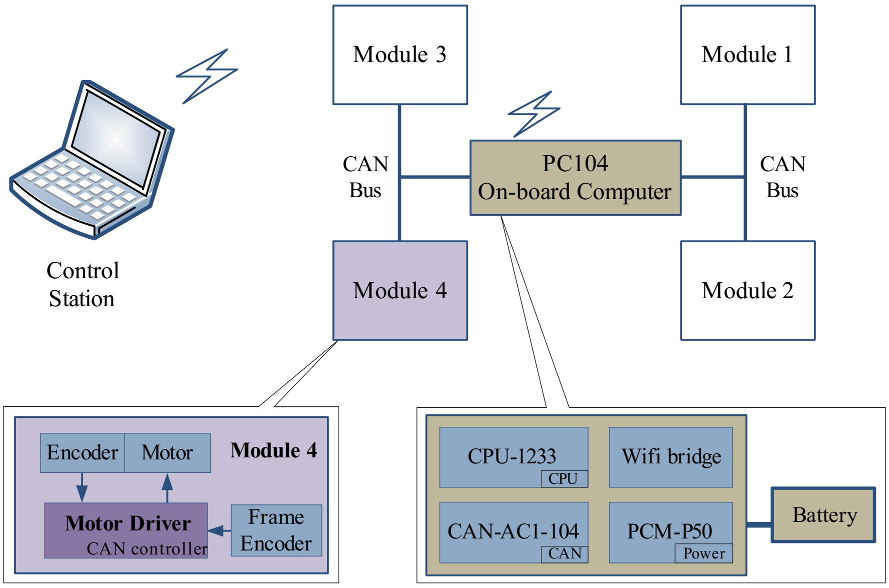

Figure C.1. The architecture of control system for four-crawler-module robot

capacity of 12 Ah is utilized to provide the power for the entire onboard components. A router made by Buffalo which is connected with computer CPU-1233 through the ethernet port communicates with the laptop in control station via the internal Wi-Fi bridge.

In order to drive each motor in the crawler module, we have developed a motor driver using MCU and motor driver ICs. The driver receives the command signal from onboard computers through CAN communication and then realizes the speed control in the internal loop. The driver not only propels the servo motor with incremental encoder, but also counts the position of the module frame. As shown in Figure C.2, the entire hardware of the control system is arranged inside the robot body.

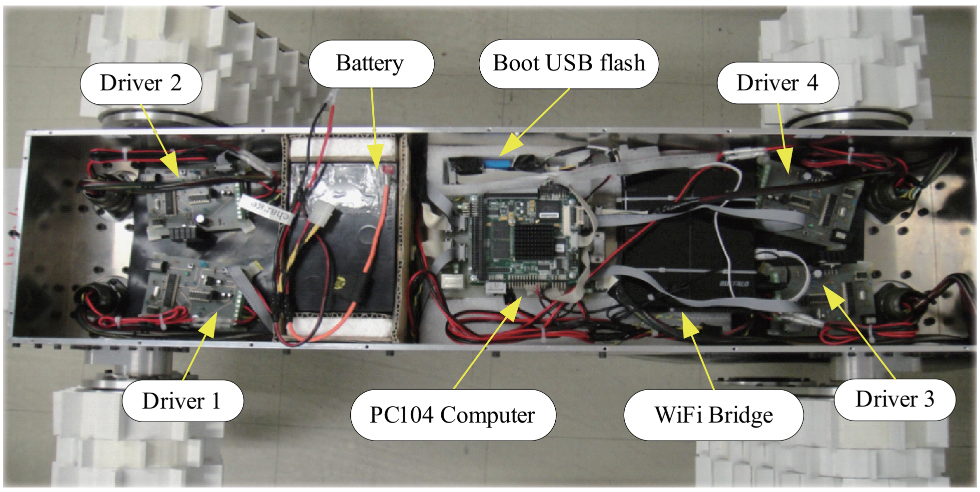

Figure C.2. Internal composition of the control hardware

(2) Software

xPC Target provides a high-performance host-target environment that enables us to connect your Simulink and Stateflow models to physical systems and execute them in real time on low-cost PC-compatible hardware. xPC Target includes proven capabilities for rapid prototyping, hardware-in-the-loop testing, and application deployment in an open hardware architecture. With xPC Target, we design our models on a host PC, generate code with Real-Time Workshop and State flow Coder and download the code to a target PC running the xPC Target real-time kernel [85].

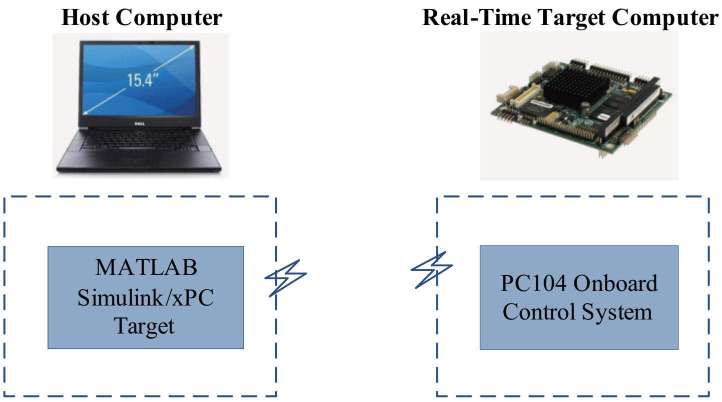

Figure C.3. Software architecture of the control system

The control program is made in the environment of Simulink/Matlab in the laptop. A controlling GUI is depicted in Figure C.4. In the GUI, the speed of each motor in the crawler module can be controlled via the slider. If the box of “Synchronize 1&2” or “Synchronize 3&4” is checked, the front two or rear two crawler modules execute the same speed obtained from the slider. On the contrary, the speed of each motor can be tuned individually via their own slider. Some experiments have been conducted in the indoor environments as shown in Figure C.5.

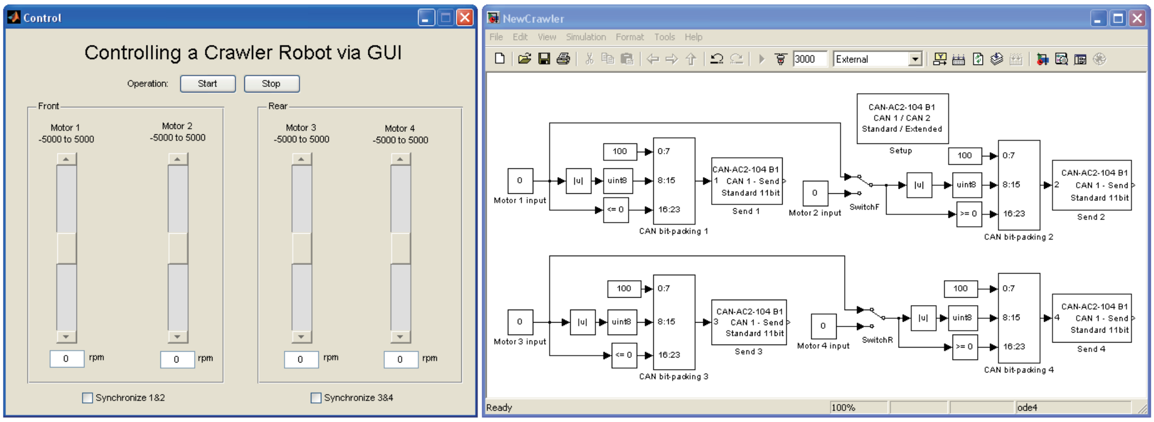

Figure C.4. View of operating program in the laptop

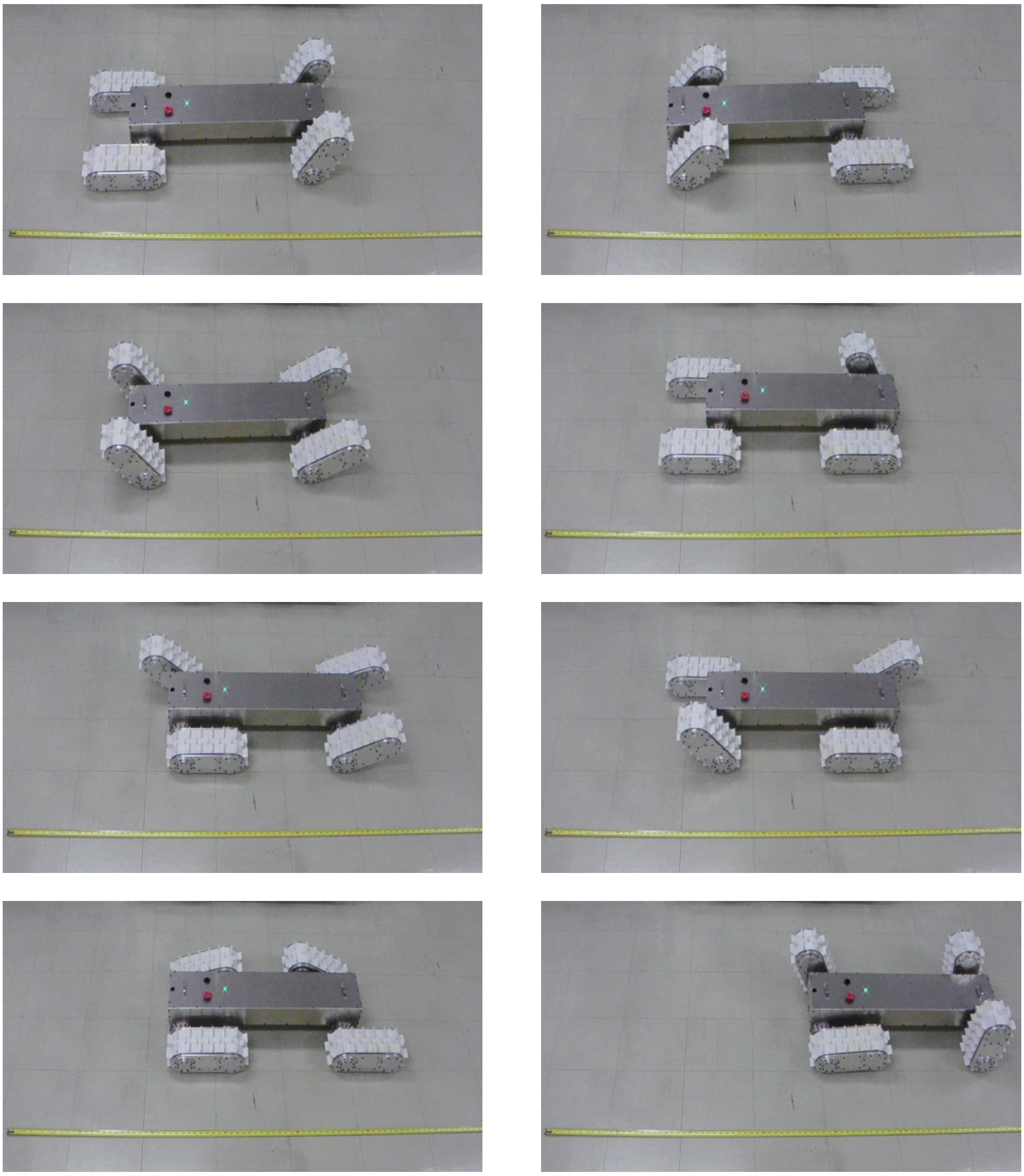

Figure C.5. Indoor experimental test using the teleoperated control system

Appendix D

Motor Driver

A self-developed motor driver with CAN communication is depicted in Figure D.1. The electronic schematic and the corresponding circuit of PCB are shown in Figure D.2 and Figure D.3, respectively.

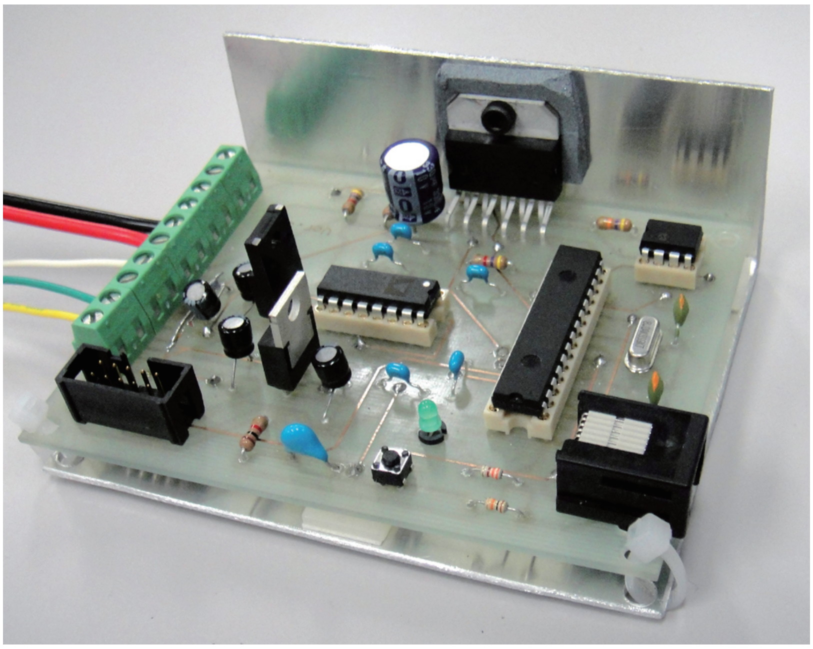

Figure D.1. The developed driver with CAN communication

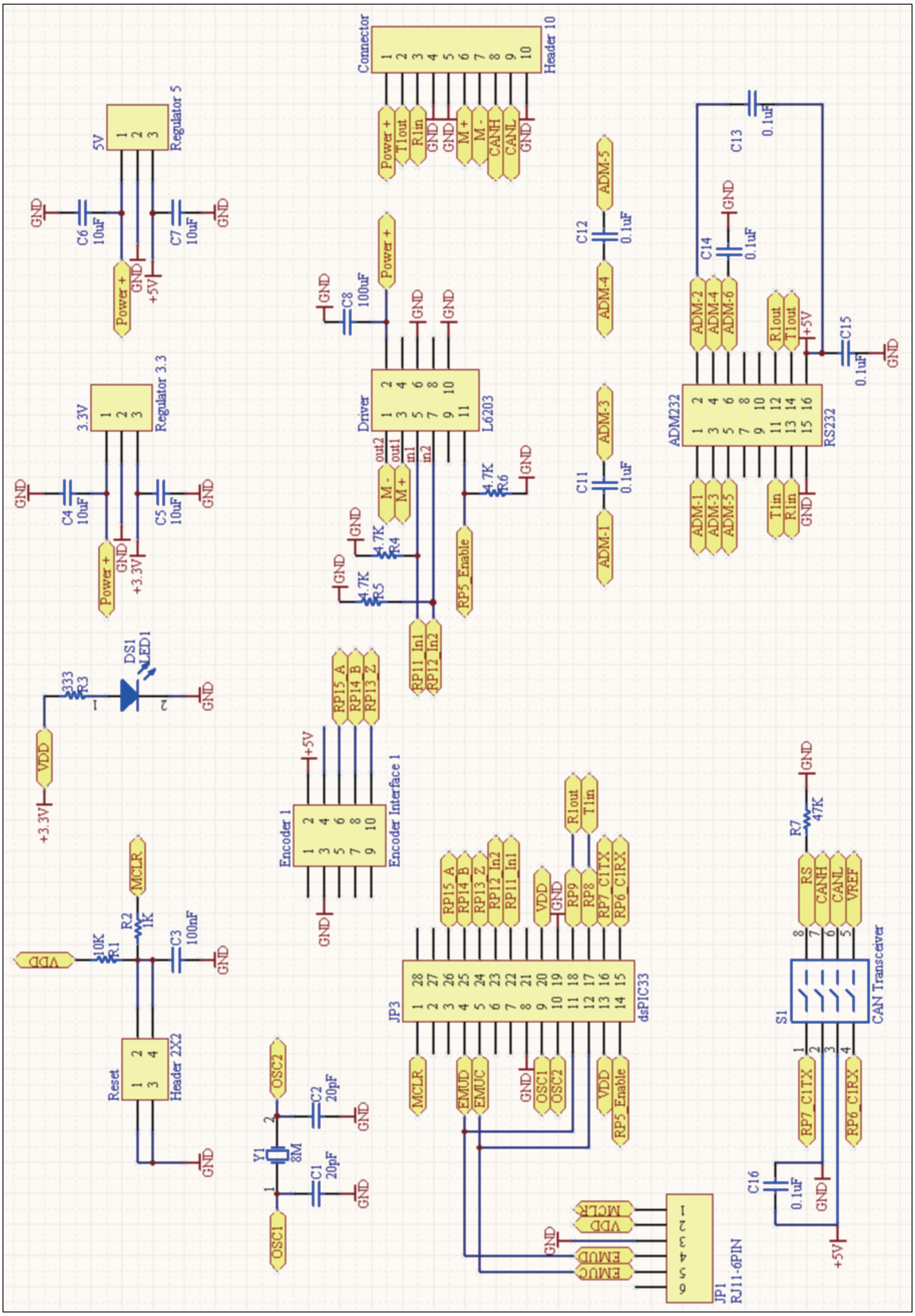

Figure D.2. Electronic schematic of the motor driver

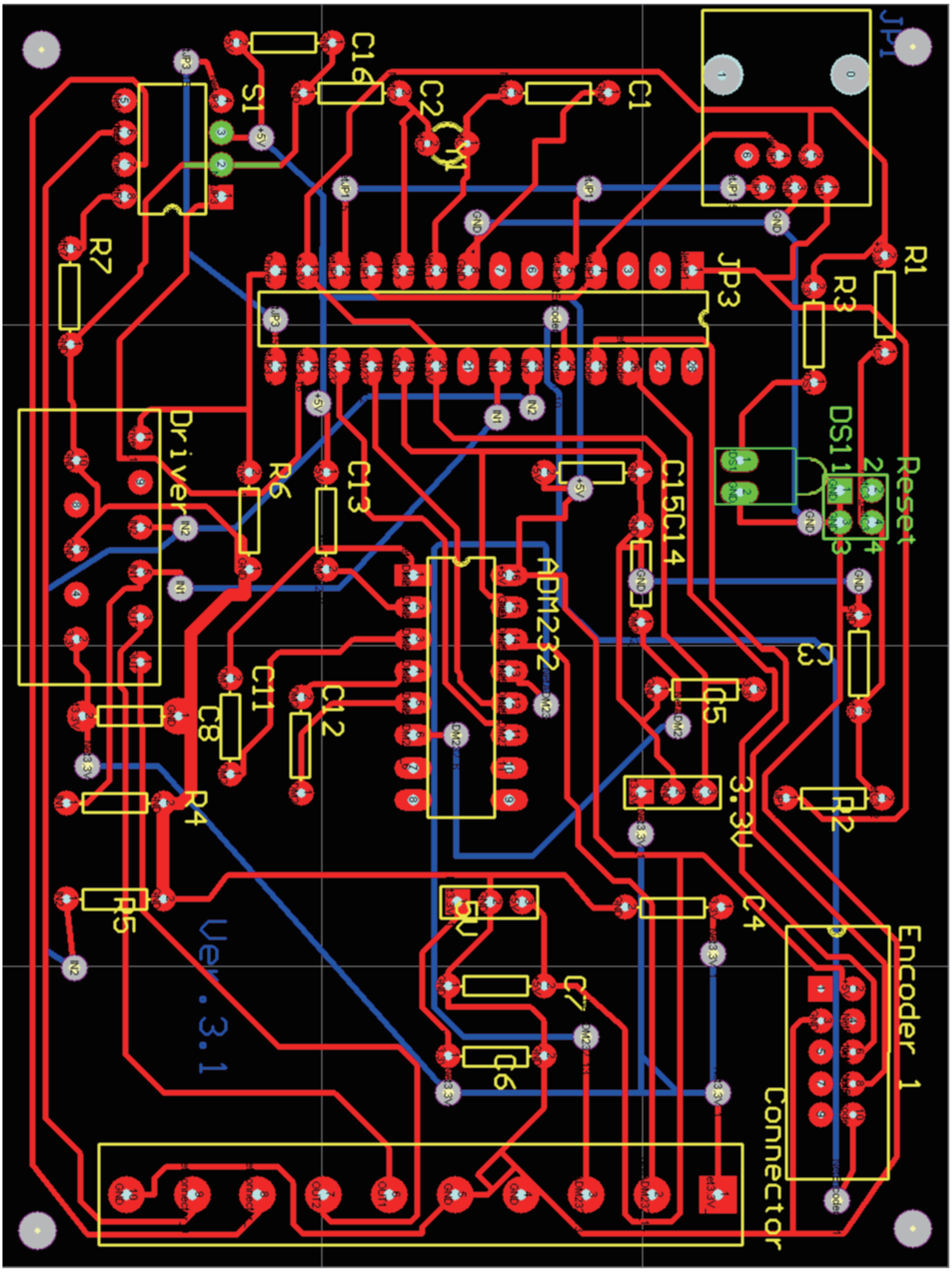

Figure D.3. Circuit of the motor driver

Published Papers During Doctoral Course

Journal Papers:

1. Qiquan Quan, Shugen Ma, and Zongquan Deng, Impact analysis of a dual-crawler-driven robot, ***Advanced Robotics***, vol.23, no.12-13, pp.1779—1797, 2009.

2. Qiquan Quan and Shugen Ma, Controllable postures of a dual-crawler-driven robot, ***Mechatronics***, vol.20, iss.2, pp.281—292, 2010.

Conference Papers:

1. Shugen Ma, Qiquan Quan, and Rongqiang Liu, Posture analysis of a dual-crawler-driven robot, *Proceedings of the 2008 IEEE/ASME International Conference on Advanced Intelligent Mechatronics*(**AIM'08**), Xi'an, China, pp.365—370, 2008.

2. Qiquan Quan, Shugen Ma, Rongqiang Liu, and Bin Li, Impact analysis of a dual-crawler-driven robot, *Proceedings of the 2008 IEEE International Conference on Robotics and Biomimetics*(**ROBIO'08**), Bangkok, Thailand, pp.800—805, 2008.

3. Qiquan Quan, Shugen Ma, Bin Li, and Rongqiang Liu, Posture control of a dual-crawler-driven robot, *Proceedings of the 2009 IEEE International Conference on Robotics and Automation*(**ICRA'09**), Kobe, Japan, pp.2977—2982, 2009.

4. Qiquan Quan, Shugen Ma, and Rongqiang Liu, Controllable postures of a dual-crawler-driven robot, *Proceedings of the 9th International Symposium on Robot Control, The International Federation of Automatic Control*(**SYROCO'09**), Nagaragawa Convention Center, Gifu, Japan, pp.319—324, 2009.

5. Qiquan Quan and Shugen Ma, A modular crawler-driven robot: mechanical design and preliminary experiments, *Proceedings of the 2009 IEEE International Conference on Intelligent Robots and Systems*(**IROS'09**), St. Louis, USA, pp.639—644, 2009.